Development of Hybrid Micro Machining Approaches and Test-bed

Wenlong Chang

Submitted for the degree of Doctor of Philosophy

Heriot-Watt University

School of Engineering and Physical Sciences

May 2012

Abstract

High precision miniature and micro products which possess 3D complex structures or free-form surfaces are now being widely used in industry. These micro products require to be fabricated by several machining processes and the integration of these various machining processes onto one machine becomes necessary since this will help reduce realignment errors and also increase the machining efficiency. This thesis describes the development and testing of several hybrid machining approaches for machines which are typically used to produce micro products such as micro fluidic moulds, solar concentrator moulds, micro grooves in brittle materials and micro structured milling cutters. These are: (a) micro milling and laser deburring; (b) micro grinding involving laser pre-heating; (c) micro milling and laser polishing.

The hybrid micro milling/ laser deburring process was tested during the fabrication of a micro fluidic injection mould. Micro burrs on the channel of micro fluidic mould generated during micro milling were completely removed by developed laser deburring process. This approach can achieve a good surface finish on a micro fluidic mould.

The hybrid laser assisted micro grinding process was investigated by fabricating a set of micro grooves on brittle materials, including Al_2O_3 and Si_3N_4. The workpiece was pre-heated by laser to increase its temperature above that of the brittle to ductile transition phase interface. It was found that lower cutting forces were apparent in the grinding process when used to machine brittle materials. It was also found that laser assisted grinding helped achieve a very good surface finish and reduced subsurface damage.

The final hybrid machining approach tested involved micro milling and laser polishing to fabricate solar concentrator moulds. Such a mould requires a good surface finish in order to accurately guide light focusing on a target. The laser polishing process was successfully used to remove any unwanted cutting marks generated by a previous micro milling process.

As a novel extension to this hybrid machine world, a focussed ion beam (FIB) fabrication approach was researched regarding the generation of microstructures on the rake faces of milling cutters with the aim of reducing cutter cutting forces and increasing tool life. The tool wear resistance performance of these microstructured tools was evaluated through three sets of slot milling trials on a NAK80 specimen with the results indicating that micro structured micro milling cutters of this kind can effectively improve the tool wear resistance performance. A microstructure in a direction perpendicular to the cutting edge was found to be the best structure for deferring tool wear and obtaining prolonged tool life. This approach can potentially be further integrated into a hybrid precision machine such that micro structure cutters can be fabricated in-situ using a laser machining process. The conceptual design of a 5-axis hybrid machine which incorporates micro milling, grinding and laser machining has been proposed as a test-bed for the above hybrid micro machining approach. Through finite element analysis, the best configuration was found to be a closed-loop vertical machine which has one rotary stage on the worktable and another on machining head.

In this thesis, the effectiveness of these novel hybrid machining approaches have been fully demonstrated through machining several microproducts. Recommendations for future work are suggested to focus on further scientific understanding of hybrid machining processes, the development of a laser repairing approach and the integration of a controller for the proposed hybrid machine.

Dedication

To my wonderful parents

HsiuFeng Chen, WuChien Chang

Acknowledgements

First of all, I would like to thank my supervisors, Dr. Xichun Luo and Professor James M Ritchie, for their great support, encouragement and guidance from the initial project inception through to the final level, which enabled me to develop a deep understanding of the research. Special thanks on given to Dr. Xichun Luo, as he has influenced me not only on my engineering research but also on my attitude in life.

I would also like to thank Heriot Watt University and the School of Engineering and Physical Sciences for the financial support which made this research possible. I also acknowledge Professor Duncan P Hand, Dr. Will Shu, Dr. Wei Wang, Mr. Chris Mack, Mr. Jining Sun, Mrs. Marian K Millar, Mr. Richard Kinsella, Dr. Ben Xu, Mr. John Mason and all my other friends and researchers within the Mechanical Engineering Department, for their assistance in machining trials and valuable advanced discussions regarding my project.

My thanks go to Professor Qingliang Zhao, Dr. Qingshun Bai, Professor Xing Yu, Dr. Xudong Li, Mr. Yi Zhao from Harbin Institute of Technology for their experimental equipment support and machining assistance. I would also like to acknowledge my former colleagues Dr. Fu-Chuan Hsu, Mr. Yin Chung and Dr. Chao-Yung Yeh in the Metal Industry and Research Development Centre for their advice and research support.

Importantly, I would like to express my appreciation to my best friend Hsing-Hsiung Wang, who gave me valuable advice and encouragement.

Finally, I am deeply indebted to my family, for their wonderful support, help and encouragement. Their love, patience, interest, unlimited moral support and welcome series of social distractions during the entire project have greatly enhanced and eased the way I conducted this research.

Declaration Statement

ACADEMIC REGISTRY
Research Thesis Submission

Name*:*	Wenlong Chang		
School/PGI:	School of Engineering and Physical Sciences		
Version: *(i.e. First, Resubmission, Final)*	Final	Degree Sought (Award **and** Subject area)	PhD Mechanical Engineering

Declaration

In accordance with the appropriate regulations I hereby submit my thesis and I declare that:

1) the thesis embodies the results of my own work and has been composed by myself
2) where appropriate, I have made acknowledgement of the work of others and have made reference to work carried out in collaboration with other persons
3) the thesis is the correct version of the thesis for submission and is the same version as any electronic versions submitted*.
4) my thesis for the award referred to, deposited in the Heriot-Watt University Library, should be made available for loan or photocopying and be available via the Institutional Repository, subject to such conditions as the Librarian may require
5) I understand that as a student of the University I am required to abide by the Regulations of the University and to conform to its discipline.

* *Please note that it is the responsibility of the candidate to ensure that the correct version of the thesis is submitted.*

Signature of Candidate*:*		Date:	

Submission

Submitted By *(name in capitals):*	WENLONG CHANG
Signature of Individual Submitting:	
Date Submitted:	

For Completion in the Student Service Centre (SSC)

Received in the SSC by *(name in capitals):*			
Method of Submission *(Handed in to SSC; posted through internal/external mail):*			
E-thesis Submitted (***mandatory for final theses***)			
Signature:		Date:	

Table of Contents

Abstract ii

Dedication iv

Acknowledgements v

Declaration Statement vi

Table of Contents vii

List of Figures xi

List of Tables xvi

Nomenclature xvii

Abbreviations xix

List of Publications from this Study xx

Chapter 1 Introduction 1

1.1 Background 1

1.2 Aim and objectives 5

1.3 Chapter plan of the thesis 5

Chapter 2 Literature review 7

2.1 Introduction 7

2.2 Precision micro machining 7

2.2.1 Micro milling and micro turning 7

2.2.2 Micro grinding 8

2.2.3 Micro laser machining 8

2.2.4 EDM 9

2.2.5 Micro ultrasonic machining 10

2.2.6 Comparative summary 10

2.3 Machining process requirements for micro products 12

2.3.1 Micro fluidic devices 13

2.3.2 Dentures 14

2.3.3 Solar concentrators 15
2.4 Benchmark precision machine tools for micro products 16
2.4.1 The micro machining centre 16
2.4.2 The micro laser machine tool 21
2.5 High precision multifunctional and hybrid machine tools 23
2.5.1 FANUC ROBONANO 23
2.5.2 AIST's hybrid machine 24
2.5.3 Takashima Sangyo's desktop hybrid machine 25
2.5.4 MIRDC's hybrid machines 26
2.5.5 MikroTools-DT110 28
2.5.6 Summary of multifunctional and hybrid machine tools 29
2.6 Summary 31
Chapter 3 A hybrid micro machining approach - micro milling and laser deburring 32
3.1 Introduction 32
3.2 Review of available deburring processes 32
3.3 Micro burrs generated in the micro milling process 33
3.3.1 Mechanics of the cutting process 33
3.3.2 Micro burr formation mechanism 34
3.3.3 Finite element analysis of micro burr generation 36
3.4 Laser deburring process 37
3.4.1 Deburring mechanisms 37
3.4.2 Laser deburring process temperature model for the laser deburring process 38
3.4.3 Laser deburring trials 40
3.5 Experimental study of the hybrid machining process and discussion 42
3.5.1 Fabrication of a micro injection mould by micro milling 42

3.5.2 Laser deburring experiment....43
3.5.3 Results and discussions....44
3.6 Summary....45
Chapter 4 A hybrid micro machining approach - laser assisted micro grinding....47
4.1 Introduction....47
4.2 Review of laser assisted turning and milling....48
4.3 Laser assisted micro grinding....49
4.3.1 Laser source for laser assisted grinding....49
4.3.2 Thermal conduction for laser heating....52
4.4 Laser assisted micro grinding trial....54
4.5 Results and discussions....57
4.5.1 Groove depth....57
4.5.2 Grinding force....58
4.5.3 Surface roughness and microstructure of the machined surface....59
4.5.4 Subsurface damage....61
4.6 Summary....63
Chapter 5 A hybrid micro machining approach - micro milling and laser polishing....64
5.1 Introduction....64
5.2 Micro milling solar concentrator moulds....65
5.3 Laser polishing trial....66
5.4 Results and discussions....67
5.5 Summary....71
Chapter 6 Structuring micro milling cutters for deferring tool wear....72
6.1 Introduction....72
6.2 Structuring micro milling cutter by focused ion beam (FIB)....72
6.3 Evaluation of micro milling trials....75
6.3.1 Cutting force and surface roughness....76
6.3.2 Tool wear....78

6.4 Summary....81
Chapter 7 Conceptual designs of a hybrid machine....82
7.1 Introduction....82
7.2 Proposed hybrid machine specification....82
7.3 Conceptual design....83
7.4 Finite element analysis of the proposed hybrid machines' mechanical structures....86
7.4.1 Finite element analysis procedure....86
7.4.2 Finite element analysis of the proposed hybrid machine mechanical structures....88
7.5 Summary....100
Chapter 8 Conclusions & recommendations for future work....101
8.1 Assessment of the research....101
8.2 Conclusions....101
8.3 Recommendations for future work....103
References....104
Appendix 1....116
Appendix 2....123
Appendix 3....129
Appendix 4....135

List of Figures

Figure 1-1 Trends in development of machining technologies in terms of machining accuracy and material removal rate....2

Figure 1-2 Comparison of traditional machining processes time and multifunctional machining process time....3

Figure 1-3 Schematic of an idealised hybrid machine tool hosting four different machining processes for the fabrication of 3D micro products....4

Figure 2-1 Micro fluidic channels....14

Figure 2-2 Denture in brittle material fabricated using grinding process....15

Figure 2-3 Illustration of the light focused by a concentrator....16

Figure 2-4 Kugler MICROMASTER® 5X....17

Figure 2-5 Ultra NANO 100....18

Figure 2-6 Freeform 700....19

Figure 2-7 Oxford Lasers' PicoLase 1000....21

Figure 2-8 PL10100....22

Figure 2-9 Ultra high precision machine FANUC Robonanoα-0iB....24

Figure 2-10 AIST's first concept of hybrid machine....25

Figure 2-11 Takashima's desk top hybrid machine....25

Figure 2-12 The micro parts polished using ECM process....26

Figure 2-13 Cross-hatched pattern of lubrication groove using CNC milling and laser machining....27

Figure 2-14 The reconfigurable machining centre with multiple machining modules....28

Figure 2-15 MikroTool's multi-process hybrid micro machine....29

Figure 3-1 Examples of burr definition after micro milling....34

Figure 3-2 Illustration of a micro milling process....35

Figure 3-3 The process of micro burr formation 35
Figure 3-4 Schematic illustration of initial and final burr formation 36
Figure 3-5 The simulation of burr generation using Deform 37
Figure 3-6 Schematic illustration of laser metal interactions during laser deburring process 38
Figure 3-7 Relationship between laser power and laser machining depth 41
Figure 3-8 Machined surface roughness under difference laser power and laser focus points 41
Figure 3-9 Setup for machining micro fluidic mould using a high speed spindle 42
Figure 3-10 CAD model of micro channel and injection mould 42
Figure 3-11 Measured burrs on the edge of the micro fluidic channels after micro milling 43
Figure 3-12 A schematic diagram of Nd:YAG laser deburring system 43
Figure 3-13 SEM image and cross section of the edge of the micro fluidic channel after micro milling 44
Figure 3-14 SEM image and cross section of the edge of the micro fluidic channel after laser deburring 45
Figure 3-15 Machined surface topography after micro milling and laser deburring 45
Figure 3-16 Flowchart of micro milling and laser deburring 46
Figure 4-1 Effect of temperature on the ultimate tensile strength for various hard-to-machine materials 48
Figure 4-2 Illustration of laser assisted machining 49
Figure 4-3 Absorption capacity of Al_2O_3 against wavelength 51
Figure 4-4 Relationship between current input and laser power output 51
Figure 4-5 Increase of temperature under different laser current for Si_3N_4 and Al_2O_3 ... 54
Figure 4-6 Experimental system of laser assisted grinding 55

Figure 4-7 The flow chart for the laser assisted grinding experiment 56

Figure 4-8 Measured groove depth for Si_3N_4 57

Figure 4-9 Measured groove depth for Al_2O_3 58

Figure 4-10 The grinding force against cutting distance 59

Figure 4-11 The 3D structure of Si_3N_4 from AFM 60

Figure 4-12 The 3D structue of Al_2O_3 from AFM 60

Figure 4-13 Subsurface damage on Si_3N_4 62

Figure 4-14 Subsurface damage on Al_2O_3 62

Figure 4-15 Flowchart of laser assisted micro grinding 63

Figure 5-1 CAD model of a simplified solar concentrator mould 65

Figure 5-2 A portable milling CNC machine for machining solar concentrator mould .. 66

Figure 5-3 The concentrator mould machined after micro milling 66

Figure 5-4 A nanosecond YAG laser system for laser polishing 67

Figure 5-5 SEM image of the machine surface after the micro milling 68

Figure 5-6 SEM images showing surface after laser polishing with 3.5W power 68

Figure 5-7 SEM images of the machine surface after laser polishing with 4.5W power 68

Figure 5-8 SEM images of machined surface after laser polishing with 4W power 69

Figure 5-9 Comparisons of surface roughness Ra after micro milling and the use of different laser power 70

Figure 5-10 Surface topography after micro milling and two laser polishing processes 70

Figure 5-11 Flowchart of micro milling and laser polishing 71

Figure 6-1 SEM images of the microstructured milling cutters and a normal milling cutter 74

Figure 6-2 Set up of the cutting trial 76

Figure 6-3 The average cutting forces on X-axis direction when using the four milling cutters 77

Figure 6-4 Measured surface roughness (Ra) in the first and third set of cutting trials..77

Figure 6-5 The cutting forces on X-axis direction when using horizontal structured tool 78

Figure 6-6 Measured flank tool wear of the microstructured tools after the third set of cutting trials.....79

Figure 6-7 Measured tool nose radius of the microstructured tools after the third set of cutting trials.....80

Figure 6-8 Variations of cutting force on X-axis direction against machining distance in the third set of slot milling trial.....80

Figure 7-1 Conceptual design 1 84

Figure 7-2 Conceptual design 2 85

Figure 7-3 Conceptual design 3 85

Figure 7-4 Illustration of finite element analysis procedure 87

Figure 7-5 Simplified structure of conceptual design 1 88

Figure 7-6 Illustration of TE4 element type.....89

Figure 7-7 Boundary conditions of 5 axes hybrid machine type 1 90

Figure 7-8 Displacement of the machine structure of conceptual design 1 91

Figure 7-9 Stress of the machine structure of conceptual design 1.....91

Figure 7-10 Mode 1 of natural frequency of conceptual design 1 92

Figure 7-11 Mode 2 of natural frequency of conceptual design 1 92

Figure 7-12 Mode 3 of natural frequency of conceptual design 1 93

Figure 7-13 Displacement of the machine structure of conceptual design 2 94

Figure 7-14 Stress of the machine structure of conceptual design 2.....94

Figure 7-15 Mode 1 of natural frequency of conceptual design 2 95

Figure 7-16 Mode 2 of natural frequency of conceptual design 2 95

Figure 7-17 Mode 3 of natural frequency of conceptual design 2 96

Figure 7-18 Displacement of the machine structure of conceptual design 3 97

Figure 7-19 Stress of the machine structure of conceptual design 3.....97

Figure 7-20 Mode 1 of natural frequency of conceptual design 3. 98

Figure 7-21 Mode 2 of natural frequency of conceptual design 3 98

Figure 7-22 Mode 3 of natural frequency of conceptual design 3 99

List of Tables

Table 2-1 Comparative summary of micro machining processes 12

Table 2-2 Specifications of micro machining centres 20

Table 2-3 Laser machine parameters 23

Table 2-4 Specifications of multifunctional and hybrid machine tools 30

Table 4-1 Material properties of Al_2O_3 and Si_3N_4 50

Table 4-2 The specifications of conventional grinding machine in HIT 55

Table 4-3 Surface roughness on Si_3N_4 60

Table 7-1 Design data of granite and Al alloy used in the machine 89

Table 7-2 Numbers of elements for three conceptual design 89

Table 7-3 Summary of these three finite element analysis machines 100

Nomenclature

A	area of the laser spot
A_b	surface transmissivity
A_v	fraction of the radiation energy absorbed to per unit volume of workpiece
C_e	capacities of the metal electron
C_l	capacities of the metal lattice
F	laser energy density
F_0	ablation threshold
F_r	laser frequency
F_q	the rate of heat transfer per unit area
I	Gaussian distribution of intensity
$I_{(t)}$	laser intensity
$Q_{(z)}$	electron heat flux
S	absorbed energy
T_e	temperature of metal electrons
T_l	temperature of metal lattices
c	specific heat of the workpiece
$erf(s)$	error function
$erfc(s)$	complimentary error function
h_0	burr width
h_f	burr height
k	thermal conductivity
k_e	metal electron thermal conductivity
t_0	undeformed chip
z	ablation rate
z_c	depth coordinate radiated

α	optical penetration depth
β	initial negative shear angle
κ	thermal diffusivity
ρ	density
ω	length from at the point of starting negative shear to the end of surface
φ	shear angle under cutting process

Abbreviations

ATCs	automatic tool changing system
AFM	atomic force microscopy
CAD	computer aided design
CAM	computer aided manufacturing
CCD	charge-coupled device
CNC	computer numerical control
ECM	electrochemical machining
EDM	electron discharge machine
FEA	finite element analysis
FIB	focussed ion beam
FTS	fast tool servo
HAZ	heat affected zone
ISO	International Organization for Standardization
LAM	laser assisted machining
LCD	light-emitting diode
R.P.M.	revolutions per minute
SEM	scanning electron microscope
STS	slow tool servo
TTM	two temperature
USM	ultrasonic machining

List of Publications from this Study

Journal Papers:

1. Xichun Luo, Jining Sun, **Wenlong Chang** and James M. Ritchie, Single point diamond turning of calcium fluoride optics, *Key Engineering Materials* (in press).
2. Jining Sun, Xichun Luo, **Wenlong Chang** and James M. Ritchie, Fabrication of freeform micro optics by focused ion beam, *Key Engineering Materials* (in press).
3. **Wenlong Chang**, Xichun Luo, Qiling Zhao, Jining Sun, Yi Zhao, Laser assisted micro grinding of high strength materials, Key Engineering Materials, Vol. 496, pp 46-49, 2012
4. **Wenlong Chang**, Xichun Luo, James M. Ritchie, Jining Sun and Chris Mark, Fabrication of micro fluidic injection moulds by a hybrid micromachining process, Proc. Inst. Mechanical Engineers Part B, J. Engineering Manufacture, Vol. 225, Issue 3, pp. 458-462, 2011
5. **Wenlong Chang**, Jining Sun, Xichun Luo, James M Ritchie and Chris Mack, Investigation of microstructured milling tool for deferring tool wear, Wear, 271(9-10), pp. 2433-2437, 2011
6. **Wenlong Chang**, Xichun Luo, James M Ritchie, Jining Sun, and Chris Mack, Laser deburring process for structured edges on precision moulds, International Journal of Nanomanufacturing, 7(3), pp. 327-335, 2011

Conference Papers:

7. **Wenlong Chang**, Xichun Luo, James Ritchie, Jining Sun and Chris Mack, Fabrication of micro fluidic mould by micro milling and laser de-burring, Proceedings of the euspen International Conference, Delft, June 2010
8. Xichun Luo, **Wenlong Chang**, Jining Sun, Comparison of micro-drilling and laser-machining holes on glass wafer for fabrication of MEMS, Proceedings of the euspen International Conference, San Sebastian, June 2009
9. Xichun Luo, **Wenlong Chang**, Jining Sun, Ning Ding, Chris Mack, Micro-drilling holes on glass wafer for fabrication of MEMS, Proceedings of the International Conference on Manufacturing Research, CD Disk, Brunel University, 2008

Chapter 1 Introduction

1.1 Background

Precision manufacturing is becoming increasingly important due to the rapidly increasing demand for high precision micro products and components in a wide range of industries such as biomedical, electro-optics, automotive, aerospace and information technology, etc [1]. The characteristics of these micro products and components are: (1) size from few micrometers up to 100 micrometers; (2) high precision tolerances, typically better than 1 micrometer; (3) good surface finish, in general surface roughness smaller than half micrometer; (4) some 3D shapes or complicated structures; (5) the use of advanced engineering materials with high hardness such as ceramics and hard steels as a substrate [2].

Many precision machining processes such as micro milling, micro turning, laser machining, micro electron discharge machining (μ-EDM), electrochemical machining (ECM), ultrasonic machining (USM), chemical etching and LIGA have been used to manufacture micro products. However, not all precision machining processes are appropriate for fabricating 3D geometries or hard-to-machine materials. It has been recognised that micro products with complex 3D shapes cannot be properly manufactured by using traditional MEMS manufacturing processes such as chemical etching or LIGA processes [3, 4]. In these, silicon is the major material and hard-to-machine materials are not suitable for fabrication using these approaches. On the other hand, high precision computer numerical control (CNC) machining processes, including micro milling and turning processes, are powerful techniques which can produce complicated miniature 3D geometries with a good surface finish on various types of materials [5].

Taniguchi's graph shown in Figure 1-1 presents the trends in improving machining accuracy from 1940 to 2000 [6]. According to his research, the trend of micro machining technology can be extended to 2010. High precision and ultra precision machining processes enable to achieve a very high accuracy from 10 nm to 100 nm and a material removal rate above 10^{-4} mm^3/s. Unfortunately, mechanical CNC machining techniques are difficult to apply to the machining of some advanced engineering materials, such as ceramics, due to excess tool wear. Even diamond cutters are limited

in fabricating non-ferrous metals. In recent years, non-traditional high precision machining processes have been applied for manufacturing hard-to-machine materials [7-10].

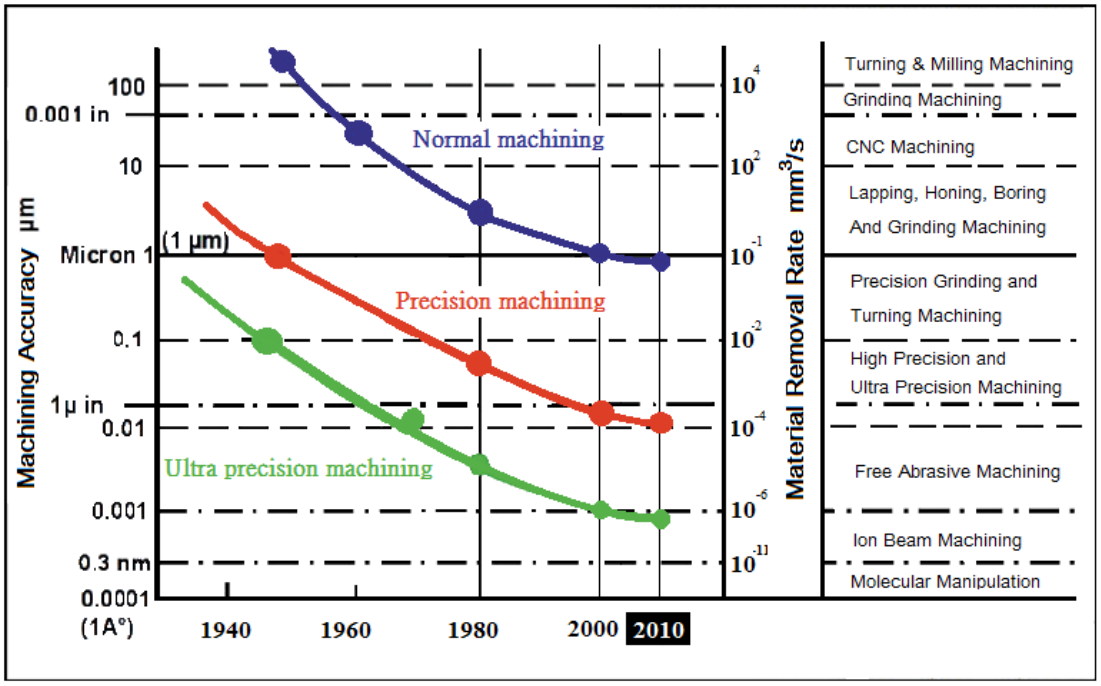

Figure 1-1 Trends in development of machining technologies in terms of machining accuracy and material removal rate [6, 11]

Currently, these highly accurate miniaturized 3D complex parts are made via a variety of separate high precision machining processes. In the last decade, multifunctional machines have been developed within the industry [12]. These integrate more than one traditional mechanical machining process, such as milling, turning, drilling, grinding and engraving, all on one machine, in order to achieve higher machining accuracy and efficiency. In 2005, Europe's premiere machine tool trade show called EMO exhibited many milling-turning machines from Japan such as Mazak, Mori Seiki and Okuma. The main advantage of multifunctional machines is implementing different traditional machining processes in one machine set-up to manufacture complex parts improving accuracy and considerably reducing both production and load times by reducing set-up and inter-operation queuing and transit times. This helps drastically reduce the production time as shown in Figure 1-2.

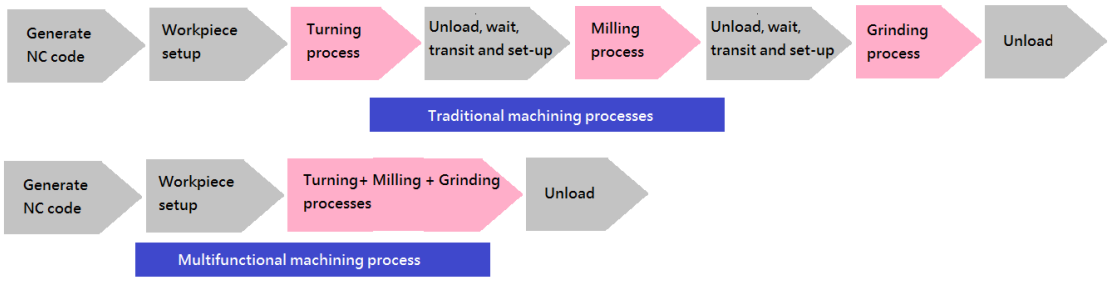

Figure 1-2 Comparison of traditional machining processes time and multifunctional machining process time

However, multifunctional machines integrate traditional mechanical material removed processes that are not always the best option for machining some advanced engineering materials such as ceramics or hard steels. Nor can they avoid the traditional shortcomings of a mechanical machining process, such as the generation of micro burrs and short tool life. On the other hand, non-traditional mechanical machining processes, such as EDM, ECM, USM, ion beam machining and laser machining can achieve better and more consistent workpiece quality and higher efficiency in the processing of hard and tough materials than traditional mechanical machining processes. However, some non-traditional processes can significantly contribute towards undesirable surface changes such as plastic deformation, hardness alteration, cracks, residual stress, metallurgical transformations and heat-affected zone.

In the future, both traditional and non-traditional micro and nano machining processes will be required to manufacture micro products, such as scalpels, optics for solar cells, micro fluidic devices and dental prosthesis.

As shown in Figure 1-3, a hybrid machine of this kind can also host and integrate traditional and non-traditional machining processes at this scale. This hybrid approach can reduce machining time and increase manufacturing precision. In order to fabricate complex parts using hard-to-machine materials, a hybrid machining capability is becoming increasingly important. It would therefore be hugely beneficial to investigate hybrid machining for the manufacture of 3D nano and micro parts which require high manufacturability and productivity.

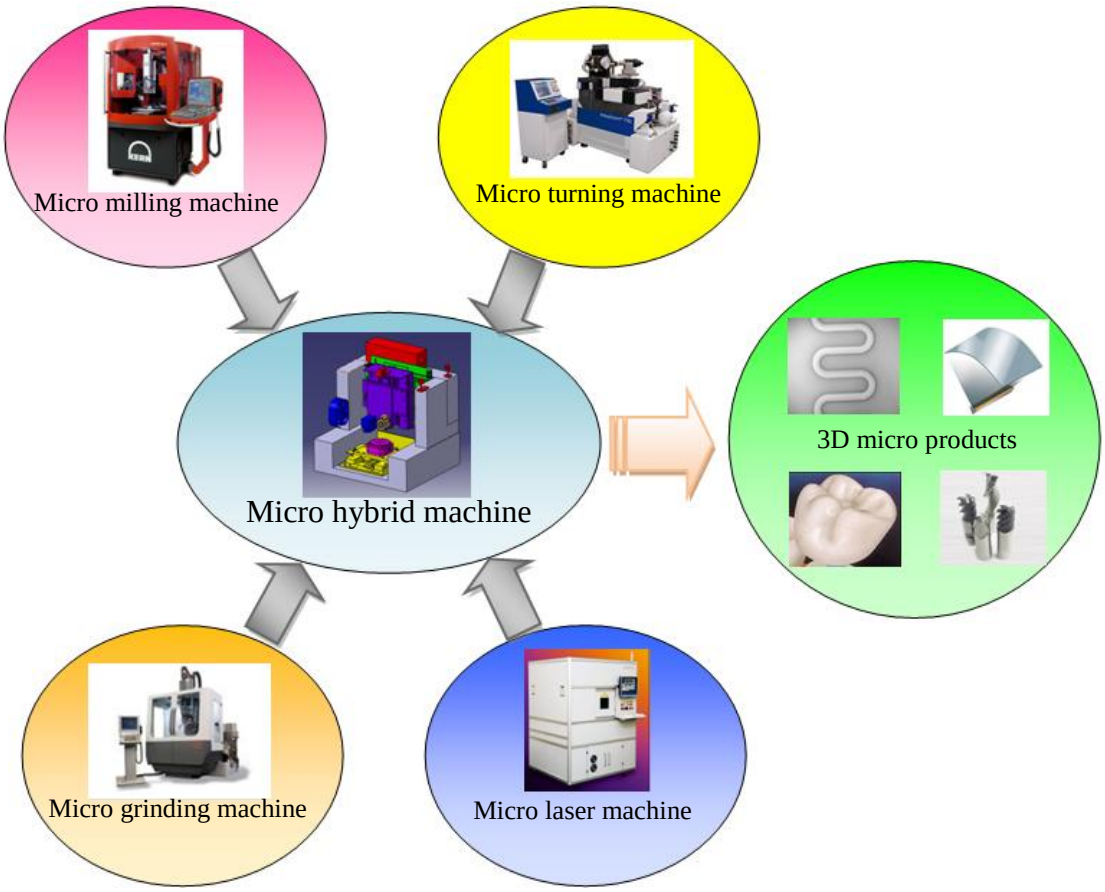

Figure 1-3 Schematic of an idealised hybrid machine tool hosting four different machining processes for the fabrication of 3D micro products

1.2 Aim and objectives

The aim of this research project is to implement and, where possible, test hybrid micro machining approaches to demonstrate the advantages offered for the manufacture of micro products which have critical demands in terms of form accuracy and surface finish.

The main objectives of this research are:

(i) To identify gaps in the current capabilities of hybrid machining micro manufacture based on both modern product machining requirements and current hybrid process limitations.

(ii) To implement and test various micro machining approaches for various products and materials by applying combinations of micro milling, micro grinding, laser machining and laser polishing with a view to addressing the gaps indentified in (i).

(iii) To develop an *in-situ* process for structuring micro milling cutters, in order to reduce the associate cutting forces and achieve a better surface finish on a workpiece.

(iv) To carry out the conceptual design of 5 axes hybrid machine.

1.3 Chapter plan of the thesis

There are eight chapters presented in this thesis. Chapter 1 explains the background, motivation, aim and objectives of this research. Chapter 2 reviews the current high precision micro products which need to be machined by using several machining processes. It also surveys and provides an international benchmark of high precision machine tools and the most recently developed hybrid machines.

Chapter 3 presents a novel hybrid micro machining approach which combines micro milling and micro laser machining for the manufacture of a micro fluidic mould. The effectiveness of this approach is accessed after measurement of machined surface roughness on the channels measured by an SEM and a white light interferometer.

Chapter 4 carries out experiments on novel laser assisted micro grinding of brittle materials. A test-bed which accommodates laser heating process and micro grinding process is developed. A series experiments are carried out to machine brittles materials including Al_2O_3 and Si_3N_4. The cutting force, surface roughness, tool wear and

subsurface damage on the brittle materials are measured and further discussed in this study.

Chapter 5 describes a novel laser assisted polishing process which is used to further improve surface roughness of workpiece machined by micro milling. The surface finish on concentrator mould is measured and presented in this chapter to show the effectiveness of this machining approach.

Chapter 6 investigates the influence of micro structures on milling cutter performance. Three different microstructure patterns are generated by a focused ion beam on three identical end mill cutters. The effects of these microstructures on tool wear resistance performance are investigated and discussed as are the cutting force, surface roughness on workpiece and tool wear.

Chapter 7 presents the conceptual design of a hybrid machine which can integrate micro milling, micro grinding, micro laser machining. Three machines configurations are proposed and the results of finite element analysis of its static and dynamic characteristics is presented and discussed.

Chapter 8 draws some conclusions resulted from this investigation and summaries contributions to knowledge. Recommendations are made for the future work.

Chapter 2 Literature review

2.1 Introduction

High precision machining processes, such as micro milling, turning, grinding, EDM, ECM and laser machining, are used to fabricate micro products in industry. The capacities and tolerance of these high precision machining processes are outlined in the following chapter. Each high precision machining process has its own limitations and is not able to meet all of the requirements of micro products. Moreover, micro products are getting increasingly more complex and require higher precision, better surface finish and require the use of hard-to-machine materials [13-16]. Typical micro products such as micro fluidic moulds, dentals and solar concentrator moulds, are fabricated by using more than one high precision machine tool, such as various combinations of micro milling, micro turning, micro grinding, EDM, ultrasonic and micro laser machine [17].

Transferring a workpiece from one machine to another will not only increase setup time but also cause an accumulation of alignment errors and potential transit and queuing [18]. These problems can be solved by combining a sequence of high precision machining processes into one machine; hence on set up. The integration of numerous manufacturing processes can fulfil the demand for a large variation of micro products and a reduction of manufacturing time and cost. In recent years, many high precision multifunctional and hybrid machine tools have been developed by research institutes and industries. This literature review surveys key micro processes and micro products which require a selection of micro machining processes, the benchmarking of high precision machine tools and the development of hybrid machines.

2.2 Precision micro machining

2.2.1 Micro milling and micro turning

Micro milling and micro turning are the most flexible micro machining processes and are able to fabricate a wide variety of complicated micro components and micro structures. Micro milling is a machining process for removing materials by relative motion between a workpiece and a high speed rotating cutter having multiple cutting edges. Each micro milling cutter tooth takes its share of the stock in the form of small individual chips. Micro turning is also a machining process and involves a cutting tool mounted on the machine to remove material from external surfaces on a rotating

workpiece; thus can involve one or more cutting edges.

The machining volumes for micro milling and micro turning machine tool are normally up to 300 mm×300 mm×150 mm and ø300 mm×300 mm, respectively. Micro milling and micro turning are defined as the downscale versions of conventional milling/turning processes involving the use of milling/turning cutters in the sub-millimetre range [19-21]. The accuracy of micro milling and micro turning processes are less than 5 μm and the material removal rate vary from 10^{-4} to 10^{-1} mm^3/s. The diameter of micro milling tools is from 0.01 mm to 1 mm. The workpiece surface can also be milled to any combination of shapes and at a roughness from Ra 0.01 μm to Ra 0.5 μm [21-26].

2.2.2 Micro grinding

Micro grinding is an abrasive process, thereby distinguishing it from most other metalworking processes. Micro grinding is especially advantageous for finishing of brittle materials which can be mirror finished because of the very small depth of cut obtained. The limitation of a micro grinding machine is that it is only for 2D features. In order to achieve 2.5D or 3D features, the jig grinding machine was developed. The original jig grinding machine was designed for grinding holes accurately to both size and location. The latest jig grinding machine can generate complex surfaces as well as internal and external shapes with different grinding wheels.

These new jig grinding machines enable to polish the workpiece size of 3D features up to 300 mm×300 mm×300 mm [27]. The accuracy of a jig grinding machine is about 3 μm and the material removal rate is from 10^{-5} to 10^{-4} mm^3/s. The diameter of the grinding wheel is from 0.75 mm to 2.5 mm and the surface roughness from Ra 0.01 μm to Ra 0.2 μm [16, 28-30].

2.2.3 Micro laser machining

Micro laser machining has become an enabling technology for micro device fabrication in many industrial applications [31, 32]. Laser beam machining is based on the conversion of electrical energy into light energy and then into thermal energy [33-36]. Although several types of laser exist, all lasers produce an intense, coherent, highly collimated beam of single wavelength light. In material processing applications, this

narrow beam is focused by an optical lens to produce a small, intense spot of light on the workpiece surface. Optical energy is converted into heat energy upon impact and the temperatures raised are high enough to melt and/or vaporize solid materials. Researchers have reported that the types of lasers currently being used for micromachining applications include CO_2, solid state, diode and excimer lasers [31, 37, 38].

Solid state pulsed lasers with micrometre and nanometre pulse widths are already used satisfactorily [37] in industry and can provide adequate processing speed and surface finish for mid-scale feature sizes (80 mm×80 mm). However, the increasing demand for component miniaturisation renders these lasers unsuitable for high quality work mainly due to the thermal nature of interaction with materials which contributes to poor feature morphology such as periodic surface structures, melt, surface swelling. Ultrafast lasers (e.g. picosecond & femtosecond laser) are of great practical importance in the sense that they completely minimise or eradicate the formation of such undesirable features without any heat-affected zone (HAZ). Ultrafast lasers are commercially available and although they have not been widely used in industrials applications, they are mainly restricted by low output power; however, they are starting to make a breakthrough [39].

The laser machine usually adopts the same machine slide configuration as a normal mechanical CNC machine tool. The motion accuracy is also less than 5 μm and the material removal rate depends on the laser source, laser power and material absorbability. The machining spot size depends on the convex mirror in the associated in laser system. The diameter of the spot size is about 1 μm to 50 μm once depends on the laser source and lens configuration. The machined surface roughness varies from Ra 0.05 μm to Ra 0.5 μm.

2.2.4 EDM

Electrical discharge machining (EDM) is a non-traditional method of removing metal using a series of rapidly recurring electrical discharges between an electrode and the workpiece in the presence of a dielectric fluid. Minute particles of metal or chips, generally in the form of hollow spheres, are removed by melting and vaporization and are washed away from the gap by the dielectric fluid which is continuously flushed

between the tool and the workpiece. The conductivity of the workpiece material is crucial for this process; however, the hardness of the material is not critical.

The machining volumes of most EDM machines are less than 200 mm×200 mm×150 mm because of a slow manufacturing process, especially for μ-EDM. Also EDM is only limited for manufacturing electric conductivity materials.

The motion accuracy of EDM is about 1 μm to 10 μm [40, 41] and material removal rate vary from 1.6×10^{-4} to 1.6×10^{-3} mm^3/s [42]. The electrode tool can be any shape and is usually fabricated using a CNC milling machine or grinding machine. The machined surface roughness is from Ra 0.01 μm to Ra 0.2 μm [16, 28-30].

2.2.5 Micro ultrasonic machining

Micro ultrasonic machining (MUSM) is a method derived from traditional ultrasonic machining in which a tool and free abrasives are employed. The tool is vibrated at ultrasonic frequency and drives the abrasive to create a brittle breakage on the work piece surface. In fact, the shape and the dimensions of the work piece depend on the tool. Since the material removal is based on brittle breakage, this method is appropriate for machining brittle materials such as glass, ceramics, silicon and graphite.

The machining volumes of MUSM are about 400 mm×300 mm×250 mm and the motion accuracy is about 5 μm to 10 μm. Its material removal rate is 10^{-2} to 10^{-1} mm^3/s [43]. A grinding wheel can be used in MUSM for the fabrication of hard materials. The grit size of grinding wheel influences the machine volume of surface finish and can achieve surface roughness from Ra of 0.01 μm to 3 μm [43].

2.2.6 Comparative summary

Table 2-1 shows the summary of a range of micro machining processes. The machining volumes of these processes are from around 300 mm×300 mm×150 mm and the motional accuracy is less than 5 micrometres and the material removal rate is between 10^{-5} to 10^{-1} mm^3/s. Micro milling, micro turning and ultrasonic processes are highly effective at removing materials. The shortcoming of the ultrasonic process is that its machining accuracy is more than 5 μm because ultrasonic head causes some vibration to

the workpiece. A micro grinding process is similar to an ultrasonic process but it is without vibrating head. In recent years, some of the multi functional machines which combined micro milling, micro turning and micro grinding processes into one machine were developed; however, these are not suited to the machining of advanced engineering materials, such as ceramics, Inconel 718 and titanium alloys. Other machining methods such as, laser machining or EDM, termed non-traditional machining processes, are very good at cutting brittle materials but have very low material removal rates.

In order to achieve a high machining efficiency and to implement the machining of advanced engineering materials in one machine tool, the, development of a hybrid machine which combines multifunctional mechanical machining processes and non traditional mechanical machining processes is essential. In non traditional mechanical machining processes, EDM is only suitable for machining electrical conductive materials. Laser machining can machine any kind of material and its variable spot size is very useful for deburring or pre-heating materials. Therefore, in this research laser machining is chosen for integration as a hybrid process with micro milling and micro grinding to evaluate their capability for fabrications of micro products and components.

Table 2-1 Comparative summary of micro machining processes

	Machining volume	Machining accuracy	Material removal rate	Tool size	Surface roughness (Ra)	Heat affected zone
Micro milling	300 mm 300 mm 150 mm	<5 μm	10^{-4} to 10^{-1} mm^3/s	0.01 to 3 mm	0.01 to 0.5 μm	N
Micro turning	ø300 mm 300 mm	<5 μm	10^{-4} to 10^{-1} mm^3/s	N/A	0.01 to 0.5 μm	N
Micro grinding	300 mm 300 mm 300 mm	<3 μm	10^{-5} to 10^{-4} mm^3/s	0.75 to 2.5 mm	0.01 to 0.2 μm	N
Micro laser machining	200 mm 200 mm 120 mm	<5 μm	N/A	1 to 50 μm	0.05 to 0.5 μm	Y
Micro EDM	200 mm 200 mm 150 mm	1 to 10 μm	1.6×10^{-4} to 1.6×10^{-3} mm^3/s	N/A	0.01 to 0.2 μm	Y
Micro ultrasonic	400 mm 300 mm 250 mm	5 to 10 μm	10^{-2} to 10^{-1} mm^3/s	N/A	0.01 to 3 μm	N

2.3 Machining process requirements for micro products

Most micro products have to be machined using more than one kind of high precision machining process. Typical micro products which have the potential to be fabricated using hybrid machining processes are presented in following section. Their requirements define the unique combination of hybrid processes used in this research

2.3.1 Micro fluidic devices

The fabrication of micro fluidic channels (shown in Figure 2-1) are strongly driven by the expanding biotechnology market with a demand for fast analytical processes for applications such as high-throughput screening, gene expression analysis and pharmacogenomics. Low cost and disposable micro fluidic devices are also made for disease diagnostic and chemical analysis [44].

These micro fluidic devices are usually made of PDMS (Polydimethylsiloxane) and PMMA (Polymethylmethacrylate) and the width of micro channels is restricted to within several micrometers to few hundred micrometers. Both good edge quality and fine surface roughness of the micro channel are crucial to produce laminar flow in the micro fluidic device [45].

Lithography, etching, laser processing and LIGA are traditionally used to fabricate these kinds of products [46, 47]. However, these machining methods are difficult to use for the manufacture three dimensional shaped channels required for the advanced functionality of some modern micro fluidic devices.

Micro injection moulding is a useful approach that suits the mass production of 3D micro fluidic devices [48]. The moulds are commonly manufactured by using micro milling process; however, this generates unwanted burrs on the mould. A mould can also be made with a micro channel having a width of 200 µm and a depth of 100 µm using a CNC machine although the micro milling process used generates micro burrs on the edges [48]; however, these burrs cause many problems such as component assembly difficulties, degraded functionality and even assembly operator injury [49, 50]. Within the micro injection mould, these unwanted burrs will be replicated onto the channel itself which in turn will cause turbulent flow on the injected part when it is being used. Therefore, an effective deburring process becomes a priority modern to achieve good edge quality and smooth surface roughness on precision moulds. In this case, a hybrid process which combines both micro milling and laser machining may be useful for the mass production of micro fluidic devices and associated channels. Such key knowledge gap in hybrid machining will be addressed in this study.

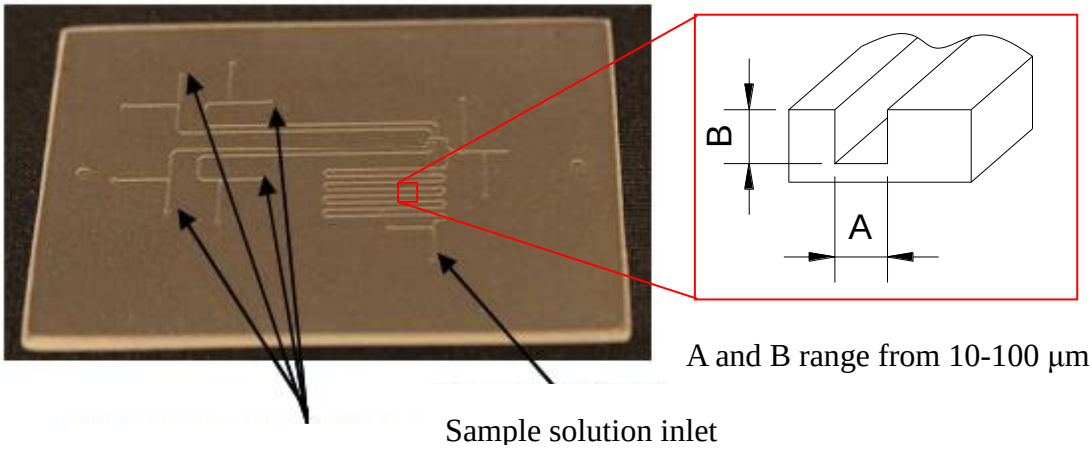

Figure 2-1 Micro fluidic channels [51]

2.3.2 Dentures

According to American Dental Association, there are approximately 113 million adults in USA missing at least one tooth. Most of these people use dentures, shown in Figure 2-2, in order to replace their missing teeth [52]. These dentures are made from either porcelain or ceramic which are both brittle materials and very difficult to be machined. Cracks and subsurface damage easily generated when CNC machining is used. However, it has been proved that thermal heating can change the brittle-ductile transition condition and hence improve machinability of brittle materials.

Laser assisted machining (LAM) uses a laser beam as a heat source to change a ceramic's deformation behaviour at brittle-ductile transition and can potentially reduce the machining force, increase machining efficiency and avoid cracks or subsurface damage on a brittle material. Therefore, a hybrid machining process which combines laser preheating and micro grinding and/or micro milling could potentially solve this problem. Currently, no such hybrid process exist; therefore, this gap will be fulfilled well by this study.

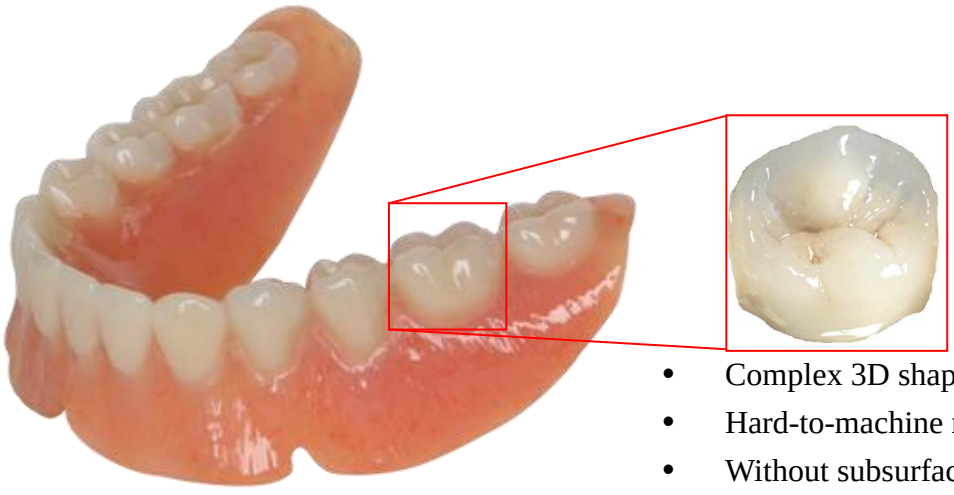

Figure 2-2 Denture in brittle material fabricated using grinding process [53]

2.3.3 Solar concentrators

The need for conserving energy and for developing energy alternatives has led to considerable research and development work in the domain of solar energy. This can be used directly in a variety of thermal applications such as heating water or air, drying, distillation and cooking. The other way in which solar energy can be used directly is through the photovoltaic effect in which it is converted into electrical energy. In order to achieve higher power generation, it is essential to produce good transparent surfaces on the solar concentrator as shown in Figure 2-3.

Solar concentrators are normally manufactured by using injection moulding or direct machining. None of these processes can avoid the appearance of micro cutting marks on the surface. These residual marks need to be removed because they can affect the light transmission through the concentrator. A mechanical polishing process can improve the concentrator surface finish and increase light transmittance; however, this is usually very time consuming. On the other hand, micro laser polishing is a developing technique which can rapidly remove cutting marks on the workpiece. Therefore, a novel hybrid process which combines micro machining and micro laser polishing is proposed to improve the machining surface finish of concentrators. Again, currently, no such a process exists and the gap in hybrid machining capability mentioned above will be explored.

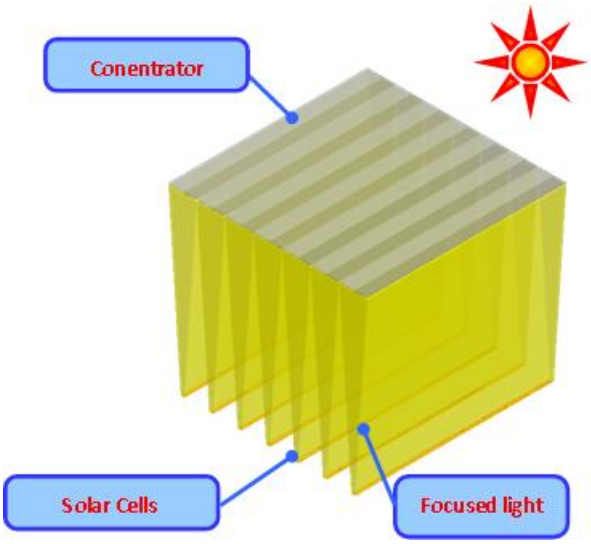

- Complex 3D shapes
- Surface roughness Ra < 300 nm

Figure 2-3 Illustration of the light focused by a concentrator

2.4 Benchmark precision machine tools for micro products

Commercially available high precision machines used for machining micro products are introduced in this section as benchmarks for the proposed hybrid micro machines. The purpose of this reviews is to highlight the current machines' capabilities, their processes and limitations; particularly with regard to contemporary hybrid commercial and research requirements.

2.4.1 The micro machining centre

2.4.1.1 Kugler's MICROMASTER® 5X

The Kugler MICROMASTER® 5X [54], shown in Figure 2-4, is an ultra precision milling CNC machine developed by Fraunhofer IPT in Aachen and Kugler Ltd. It is equipped with hydrostatic linear guides on a granite machine base. The strokes of the three linear axes (X, Y and Z) are 300 mm, 200 mm and 200 mm, respectively. High resolution linear scales are integrated into these axes. B and C axes are based on the work table and enable 5 axes milling to be carried out.

The powerful motion controller and the use of the optional tilt swivel unit expand the machine into a fully simultaneous five axis tool. This advantage offers the best qualification for the machining of 2.5D and 3D freeform surfaces at the highest quality. A pneumatic vibration insulation system is used to effectively suppress oscillations with frequencies above 5 Hz. Depending on the choice of machining spindles and tools, a

variety of non-ferrous metals, brittle and hard materials can be processed with high precision. The arbitrarily programmable CNC-control for process sequences and machining paths also enables the manufacture of microstructure and free-form surfaces with almost optical quality. The detailed specifications of Kugler MICROMASTER are shown in Table 2-2.

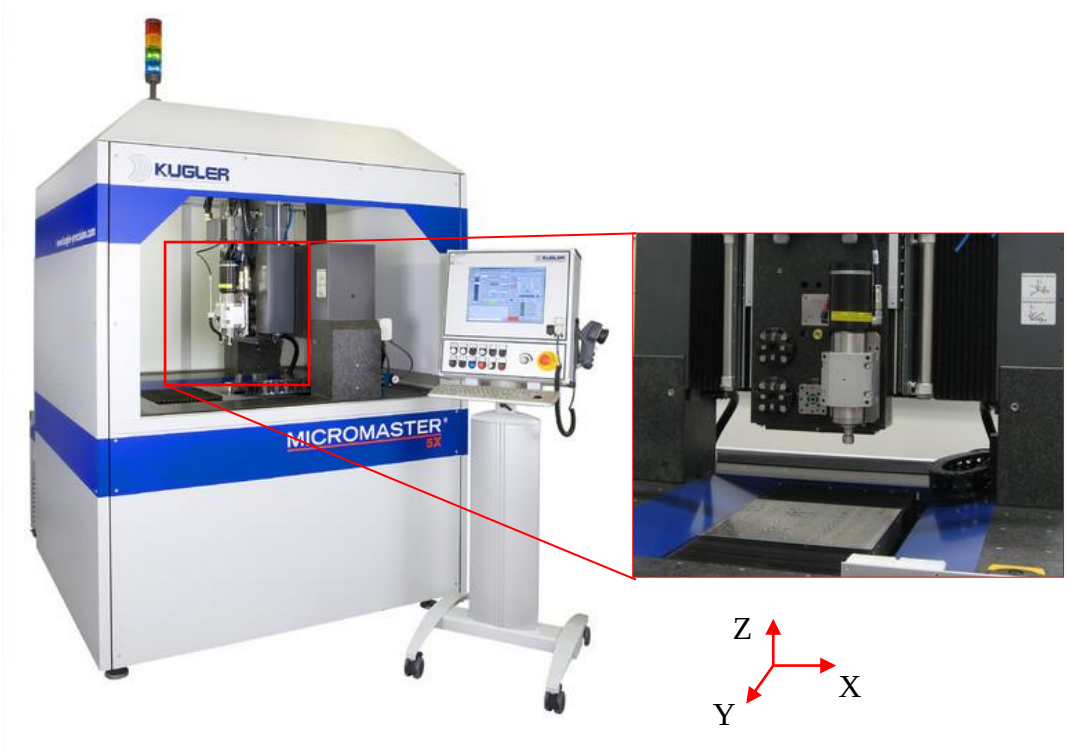

Figure 2-4 Kugler MICROMASTER® 5X [54]

2.4.1.2 Sodick's Ultra NANO 100

Sodick Co. Ltd. developed an ultra-high-precision machine named Ultra NANO 100 which is shown in Figure 2-5. The maximum travel distance for the linear axes (X, Y and Z) are 100 mm, 100 mm and 55 mm, respectively. The linear motional control resolution is 0.07 nm for these three axes. Two additional rotary axes (A axis: 180° and C axis: no limitation) enables turning operations as well as milling and grinding using rotating micro milling cutters and grinding wheels. The motion accuracy of this machine is less than 5 nm.

The combination of ceramic air bearings with linear motors eliminates contact portions from drive systems to realize a smooth, high-response without backlash and an ultra

high precision axial drive. The Ultra Nano 100 has been applied to the manufacture of dies for a wide variety of products such as diffraction gratings, light guide plates, spherical and non-spherical lenses and spherical/non-spherical micro-lens arrays. Table 2-2 shows more detailed specifications of Ultra NANO 100.

Figure 2-5 Ultra NANO 100 [55]

2.4.1.3 Precitech's Freeform 700

The Freeform 700, shown in Figure 2-6, is an ultra precision diamond machining system developed by Precitech Co Ltd. The X, Y and Z axes of travelling strokes on Freeform 700 are 350 mm, 150 mm and 250 mm, respectively. Optional B and C rotary axes are configured on the Freeform 700 which can run up to 5-axes motions. Its motional accuracy is about 300 nm thanks to oil hydrostatic bearings, linear motors and high resolution encoder. The machine has its own build-in metrology systems for form measurement [56].

The Freeform 700 is designed based on diamond turning machine which is capable of single point diamond turning, grinding and milling of spherical, aspheric and non-axes symmetric (freeform) optics, optical moulds and precision mechanical components. Moreover, the Precitech fast tool servo (FTS) is applied for the rapid manufacturing of

small departure (up to 1,000 μm) freeform components and micro-structures. It can also use slow tool servo (STS) to manufacture large departure freeform components. The FTS and STS systems on Freeform 700 have been used to machine micro prisms, lens arrays, torics (toric lens) and off-axis aspheres. The detailed specifications of Freeform 700 are shown in Table 2-2.

Figure 2-6 Freeform 700 [57]

2.4.1.4 Discussion on stand-alone micro milling/ turning machines

The specifications of the above micro milling/turning machines are summarized in Table 2-2. The common features of these include 5 axes, nanometre scale resolution, high accuracy, spindle speed, feedrate and large strokes on each axis. In recent years, 5-axis ultra-precision milling has attracted considerable interest because of its machining capability for the fabrication of three-dimensional small parts with complex shapes [58]. In order to fabricate high precision products, such as fly-eye mirrors [59], these machines have applied this design principle with high resolution and accuracy. In the Ultra-Nano 100, the control of the motion on the linear axes by a 0.07 nm is the state-of-the-art. However, these machines are very high cost and have low flexibility to fabricate micro-components which require different machining processes.

Table 2-2 Specifications of micro machining centres

	Micromaster ® 3/5X	UltraNano 100	Freeform 700
Axis	3 or 5 axes	5 axes	4 or 5 axes
Linear Motion Resolution	150 nm	0.07 nm	10 nm
Rotation Resolution	N/A	0.0000008°~ 0.0003°	0.0001°
Accuracy	< 500 nm	< 5 nm	<300 nm
Maximum Acceleration	10 m/s^2	N/A	N/A
Maximum Feed rate (mm/min)	6,000	3,000	1,500
Maximum Spindle Speed (RPM)	200,000	120,000	<5,000
Slide Travel	X 300 mm Y 300 mm Z 200 mm	X 100 mm Y 100 mm Z 55 mm	X 300 mm Y 150 mm Z 300 mm
Rotation Angle	360°	A 180° C 360°	360°
Processes	Milling	Milling/ Turning	Milling/Turning

2.4.2 The micro laser machine tool

2.4.2.1 Oxford Lasers' PicoLase 1000 system

Oxford Lasers' PicoLase 1000 system (shown in Figure 2-7) [60] features a picosecond laser system with 532 nm and 355 nm harmonics and 12-axis motion control system. This laser source developed by LUMERA Laser GmbH enables to machine virtually any materials with resolution of 5 μm. The system's special features include a dual beam line, automated trepanning systems and special micro milling routines for ablating complex structures. The system can be used for product miniaturization and provide a manufacturing platform for next generation of micro systems-based products.

Figure 2-7 Oxford Lasers' PicoLase 1000 [60]

2.4.2.2 EKSPLA's PL10100

PL10100 shown in Figure 2-8 [61] is an ultra short pulse picosecond laser machine tool developed by EKSPLA Company. It adopts a high repetition rate diode pumped laser, providing up to 100 kHz. Its advanced optical set-up ensures small, down to 5 μm laser beam spot size in combination with a relatively long 150 mm working distance. Laser machining trails using the PL10100 prove that it is close enough to industry requirements, due to its capability to directly machine a wide range of micron-scale features in almost all materials at relatively high speed.

Full automatic control of this machine makes it easy to use and its functionality is enhanced through open customizable software: the system can be made either flexibly adaptive. It possesses a class 1 laser safe and clear room compatible enclosure with a rigid

vibration isolated granite platform to ensure robustness and reliability. It is widely used to machine light-emitting diode (LCD) filter, silicon wafer, masker for organic light-emitting diode (OLED), PMMA for micro fluidic devices and glass with light guiding channels.

Figure 2-8 PL10100 [61]

2.4.2.3 Comparison of micro laser machines

Currently, most of micro laser systems are used only for drilling holes, grooving channels or any other features for 2.5D applications. The parameters of these two machines are summarized in Table 2-3. Using picosecond lasers, both can achieve a good surface finish and precision tolerance because the laser power is much less than a CO_2 equivalent. The wave length of the PicoLase 1000 is near ultraviolet so it can be used to cut transparent materials such as glass and plastics.

Table 2-3 Laser machine parameters

	PicoLase 1000	PL10100
Laser System	8 ps	10 ps
Mode	Nd:YVO_4	Nd:YVO_4
Wave Length	355 ~532 nm	1024 nm
Power	2.9 W	10 W
Machining Capacity	2.5D	2.5D
Accuracy	< 2 μm for X and Y axes < 10μm for Z axis	< 3 μm X, Y and Z axes
Slide Travel	X 600 mm Y 300 mm Z 100 mm	X 200 mm Y200 mm Z 100 mm

2.5 High precision multifunctional and hybrid machine tools

2.5.1 FANUC ROBONANO

FANUC Ltd. in Japan has commercialized a high precision machine named FANUC ROBONANOα-0iB (shown in Figure 2-9(a)) [62]. This multifunctional machine can work as a 5-axis milling, a turning, a 5-axis grinder, a 5-axis shaping machine and a high speed shaper. Figure 2-9(b), (c), (d) shows these operations. The turning operation is nominally accomplished by a single crystal diamond tool. For milling, an air turbine spindle is employed to provide a rotational speed up to 50,000 rpm. Shaping is performed using a high speed shuttle unit capable of producing three grooves per second and a 3 kHz fast tool servo using a PZT actuator. However, the various machining processes are required to change the different type of processing modules such as milling process requires to set milling module on the head. The resolution of the linear axes is 1 nm and 0.00001° for the rotational axes. The actual trace rate to NC command is ±2 nm at straight line and ±5/100,000 degrees at indexing.

(a) FANUC ROBONANOα-0iB

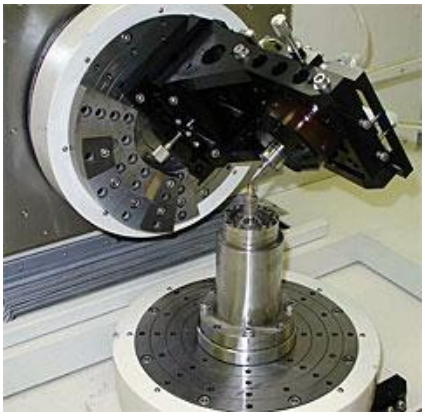

(b) Milling/ Grinding

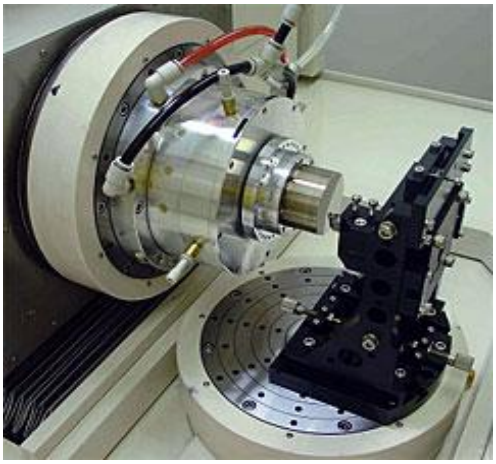

(c) Turning

(d) scribing

Figure 2-9 Ultra high precision machine FANUC Robonanoα-0iB [62]

2.5.2 AIST's hybrid machine

Currently, there are many universities, companies and research centres developing different kinds of hybrid machines. The advanced Industrial Science and Technology (AIST) in Japan has developed many different machining modules, such as milling, grinding, EDM and ECM processing, which can be interchanged on the machine head (shown in Figure 2-10) [63]. These modules can be changed manually in order to machine different products. Realignment of workpiece is unnecessary due to the component staying on the same machine but there are still some minor errors incurred from the need to manually change the processing modules.

Figure 2-10 AIST's first concept of hybrid machine [64]

2.5.3 Takashima Sangyo's desktop hybrid machine

Takashima Sangyo Co., Ltd. in Japan developed an new hybrid machine (shown in Figure 2-11) which is based on the concept of AIST's hybrid machine [65]. It is a desk top hybrid machine which integrates an one-touch head change system that can reduce manual changing module errors. There are five different modules including EDM, micro EDM, milling, micro milling and grinding. In 2004, the Advanced Manufacturing Research Institute and AIST developed a new concept desk top machine tool which combined laser and ECM [66]. These machines require only a desk size space to carry out all its processes. This desk top machine is very easy to move and place but the stiffness of the small size machine is not strong enough to avoid vibration.

Figure 2-11 Takashima's desk top hybrid machine [67]

2.5.4 MIRDC's hybrid machines

In 2010, Metal Industry Research and Development Centre (MIRDC) in Taiwan developed a hybrid machine which combines micro EDM, ECM and micro milling [68]. The main structures of the machine are made of natural granite to reduce thermal and vibration problems. The high precision, stiffness and stability in the moving stages and frames afford better performance of machining precision. A typical micro part manufactured through the machining processes on this machine are shown in Figure 2-12. Firstly micro EDM is used for rough process, then micro milling for a sharp edge and finally ECM for finished polishing. As this hybrid machines include EDM/ECM processes which require the conduction of electricity; therefore, it can only work on metals.

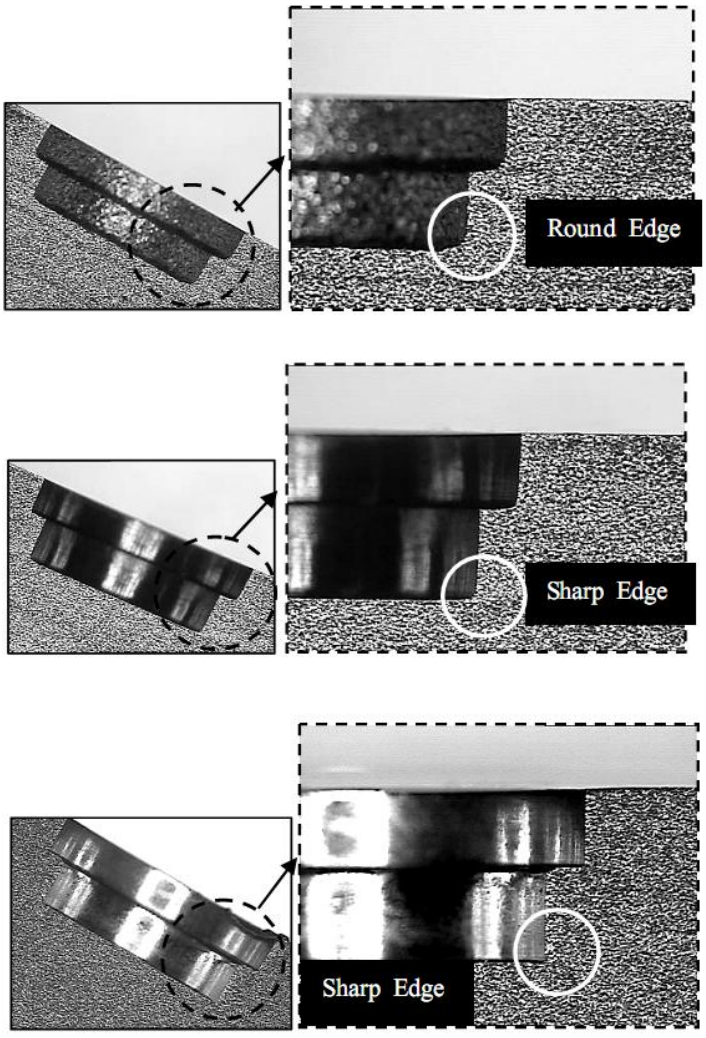

Figure 2-12 The micro parts polished using ECM process [68]

Shin et al. [69] combined laser and CNC processes in another MIRDC hybrid machine to fabricate a groove on linear guides. The laser machining process is very useful because the conventional processes are limited to fabricate hard brittle materials, such as ceramic, glass and tool steel. In this experiment, the milling process was used for manufacturing linear guides and the laser system for fabricating a micro pattern as shown in Figure 2-13.

In 2011, MIRDC developed a reconfigurable micro machining system with multiple machining modules which include a laser and a milling process as well as a measuring system [70]. In the experiment, laser machining is used to rapidly remove material, then the milling process is applied for the finish cut. This hybrid machine which incorporates a laser system on a CNC machine that can achieve high efficiency, high machining accuracy and is very cost effective; however, this high power laser causes heat affected zone (HAZ) on material.

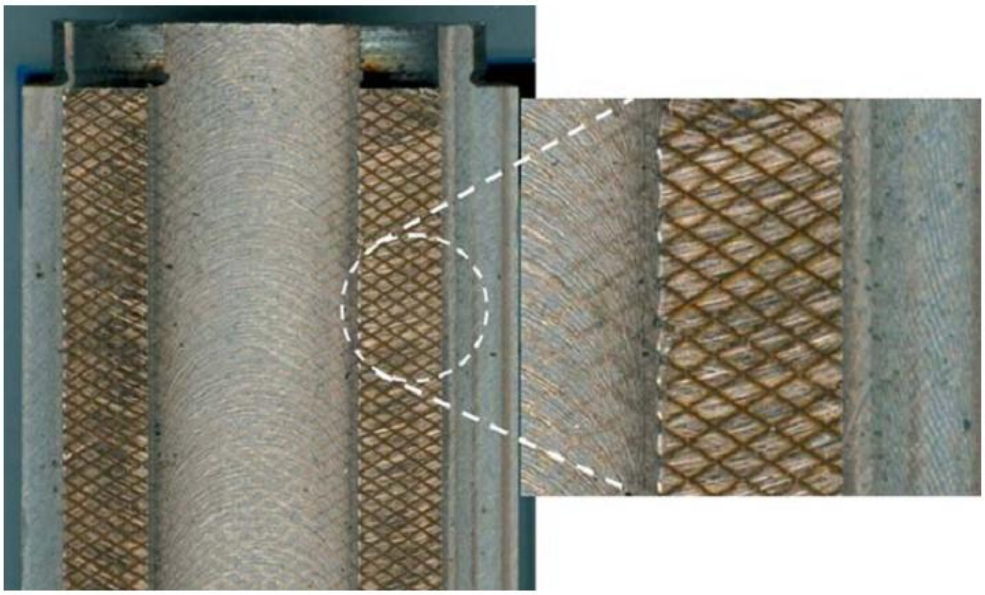

Figure 2-13 Cross-hatched pattern of lubrication groove using CNC milling and laser machining [69]

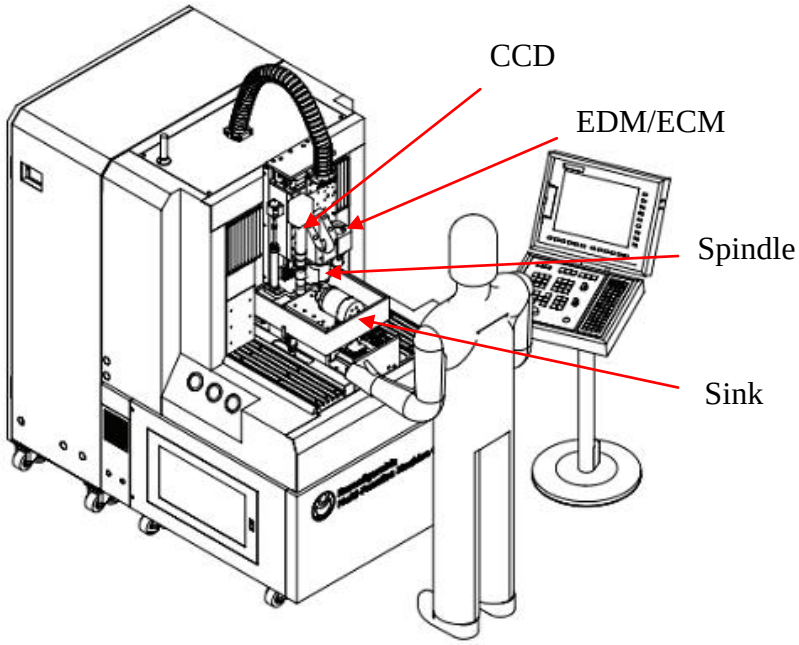

Figure 2-14 The reconfigurable machining centre with multiple machining modules [70]

2.5.5 MikroTools-DT110

The MikroTools-DT110 developed in Singapore, as shown in Figure 2-15 is a three axes hybrid machining centre which combines micro milling, turning, EDM, wire EDM, wire electrical discharge grinding (WEDG) and grinding processes on a single station. The travelling distances of X, Y and Z axes are 200 mm, 100 mm and 100 mm, respectively. The resolution and repeatability are only 0.1μm and 1 μm for each axis. The air bearing milling spindle has a maximum rotational speed of 200.000 rpm. A charge-coupled device (CCD) for on-machine inspection is also integrated into this machine. The hybrid machine can adopt turning to fabricate a shaft and then machine it to micro pin using wire EDM. These micro pins can machine micro holes on any conductive materials using EDM process. These multi task machining processes can be applied to many products which require micro holes; however, the EDM process is required to take place in a tank with non-conductive liquid. Machined products have to be uploaded from outside into the tank of the working table. It is likely that the parts need to be moved from one machine to the other.

Figure 2-15 MikroTool's multi-process hybrid micro machine [71]

2.5.6 Summary of multifunctional and hybrid machine tools

The specifications of the above multifunctional and hybrid machine tools are summarized in Table 2-4. The common machining process of these include milling, turning, grinding, EDM and ECM. Multifunctional machine, ROBONANO, can provide three traditional machining processes to manufacture parts with high precision and accuracy but these machining processes are not easy to fabricate hard-to-machine materials. These hybrid machines with EDM and ECM processes are used to manufacture hard-to-machine materials but they can only fabricate the products in metal. In recent years, MIRDC developed a hybrid machine which combine a high power laser for rough machining but this high temperature causes residual stress on workpiece. However, these 3 axes hybrid machines are very difficult to manufacture novel complex surfaces or products in industry.

Table 2-4 Specifications of multifunctional and hybrid machine tools

	FANUC ROBO-NANO	AIST's hybrid machine	Takashima Sangyo's desktop hybrid machine	MIRDC's hybrid machines	MikroTools-DT110
Processes	Milling Turning Grinding	Milling Grinding EDM ECM	Milling Grinding EDM	Milling Grinding EDM ECM +High power laser	Milling Turning EDM EDG
Axis	5 axes	3 axes	3 axes	3 axes	3 axes
Linear Motion Resolution	1 nm	0.1 μm	0.1 μm	0.1 μm	0.1 μm
Accuracy	4 nm	<10 μm	<4 μm	<2 μm	<4 μm
Maximum Spindle Speed (RPM)	50,000	60,000	80,000	60,000	200,000
Slide Travel	X 300 mm Y 300 mm Z 200 mm	N/A	X 200 mm Y 200 mm Z 110 mm	X 200 mm Y 200 mm Z 120 mm	X 200 mm Y 100 mm Z 100 mm
Feedrate (mm/min)	X 200 Z 200 Y50	N/A	12	1,000	N/A

2.6 Summary

According to this literature review, most micro products or compounds have to be machined using several machining operations. High precision machines, such as Kuler Micromaseter and Sodick Ultra nano 100, can provide one single process for machining parts with high precision and accuracy. With the increasing demand for high accuracy, surface finish, reduction in size and use of harder material properties for micro products, a stand-alone machine is not an ideal solution to meet the required specifications. Product setting from one machine to another also produces many problems. Realignment in the machining process is a basic problem which can cause errors and increases loading and inter-operation time. In recent years, many research groups have developed hybrid machines to fabricate micro parts in order to avoid alignment errors and workpiece re-setting times. The hybrid machine which combines micro milling, micro grinding and a laser machining system is very promising as it can fabricate products in various materials. It can also achieve high machining accuracy, efficiency and low machining time.

Chapter 3 A hybrid micro machining approach - micro milling and laser deburring

3.1 Introduction

Normally, lithography, etching, laser processing and LIGA are adopted to machine micro fluidic devices [46, 47]. These technologies are costly and time consuming. Moreover, they are restricted to machine 2D or 2.5D shape channels on micro fluidic devices. On the other hand, injection moulding is a very cost effective approach to fabricate micro fluidic devices. Due to the increasing complexity of the design and surface quality required for moulded micro products, the majority of micro injection moulds have to be manufactured through several operation processes, such as milling, turning, grinding, EDM, etc. Moving the workpiece around different stand-alone machine tools introduces machining errors due to workpiece repositioning and also increases lead times.

The development of hybrid machining centres will provide a promising machining solution at the micro level since it can integrate several operations in one machines. Micro milling is an efficient machining process to manufacture complex shape products. However, the burrs inevitably generated by the micro milling part of the process become problematic [48, 72, 73]. Any burrs on the edge of the channel will be replicated on the associated fabricated micro chip and may result in catastrophic turbulent flow within the micro fluidic devices. Therefore, a deburring process has to be carried out after micro milling. In this chapter, a hybrid machining process is to test the feasibility of machines a micro fluidic injection mould in one set up.

3.2 Review of available deburring processes

In recent years, several deburring methods have been developed [74]. DeLitzia and Ferrara [75, 76] used tumbling or vibratory finishing to remove materials from the confined edges of surfaces. Sonego [77] investigated to remove burrs by using electrochemical deburring methods. Micro electrical discharge machining (micro-EDM) using low discharge energy and a small-diameter cylindrical tool have also been used to remove micro burrs [78]. There are other methods for removing burrs on micro features, including abrasive jet machining [79], magnetic abrasive finishing [80] and ultrasonic machining [81]. However, these methods are limited to certain applications and have some shortcomings, such as damaging finished surface, changing properties of surface

material or damaging the edge material from the workpiece. In addition, these methods are either expensive or difficult to integrate onto a micro milling machine.

Lee [49] developed an effective way of deburring precision components by using a high power CO2 laser. Minimal material properties have been changed by a heat affected zone. Today, higher accurate and more powerful laser machines have been developed and used for micro machining, surface polishing, product marking and laser assisted processes.

3.3 Micro burrs generated in the micro milling process

3.3.1 Mechanics of the cutting process

Micro milling is a process of removing material with a sub micron depth of cut when feeding a workpiece onto a rotating tool where the cutting action of many teeth around the milling cutter produces a fast material removal method [21-23, 82]. Micro burrs are commonly observed after using micro machining processes, such as micro milling, micro turning and micro grinding, and are undesirable projections of ductile materials formed as the result of the plastic flow from cutting or shearing processes [83].

Four types of burrs are classified by Gillespie and Blotter [84], there are Poisson, rollover, tear and cut-off burrs. Rollover burrs and tear burrs as shown in Figure 3-1 are described as entrance/exit and top burrs respectively when produced by micro milling [85]. Micro milling often fails to produce smooth or well finished edges on parts due to these generated burrs [86, 87]. The Poisson burr is the result of a workpiece bulging to one side when it is compressed by a milling cutter causing permanent plastic deformation. Tear burrs appear when a chip is torn from the workpiece rather than shearing away [88].

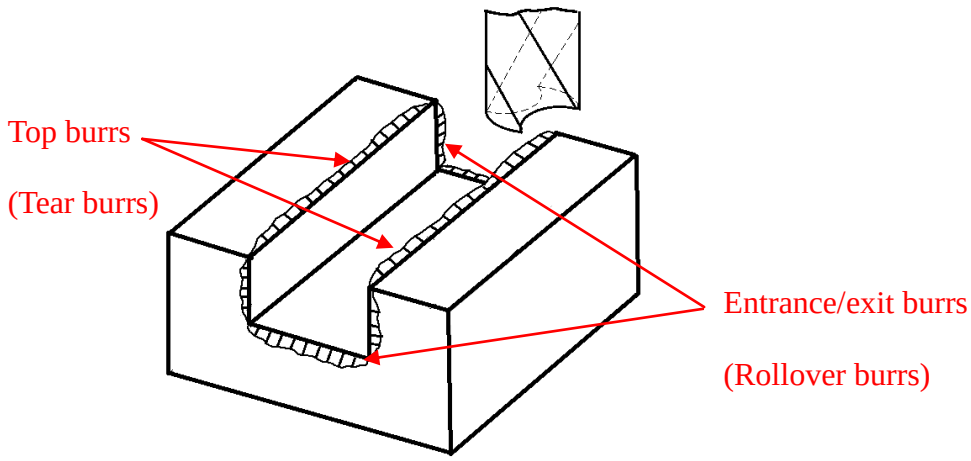

Figure 3-1 Examples of burr definition after micro milling

In recent years, many researchers have investigated the generation mechanisms associated with burrs and the influence of machining parameters on micro burrs [89, 90]. Fang and Liu [91] carried out both on experimental and theoretical study to minimize the generation of burrs in micro cutting. Although burrs can be minimized using optimized parameters, they cannot be completely avoided the generation [92].

3.3.2 Micro burr formation mechanism

The prediction of burr formation or fracture is required in order to remove unwanted burrs generated using micro milling. A 3D illustration of a micro groove fabrication on a workpiece by a micro milling process is shown in Figure 3-2(a). Micro burrs are generated on the edge of slot on the top surface of the workpiece. The 3D model of micro milling process at section A-A in Figure 3-2(a) can be simplified to a 2D model of a micro cutting process as shown in Figure 3-2(b). The burrs can be predicated using a burr formation model for the machining process [93]. In 2004, Ko and Dornfeld [94] improved the burr formation model for the oblique cutting process which is applied for different angles of cutting direction.

Both theoretical analyses and experimental studies show that the burr formation can be described in four steps (Figure 3-3) [95]. In the first step, the chip formed under the action of the cutting tools has a positive shear angle φ as shown in Figure 3-3(a). When the cutter is close to work edge, the primary shear zone is extended to the work edge. The shear angle φ reduces and then primary shear angle becomes negative as shown in Figure

3-3(b). While the negative shear angle is pushed towards the work edge by the cutting edge, the work material pivots as shown in Figure 3-3(c). In the final step, the cutter continues pushing the material and causes the chips to separate leaving a burr formation as shown in Figure 3-3 (d).

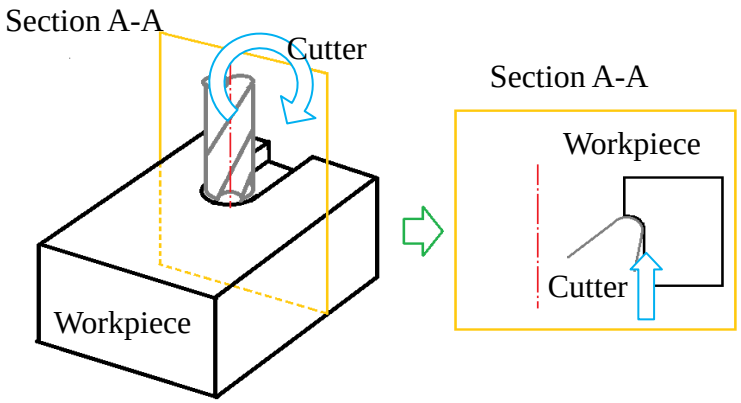

(a) 3D model process (b)Simplified model as a 2D process

Figure 3-2 Illustration of a micro milling process

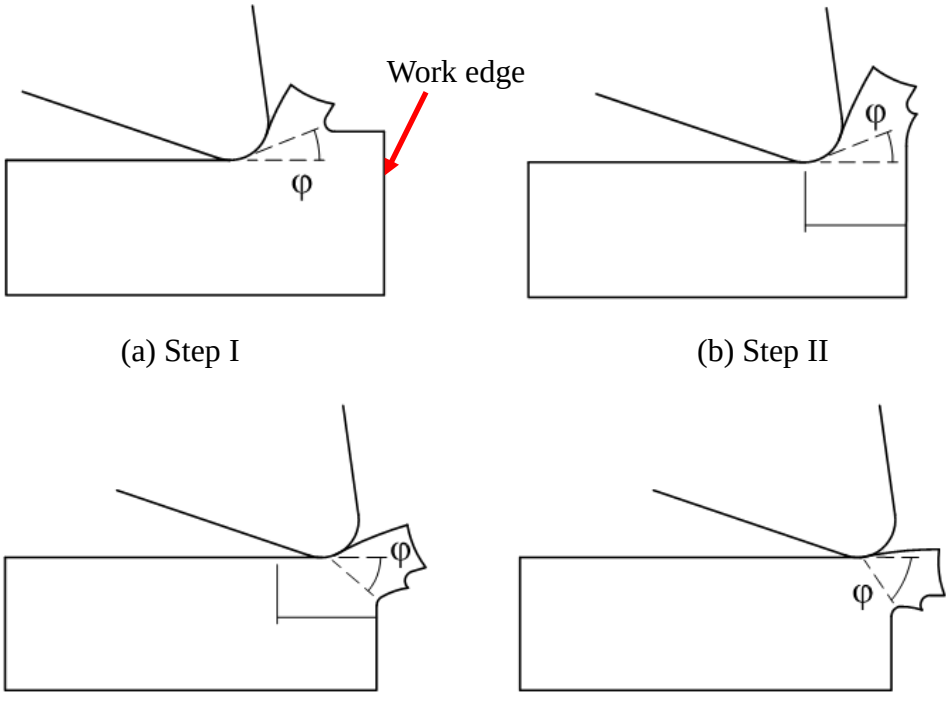

(a) Step I (b) Step II

(c) Step III (d) Step IV

Figure 3-3 The process of micro burr formation

In the machining process, the chip formation stops and burr formation begins at the transient point, A, as shown in Figure 3-4(a). The burr continues growing towards the end surface of the workpiece. As shown in Figure 3-4(b), the burr height and width can be used to geometrically characterize the final shape of the remaining burr on the workpiece. The burr height, h_f, can be calculated by using the following equation [94],

$$h_f = (t_0 + \omega \tan\beta)\sin(90° - \beta) \tag{3-1}$$

Where t_0, ω, β are undeformed chip thickness, the length from at the point of starting negative shear to the end of surface and initial negative shear angle, respectively.

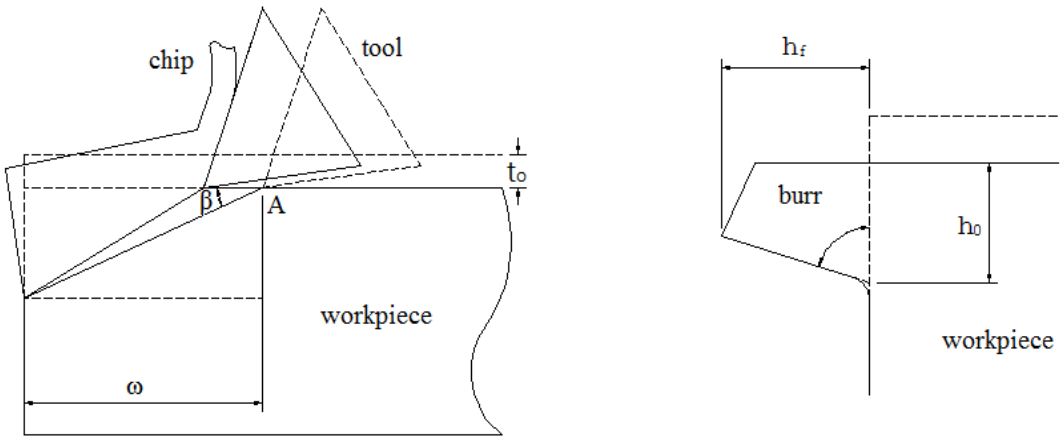

(a) Schematic illustration of initial burr (b)Representation of final burr geometry

Figure 3-4 Schematic illustration of initial and final burr formation

3.3.3 Finite element analysis of micro burr generation

According to Eq (3-1), the height of the burr depends on the length from the starting point of negative shear to the end of surface. Since the micro milling process is used in this experiment, the length of ω changes at the different positions. The initial negative shear angle, β, is caused by the flow stress of the material. Finite element analysis (FEA) software - Deform was used to simulate the formation of burrs. In Figure 3-5, the FEA and process of burrs generation formed a cutting tool is shown. The cutter assumed to be a rigid body and the workpiece material is NAK80. The Young's modulus and Poisson ratio are 200,000 kgf/mm^2 and 0.33, respectively. In the milling process, the spindle

speed is 25,000 rpm and the feedrate is 1300 mm/s in the cutting process. The FEA simulation shows the primary shear zone extended towards the work edge (Figure 3-5(b)). As the shear angle reduces and the primary shear angle become negative Figure 3-5(c). The burr is generated when the cutter continues pushing (shown in Figure 3-5(c)) and separates from the workpiece. The result shows the burr height is 10.5 μm while these parameters are used in milling NAK80.

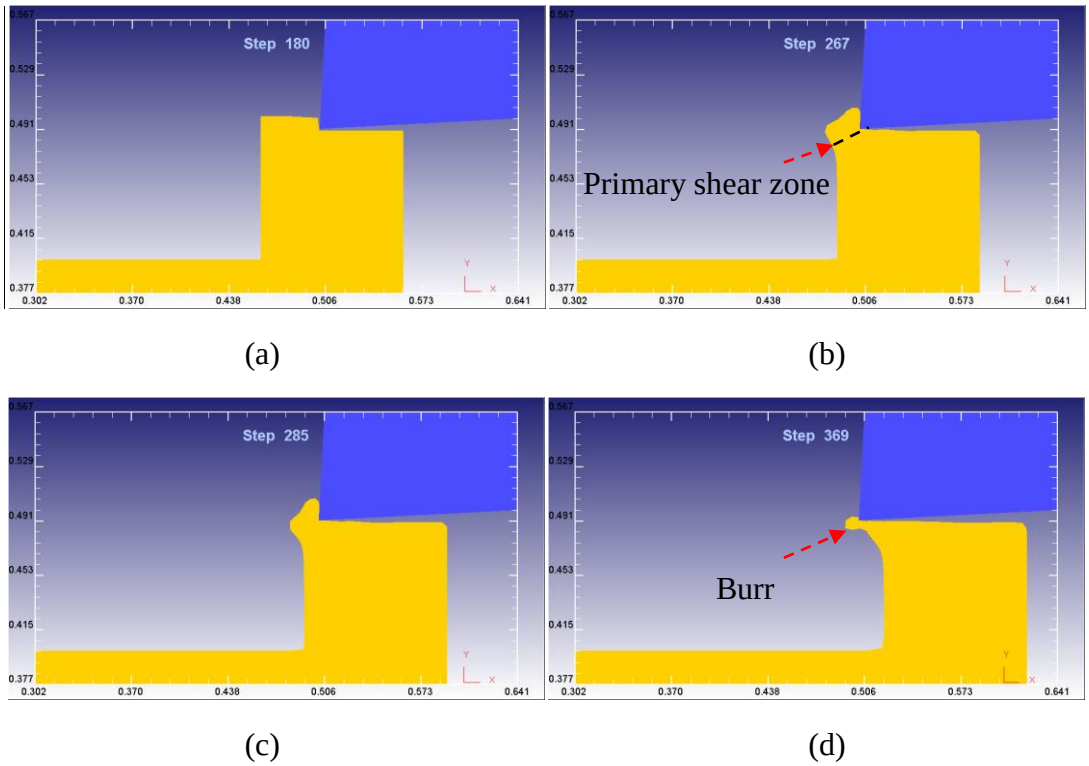

(a) (b)

(c) (d)

Figure 3-5 The simulation of burr generation using Deform

3.4 Laser deburring process

3.4.1 Deburring mechanisms

Removing burrs on the metal mould using laser radiation is a thermal process which can be illustrated in Figure 3-6. Firstly, the laser beam is focused on the target surface. The laser thermal energy is absorbed by the free electrons in the metal material during the interaction of laser pulse radiation. After that, the thermal energy will be transferred from the electrons to the lattices of the metal materials by thermal conductivity but some energy will disappear by thermal diffusion. The thermal energy produced is then used to melt or break the metal to cause removal of burrs from the metal mould. The advantage of laser deburring is that it is suitable for machining hard materials, especially the

materials with low thermal diffusivity and conductivity. The effectiveness of the laser deburring process depends on the thermal properties and optical properties of the material rather than its mechanical properties [96].

In the past, substantial research has been performed to predict the cutting shapes attainable by analyzing the laser properties. In 1977, Glass [97] had developed a model of numerically derived temperature and thermal stress fields to calculate proper material removal during a laser deburring glass experiment. The energy loss and temperature in the material were predicted in the deburring experiment. Rajaram and Coyle [98] investigated the depths and widths of the heat affected zone in laser material processing. Smith et. al. [99] used laser machining experiments to determine the influence of workpiece thickness, spot size, cutting speed and laser power on aluminium oxide. In a thermal analysis for laser heating and melting materials, Cline and Anthony [100] related the temperature distribution, cooling rate distribution and depth of melting to the laser spot size, velocity and power level. In this chapter, the laser cutting depth and other parameters, such as laser energy, density and laser power, are regarded as primary factors which can influence the laser deburring process.

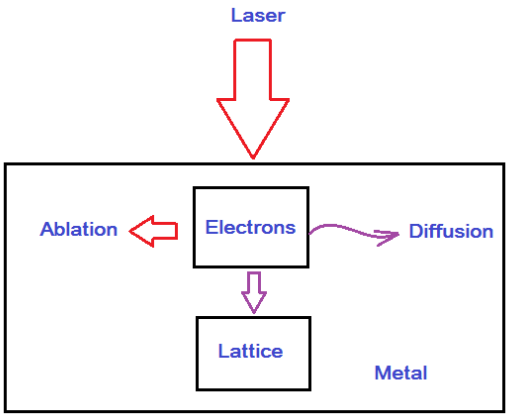

Figure 3-6 Schematic illustration of laser metal interactions during laser deburring process

3.4.2 Laser deburring process temperature model for the laser deburring process

Laser energy density and laser power are two critical laser machining parameters for obtaining high quality model during the laser deburring process. They can be calculated

through a two temperature model (TTM) [101] in which the metal electrons and metal lattices shown in Figure 3-6 are treated as two separate heat baths with temperature T_e and T_l respectively. The diffusion equation between the metal electrons and the metal lattices can be described as:

$$C_e \frac{\partial T_e}{\partial t} = -\frac{\partial Q(z)}{\partial z} - \gamma\left(T_e - T_l\right) + S \tag{3-2}$$

$$C_l \frac{\partial T_l}{\partial t} = \gamma\left(T_e - T_l\right) \tag{3-3}$$

where C_e, C_l, S and z are the capacities of the metal electron, the metal lattice, the absorbed energy in material and the ablation rate to the target surface, respectively. $Q(z)$ is the electron heat flux and can be calculated by:

$$Q(z) = -k_e \partial T_e / \partial z \tag{3-4}$$

where k_e is the metal electron thermal conductivity. As a nanosecond laser source is used in this research, the metal electrons and metal lattices are in a thermal equilibrium state, i.e. $T_e = T_l$. Therefore, equation (3-2) can be simplified as [101]:

$$C_e \frac{\partial T_e}{\partial t} - \frac{ke\,\partial T_e / \partial z}{\partial z} = S \tag{3-5}$$

After integration, the absorbed energy S in equation (3-5) can be expressed as:

$$S = I_{(t)} A_b \alpha e^{-\alpha z} \tag{3-6}$$

where $I_{(t)}$ is the laser intensity. A_b and α are the surface transmissivity and optical penetration depth, respectively.

The temperature of the metal electrons can be described as integration by an Eq (3-2):

$$T_e = \left[\frac{2It_{(t)} At\alpha e^{-\alpha z}}{\dot{C}_e}\right]^{\frac{1}{2}} \tag{3-7}$$

The temperature of the metal lattice can be simplified as $T_i \approx T_e t/C_i$. The temperature of the metal lattice can also be determined by the average cooling time of the electrons ($t = C'_e T_e/2$), so it can be described as [101]:

$$T_i \approx T_e^2 \frac{C'_e}{2C_i} \approx \frac{F\alpha}{C_i} e^{-\alpha z} \tag{3-8}$$

where F is the laser energy density. The ablation threshold, $F_0 \approx T_l C_l/\alpha$ can be described by the Arrhenius- type equation. Equation (3-8) can be written as:

$$F \approx F_0 e^{-\alpha z} \tag{3-9}$$

The ablation threshold and the optical penetration depth are the metal material parameters. The ablation rate can be assumed to be equal to the height of burrs to be removed per pulse. Therefore, the energy density can be obtained through Eq (3-9).

According to the definition of the energy density, the power of the laser system (P) to be used in the laser deburring process can be obtained as:

$$P = F \cdot F_r \cdot A \tag{3-10}$$

where F_r and A are the laser frequency and area of the laser spot, respectively.

3.4.3 Laser deburring trials

In order to validate the predicted relationship between laser depth and laser power, a piece of un-machining NAK80 material was tested using different laser powers before deburring. Each different parameters were tested three samples. The parameters of the optical penetration depth and the ablation threshold of NAK80 are 0.3 μm^{-1} and 2.5 J/cm^2 respectively [102, 103]. The energy density calculated by Equation (3-9) is 50 J/cm^2. A laser frequency of 15 kHz and a spot size of 20 µm diameter are used in this experiment. Four slots were manufactured by using laser power of 2.5, 2.52, 2.54 and 2.57 W, respectively. A comparison of the theoretical and experimental values shows the relationship between laser power and laser machining depth in Figure 3-7. This shows that the model can accurately predict laser machining depth because some errors from

material parameters and laser energy diffusion. There is only 0.2 μm difference at laser power of 2.5 W. The surface roughness was measured using a white light interferometer (Zygo New view 5000) and the results are shown in Figure 3-8. When the laser power was smaller than 2.54 W, the surface roughness (Ra) machined by using the laser was smaller than that achieved using a milling process. The best surface roughness in the experiment was achieved when using a 2.5 W laser power and setting the focus point of laser on the top surface of workpiece.

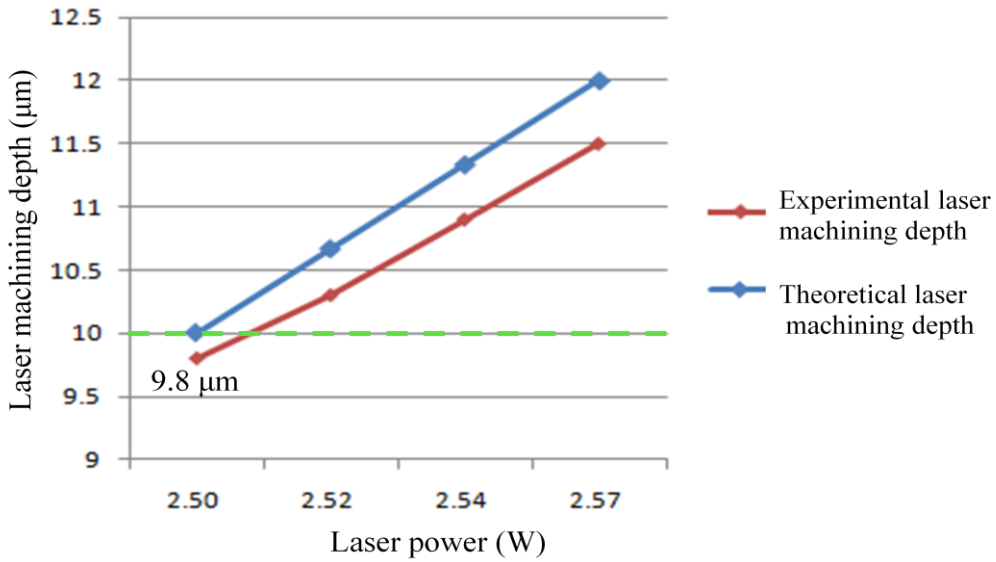

Figure 3-7 Relationship between laser power and laser machining depth

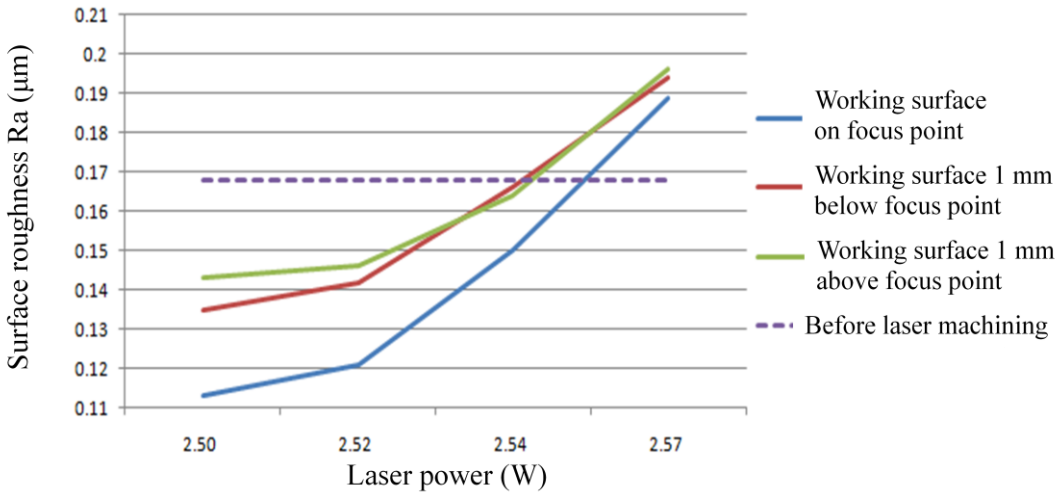

Figure 3-8 Machined surface roughness under difference laser power and laser focus points

3.5 Experimental study of the hybrid machining process and discussion

3.5.1 Fabrication of a micro injection mould by micro milling

In the experiment, a NAK80 black which is commonly used material for micro injection mould was fabricated by micro milling on a CNC machining centre Takang VMC-1020. To instead of the conventional spindle, the high speed spindle SF3060-ST32 was used in the experiment as shown in Figure 3-9. A metal carbide end mill with a diameter of 1 mm was chosen as the cutting tool. A spindle speed, a feedrate and a depth of cut of 25,000 rev/min, 100 mm/min and 0.5 mm were applied. After micro milling processes, the edge of the micro channel was observed under a SEM (FEI Quanta3D FEG). Figure 3-11 shows the maximum height of the burrs generated on the channel was approximate 10 μm.

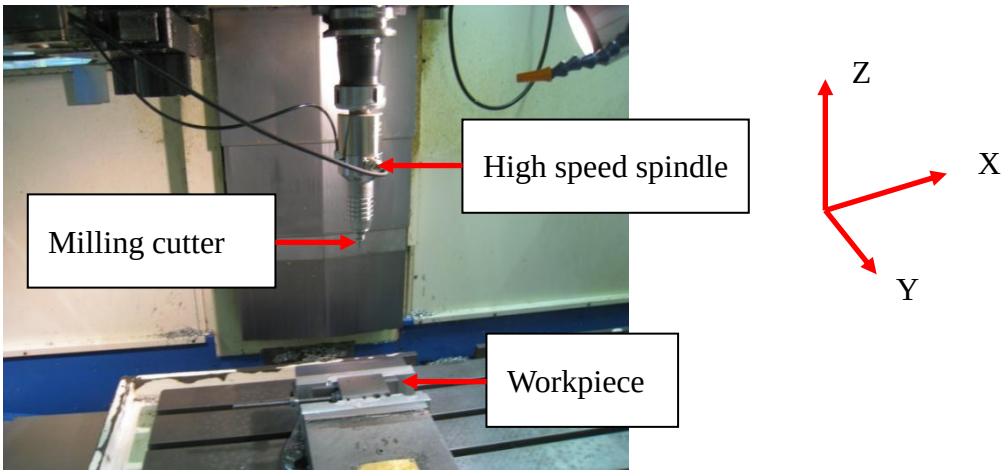

Figure 3-9 Setup for machining micro fluidic mould using a high speed spindle

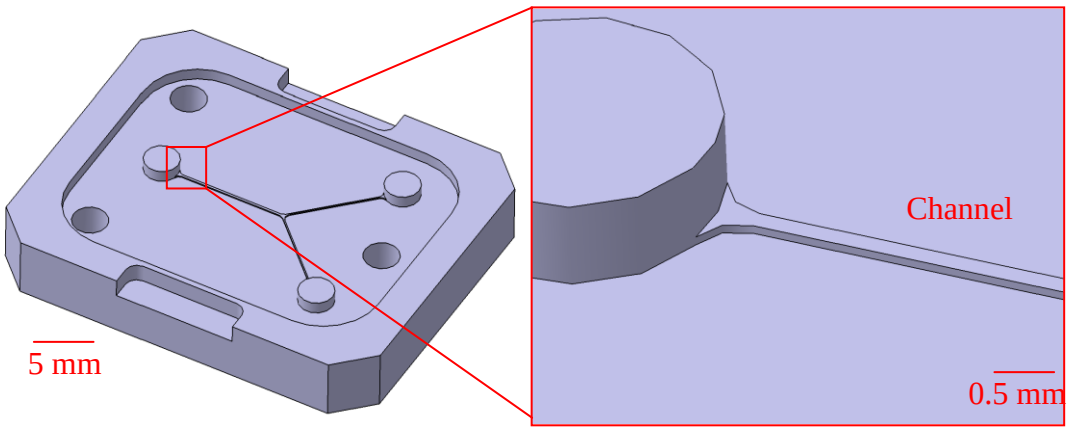

Figure 3-10 CAD model of micro channel and injection mould

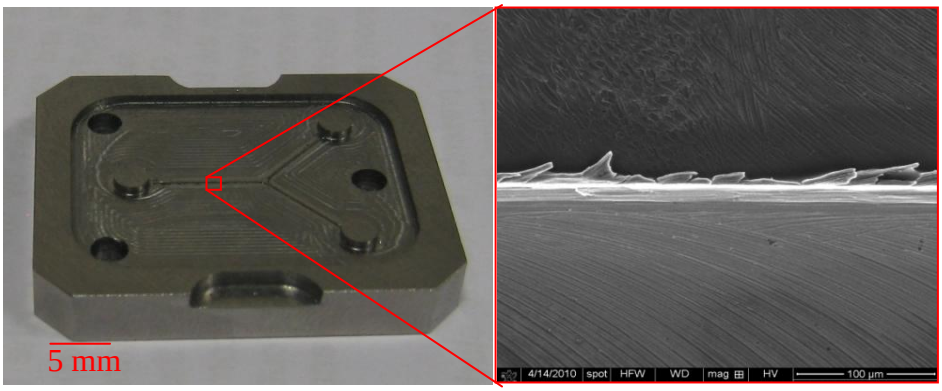

Figure 3-11 Measured burrs on the edge of the micro fluidic channels after micro milling

3.5.2 Laser deburring experiment

An Nd:YAG nanosecond laser machine was used in this experiment and its maximum power, wavelength, frequency, pulse duration time and the smallest spot size are 5 W, 355 nm, 15000 Hz, 65 ns and 20 µm, respectively. A schematic diagram of the laser system for deburring is shown in Figure 3-12. The workpiece was fixed on working table with motional resolution of 1 µm.

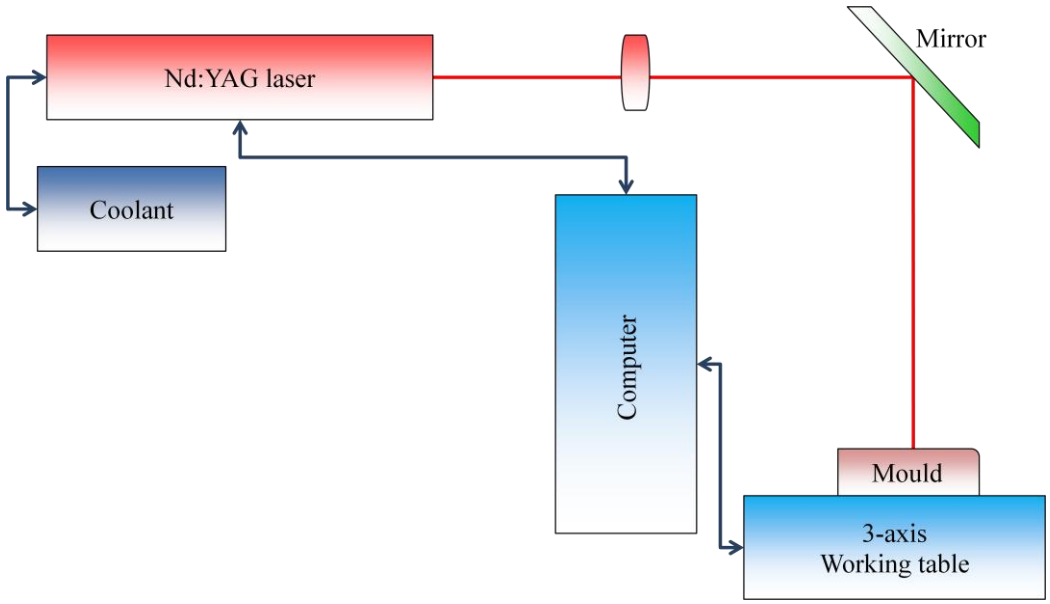

Figure 3-12 A schematic diagram of Nd:YAG laser deburring system

In the deburring process, the measured maximum height of burrs using a Form Talysurf was 10 µm (shown in Figure 3-13). According to chapter 3.4.3, the laser power, frequency and spot size were set up as 2.5 W, 15 kHz and 20 µm diameter, respectively.

The laser was focused on micro burrs and moved along the edge of the micro channels with a speed of 5 mm/min to remove burrs.

3.5.3 Results and discussions

Figure 3-14 shows a SEM image of an edge on the micro fluidic mould channel after the laser deburring process. It could be seen that the burrs generated in the micro milling process had been removed completely. Compared with Figure 3-13, the edge quality of the micro channels on the micro fluidic mould has been dramatically improved. The surfaces of the micro channels before and after laser deburring observed by the SEM are shown in Figure 3-15. It shows that there are some cracks generated on the machined surface after the micro milling process. However, after the laser deburring process the cracks had been removed. The surface roughness of the machined surface was also measured by the white light interferometer. The measurement results showed that the average surface roughness (Ra) of the machined surface had been reduced from 0.169 μm to 0.114 μm after the laser deburring process. Therefore, laser deburring process cannot only remove micro burrs on the micro fluidic channel but also improve the surface roughness on the top of channel.

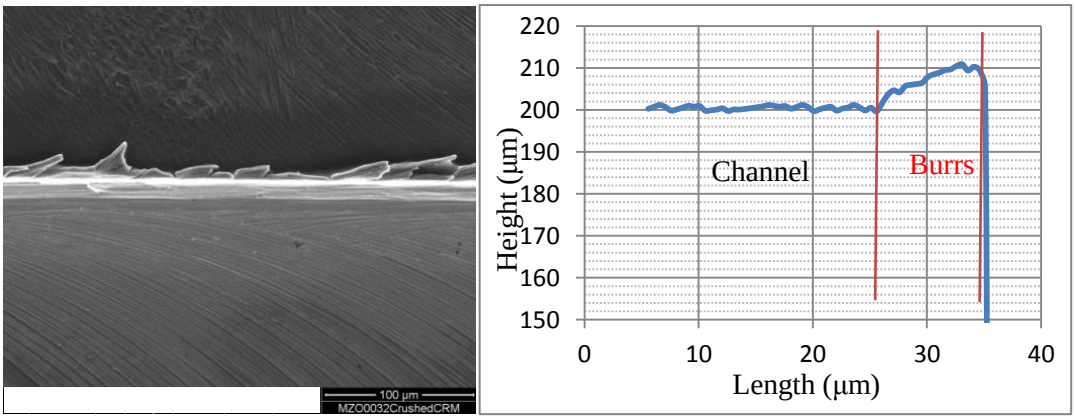

Figure 3-13 SEM image and cross section of the edge of the micro fluidic channel after micro milling

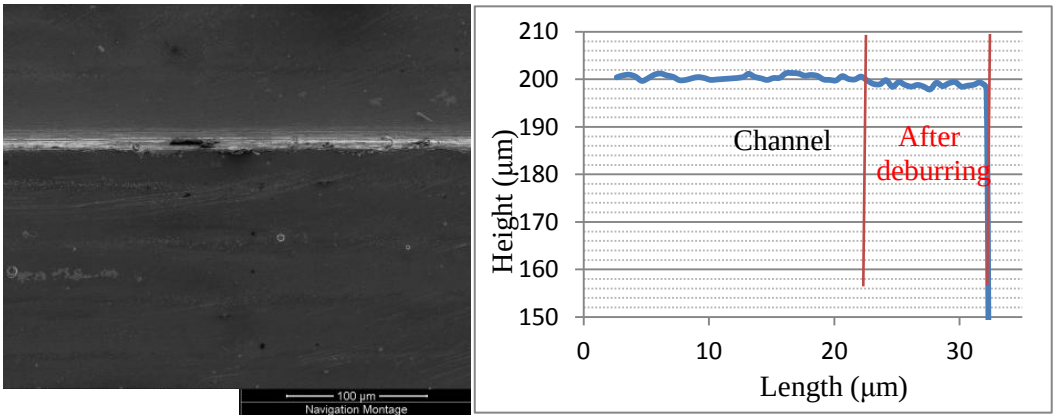

Figure 3-14 SEM image and cross section of the edge of the micro fluidic channel after laser deburring

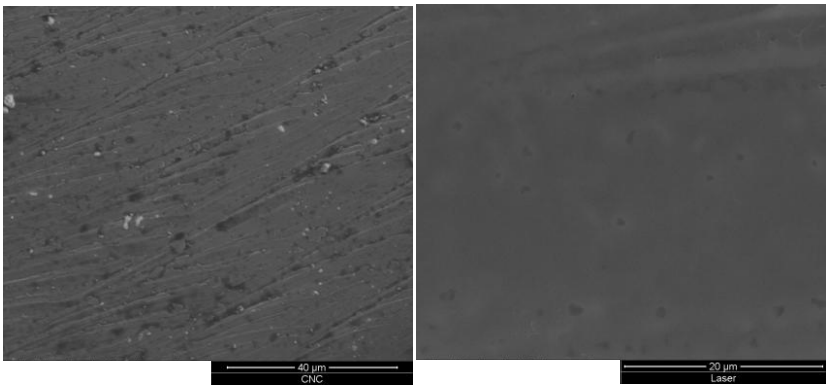

(a) After micro milling (b) after laser deburring

Figure 3-15 Machined surface topography after micro milling and laser deburring

3.6 Summary

In this chapter, a potential hybrid micro machining approach was developed to fabricate a micro fluidic injection mould. The micro fluidic channels, 100 µm (width) × 100 µm (depth), were micro milled using a high speed spindle with spindle speed of 25,000 rev/min and feedrate of 100 mm/min. The result in the finite element analysis shows that the burr height was 10.5 µm when NAK80 was adopted. It was very close to theoretical and experimental results. The burrs height can be calculated or simulated before micro milling process was applied. In this experiment, the micro burrs which inevitably formed at the channel edges during the micro milling process were completely removed by using an Nd:YAG nanosecond laser. The average surface roughness (Ra) of the machined surface was 0.169 µm but the surface roughness was improved down to 0.114 µm after laser deburring. Therefore, laser deburring process

cannot only remove micro burrs on the micro fluidic channel but also help to achieve good surface finish on the mould. The results demonstrated that high quality micro injection moulds can be obtained by applying this hybrid micromachining approach. This work justified the importance of development of a hybrid micro machining centre which can integrate micro milling and laser machining to obtain high quality micro products.

This flowchart of this hybrid micro machining approach, i.e. micro milling and laser deburring, is shown in Figure 3-16. An un-machined workpiece is setup in a hybrid machine. Then, the micro milling cutter which follows the path of NC-code is used to fabricate the 3D complex surface. Laser deburring process is applied for removing unwanted burrs on the edge. In the micro milling process, spindle speed, feedrate and depth of cut will have significant influence on the height of burrs. The laser parameters, such as laser power, frequency, wavelength and scanning speed are used to control the removal of such micro burrs. These parameters can be calculated using Equation (3-9) with material parameters, optical penetration depth and ablation threshold as inputs.

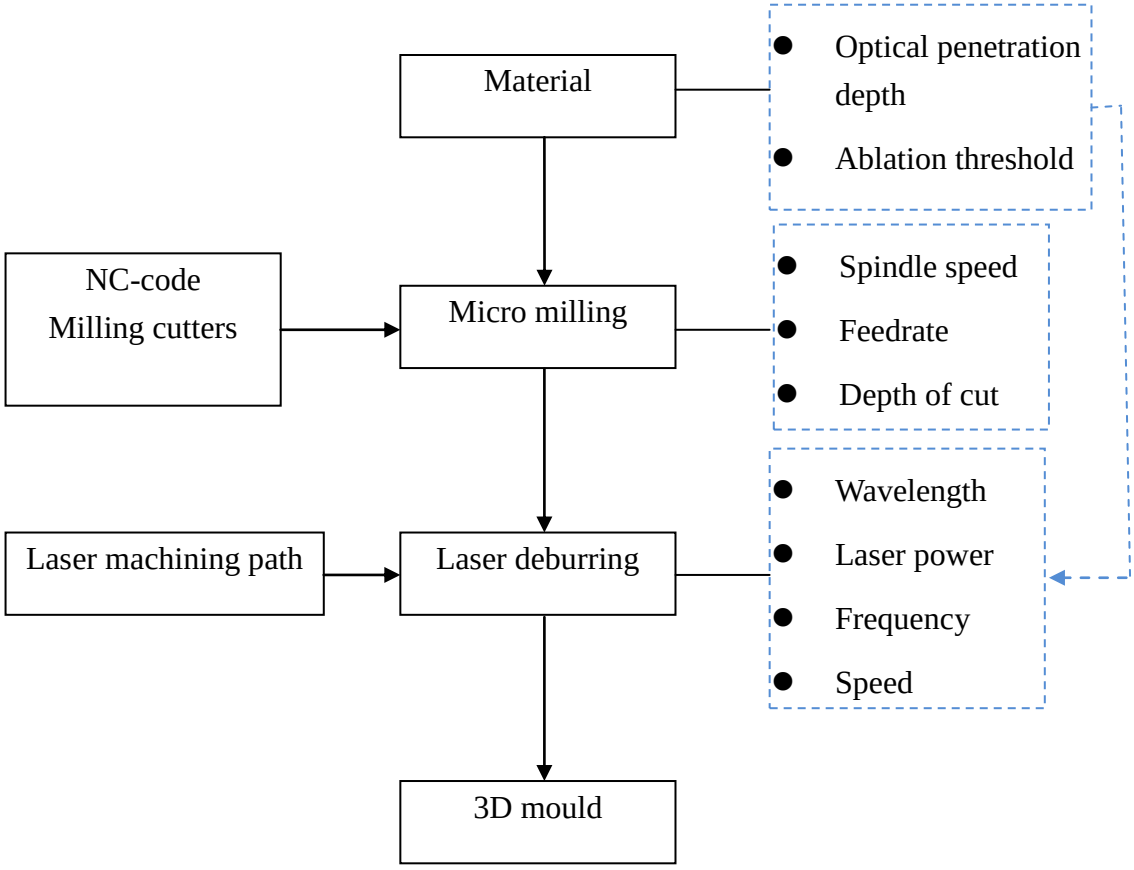

Figure 3-16 Flowchart of micro milling and laser deburring

Chapter 4 A hybrid micro machining approach - laser assisted micro grinding

4.1 Introduction

High strength materials, such as silicon nitride (Si_3N_4) and aluminium oxide (Al_2O_3), have been increasingly used to make precision products, such as bearings, tooth implants, cutting tools, artificial joints in aerospace, automotive engine and medical industries. Such materials offer high strength, thermal and chemical stability at elevated temperatures and good wear resistance [104].

However, these materials are ranked as hard-to-machine because of their high hardness and brittleness [8]. Currently, 95% of high strength material components are made using conventional machining approach such as diamond grinding, diamond milling and diamond turning. Diamond grinding is the most commonly used industrial machining method as it can achieve the required accuracy for ceramic products. However, it is a costly process due to low material removal rates and high diamond wheel wear rates. In addition, it causes subsurface damage on products which require a subsequent time consuming polishing process to remove.

Figure 4-1 shows variations of the tensile strength of different materials against temperature [105]. It shows that tensile strength significantly decreases when they are heated to higher temperatures. Bearing in mind, thermal heat treatment is a technique which can be used to soften a workpiece material by pre-heating it before machining [106-110]. Compared to other heat treatment methods, such as flame heating, plasma beam, friction resistance or induction, laser radiation offers a higher power density, a more precise focal point, power shaping capability and coherence [111, 112]. In recent years, research has indicated that laser assisted machining (LAM) is a promising technique for decreasing the cost, improving the efficiency and reducing the subsurface damage for machining hard-to-machine materials [113]. Heating using a laser to modify the deformation behaviour of ceramic can change its property from brittle to ductile. It can also reduce the yield strength of the ceramic to a value below the fracture strength, thereby eliminating melting or sublimation of the workpiece surface or destruction of the subsurface. [114-116].

This chapter presents an experimental study of a laser assisted micro grinding approach and a diode laser system has been integrated into a grinding machine as a test-bed for machining Si_3N_4 and Al_2O_3. The machining accuracy, grinding force, surface roughness, microstructure of machined surface and subsurface damage on the workpiece are discussed in this study.

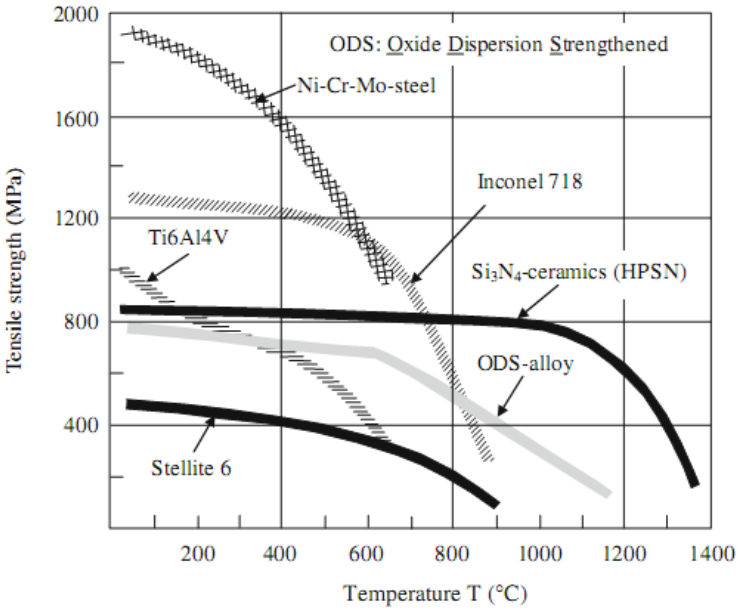

Figure 4-1 Effect of temperature on the ultimate tensile strength for various hard-to-machine materials [105]

4.2 Review of laser assisted turning and milling

Figure 4-2 illustrates the setup for laser assisted turning and laser assisted milling. Laser is used to preheat the workpiece immediately before the turning or milling operations. Many studies show laser assisted machining offers many machining advantages comparing to conventional machining processes [113]. Melkote and Shelton [7, 117] achieved high dimensional accuracy and good surface finish using a laser assisted micro milling approach. Some researchers have used laser assisted machining processes to fabricate hard-to-machine steels [7, 117-119]. It has been demonstrated that the cutting force can be reduced up to 64% during laser assisted micro milling 1018 steel and 6061-T6 aluminium [120]. Anderson summarized that the benefits of laser assisted machining are reductions of 25% in cutting energy, a 2-3 fold improvement in surface finish and an increase of 200% - 300% in tool life in compared to normal machining [118].

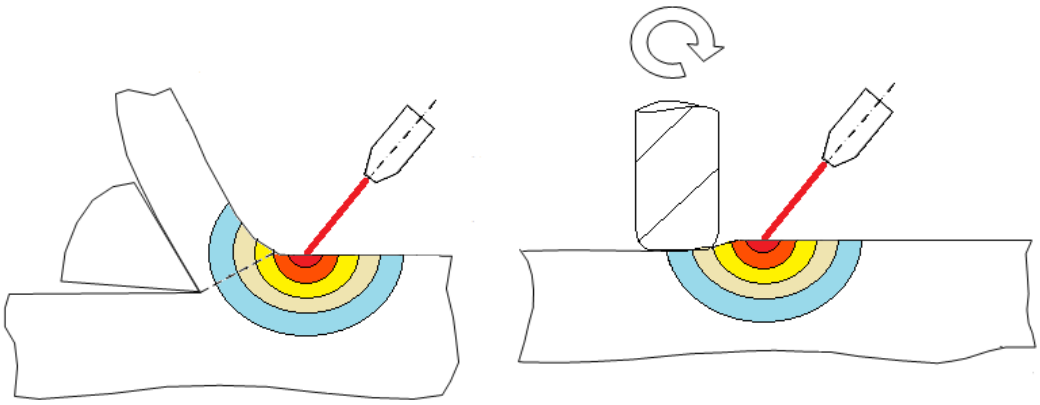

(a) Laser assisted turning (b) Laser assisted milling

Figure 4-2 Illustration of laser assisted machining

In recent years, much research has focused on the laser assisted machining ceramic materials. Yang and Lei [121] found that laser heating could improve the machinability of silicon nitride ceramics in terms of reduction of cutting force and workpiece edge chipping as well as increase of tool life. Brecher's research showed that laser assisted milling can obtain a much better surface finish than normal milling [122]. Singh and Melkote [123] investigated the influence of laser power, spot size, cutting speed and depth on cutting forces and dimensional accuracy when laser assisted turning is used to fabricate hard-to-machine materials. Kim et al. [124] also found that when the laser power increased, the cutting efficiency and tool life would all rise. Wang carried out laser assisted machining of Al_2O_3. In this study, the cutting force and tool wear were found to reduce 30 - 50% and 20 - 30%, respectively. The machined surface quality also improved when compared with conventional cutting. Although laser assisted milling/turning processes have been studied in the past, very limited work has been reported on laser assisted micro grinding [125].

Following this review, micro-groove machining experiments were conducted in order to understand the influence of the laser variables (laser power, beam location with respect to tool) and grinding parameters (depth of cut, cutting speed and tool width) on the cutting forces and dimensional accuracy of a machined part.

4.3 Laser assisted micro grinding

4.3.1 Laser source for laser assisted grinding

Si_3N_4 and Al_2O_3 are important ceramic materials which offer high temperature stability,

corrosion resistance and the toughness necessary for a wide range of applications [113]. The material properties of these are shown in Table 4-1. In this study, these two materials are heated using a laser since rising temperature of the workpiece should help to decrease material hardness. This technique is also used to increase the ductility and decrease the tensile strength and compression strength of the ceramics.

The absorption capacity Al_2O_3 under different wavelengths of laser is shown in Figure 4-3. The best absorption capacity is found to be at a wave length in the range 900 nm and 1200 nm. There is also 75% absorption capacity when a wavelength of 808 nm is used. A diode laser with a wavelength of 808 nm developed in Harbin Institute Technology (HIT) was used in this experiment. The relationship between the input current and output power is shown in Figure 4-4; its maximum output power is approximate 90 W.

Table 4-1 Material properties of Al_2O_3 and Si_3N_4

Material properties			Al_2O_3 (99%)	Si_3N_4 (hot pressed)
Physical Property	Density	g/cm^3	3.9	3.2
	Sinter Temperature	℃	1700	1800
Mechanical Property	Rockwell Hardness	HV	1700	1400
	Compression Intensity	Kgf/mm^2	30,000	23,000
	Elastic Modulus	GPa	375	310
Thermal Property	Maximum working temperature	℃	1,500	1,400
	Thermal expansion coefficient	/℃	8.0×10^{-6} (0-1,000℃)	4.0×10^{-6} (500-1,000℃)
	Thermal Conductivity	W/mK	35	30

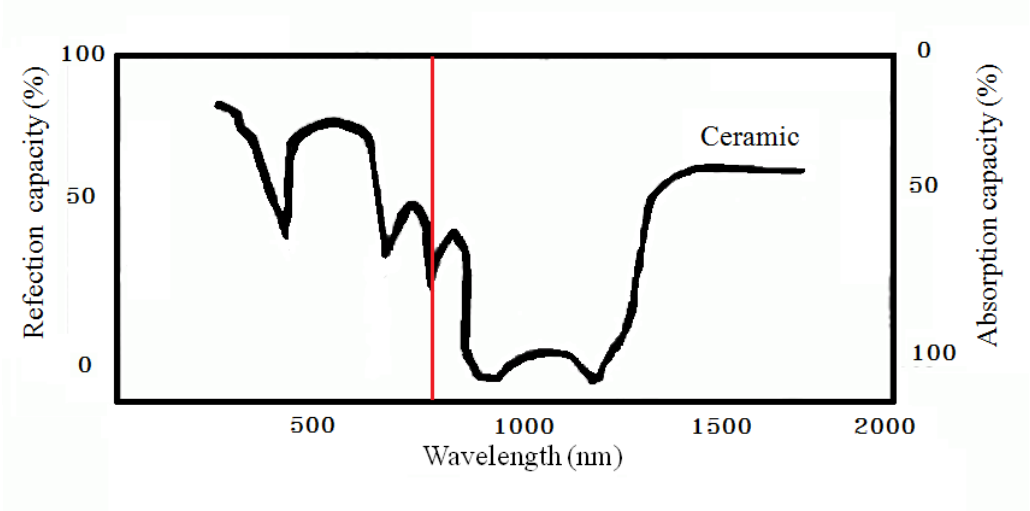

Figure 4-3 Absorption capacity of Al_2O_3 against wavelength [126]

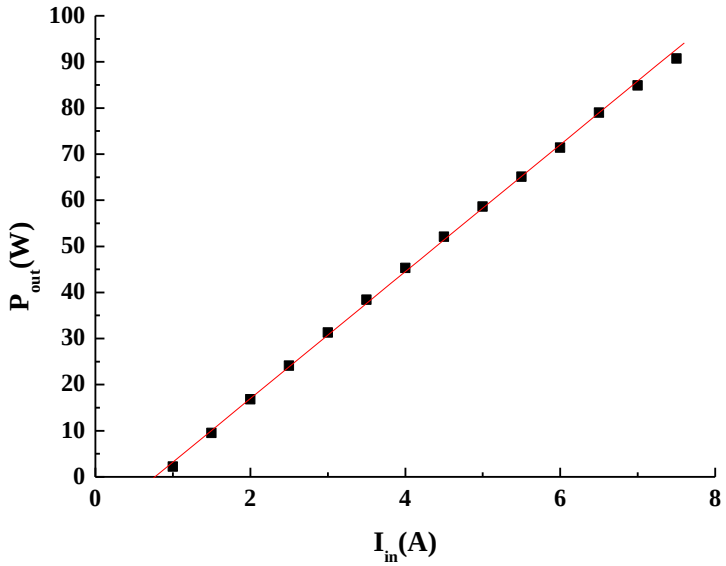

Figure 4-4 Relationship between current input and laser power output

4.3.2 Thermal conduction for laser heating

Many researchers have utilized laser heating to achieve temperatures of 850 - 950 ℃ in the micro milling/turning region [113-115]; however, the temperature decreases from the laser heating target surface to the micro machining region due to heat conduction.

The surface temperature heated by the laser machine can be calculated by Fourier's law. The heat conduction in an isotropic material assumes that the rate of heat transfer per unit area F_q is proportional to the thermal conductivity (k) and the temperature gradient in the direction of normal to an isothermal surface [127, 128]

$$F_q = -k\nabla T \tag{4-1}$$

where T is the temperature of the workpiece. This equation is sufficient for steady-state heat-transfer problems but laser applications seldom lead to steady-state situations. Therefore, the non steady-state heat conduction can be described as

$$\nabla^2 T = \frac{\rho c}{k}\frac{\partial T}{\partial t} - \frac{A_v I(x,y,z,t)}{k} \tag{4-2}$$

where ρ and c are the density and the specific heat of the workpiece, respectively. A_v is the fraction of the radiation energy absorbed to per unit volume of the workpiece and I is the Gaussian distribution of intensity. This equation allows for the evaluation of the temperature field not only during the laser pulse but also after the laser is switched off.

In a laser assisted grinding process, radiation and convection are not significant sources of heat loss and are therefore negligible. Carslaw and Jaeger have further improved the energy balance approach given in Eq. (4-2). The complete solution for the uniform, constant irradiance is:

$$T(z_c,t) = \frac{2I_o}{k}\left[\left(\frac{\kappa t}{\pi}\right)^{1/2} e^{\left(-z_c^2/4\kappa t\right)} - \frac{z_c}{2}\,erfc\,\frac{z_c}{\sqrt{4\kappa t}}\right] \tag{4-3}$$

where

$$\kappa = \frac{k}{\rho c} \tag{4-4}$$

$$erf(s) = \frac{2}{\sqrt{\pi}} \int_0^s e^{-x^2} dx \tag{4-5}$$

where $erf(s)$ is the error function and $erfc(s)$ is the complimentary error function or *1-erf(s)*. I_0 is the irradiance. κ is the thermal diffusivity of the workpiece and z_c is the depth coordinate radiated into the sample. Tables of the error function are available in most compilations of mathematical tables, such as Jahnke and Emde (1945). The surface temperature of the semi infinite solid is given by

$$T_s(0,t) = \frac{I_o}{\kappa}\left(\frac{4\kappa t}{\pi}\right)^{1/2} \tag{4-6}$$

Equation(4-6) thus shows the temperature rise is caused by releasing the heat (F_q) per unit area. Note that for very long heating durations ($t \to \infty$), the temperature increase on the surface, $T \sim \sqrt{t}$ would be unlimited. This is useful for estimating the time required to reach a specified surface temperature for a given laser irradiance.

The distance between the laser target and the micro grinding wheel is 10 mm and the temperature at the micro grinding wheel is 900 ℃. According to Eq (4-3) and (4-6), the temperature at the laser machining point is 1,000 ℃ on ceramics. In this experiment, both ceramics are heated to temperature 1,000 ℃ during the laser assisted micro grinding. Figure 4-5 shows the increase of temperature as a function of the laser current for Si_3N_4 and Al_2O_3. It can be seen that to reach a surface temperature of 1,000 ℃ on Si_3N_4 and Al_3O_4 are used, the laser current need to be set at 4 and 5.8 A, respectively.

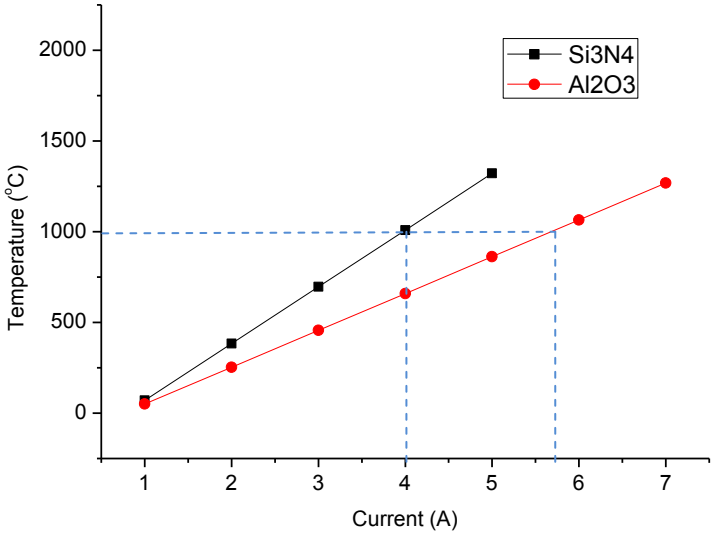

Figure 4-5 Increase of temperature under different laser current for Si_3N_4 and Al_2O_3

4.4 Laser assisted micro grinding trial

The experimental test-bed for laser assisted micro grinding approach is shown in Figure 4-6. A grinding machine (MUGK7120X5) is adopted as the host machine and consists of two servo motors on the X and Z axes and a linear motor on the Y axis. The specifications of the grinding machine are shown in Table 4-2. A high speed spindle (SF3060-ST32) with rotational speeds up to 60,000 rpm and laser focus lens were fixed onto the grinding machine. A 3 mm diameter grinding wheel with a grit size of 70 - 80 μm was used in the experiment. The thickness of diamond layer was 0.3 mm and the length 15 mm. The workpiece was fixed on a small vice which was mounted on a Kistler dynamometer (9256C). Si_3N_4 and Al_2O_3 were machined in this experiment.

A flow chart shown in Figure 4-7 explains the experimental process. According to Figure 4-4 and Figure 4-5, the diode laser power was set 45 and 70 W for Si_3N_4 and Al_3O_4, respectively. The wavelength of laser chosen was 808 nm due to the 75 % absorption on ceramic. After a few laser machining trials on the ceramics, a spot size of 3.2 mm and the focal point were found. In the experiment, a spindle speed of 5,000 - 15,000 rev/min, a feedrate of 8 - 20 mm/min and cutting depth of 1 to 5 μm were used in order to find the optimized machining parameters.

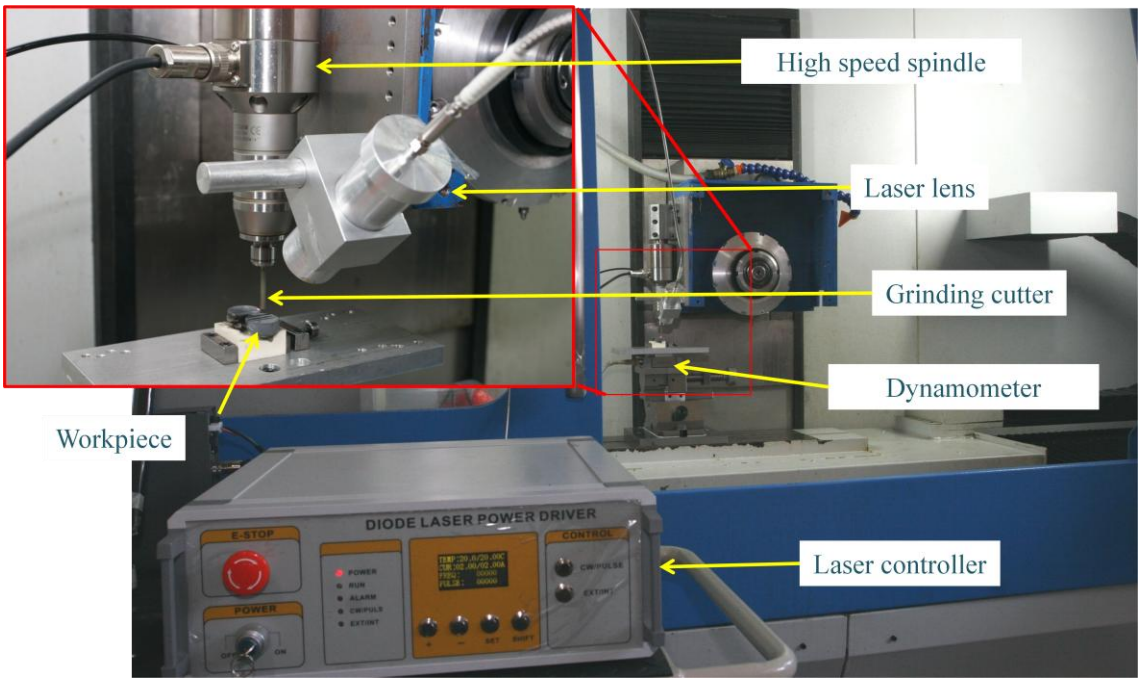

Figure 4-6 Experimental system of laser assisted grinding

Table 4-2 The specifications of conventional grinding machine in HIT

	Parameters
Travelling distance	650 mm × 230 mm × 250 mm
Table size	200 mm × 500 mm
Maximum feedrate of X axis	1500 mm/min
Feedrate range for Y axis	10-1500 mm/min
Feedrate range for Z axis	0.01-35 mm/min
Control resolution	0.1 μm
Controller	FANUC 18i-MB
Maximum weight on working table	82.4 Kg

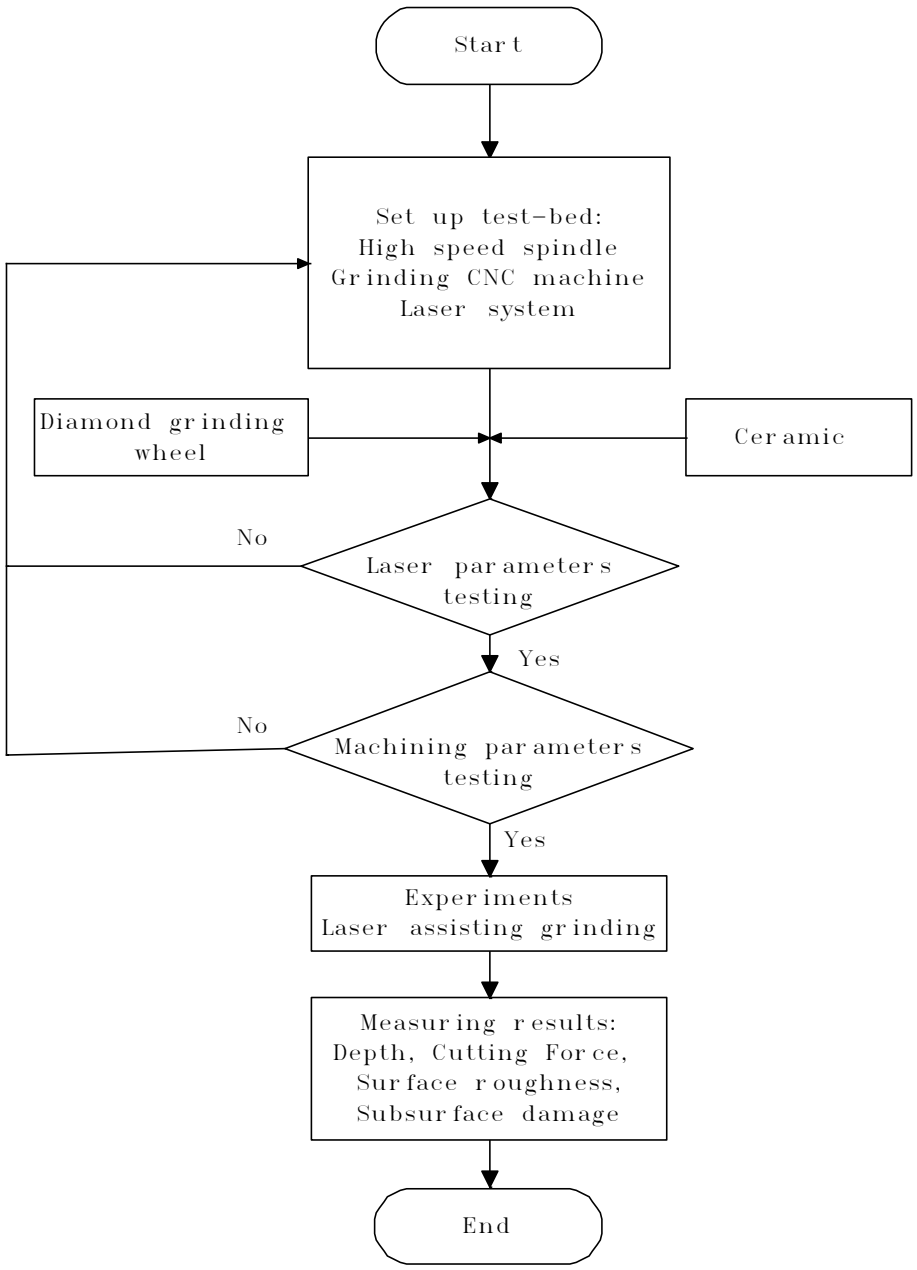

Figure 4-7 The flow chart for the laser assisted grinding experiment

In the experiments, three grooves were machined on each material. The first groove was fabricated by using the traditional grinding approach with a soluble oil coolant. The second groove was machined by using laser assisted grinding with an air coolant blowing on the grinding cutter. The last groove was manufactured using laser assisted grinding without applying any coolant. The spindle speed, feedrate and cutting depth were 10,000 rpm, 10 mm/min and 3 μm, respectively. The laser power was set to 45 W and 70 W on the Si_3N_4 and Al_2O_3. Three samples of each parameters were tested in this research.

4.5 Results and discussions

4.5.1 Groove depth

To assess the dimensional accuracy under different machining conditions, the groove depth was measured at 10 points along the machining direction by using a Form Talysurf (Taylor-Hobson Talysurf 4-120). The results for Si_3N_4 and Al_2O_3 are shown in Figure 4-8 and Figure 4-9, respectively, which indicate that the groove depth is relatively close to 3 μm. When a laser assisted process was used, the groove depth was grater then 3 μm due to thermal expansion of the workpiece. In addition, the thermal expansion of the tool during laser heating also affected the dimensional accuracy of the groove depth. The grinding depth manufactured by laser assisted grinding with air cooling was found to be between the cutting depth machined using the conventional grinding process and laser assisted process. The workpiece was heated by laser but the air coolant counteracted such a thermal effect and kept the temperature constant.

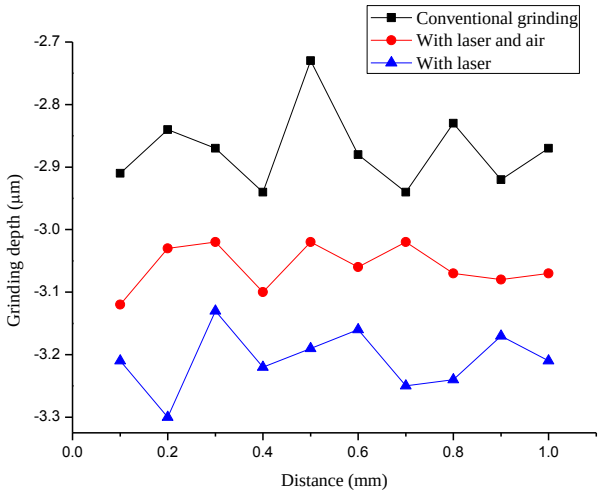

Figure 4-8 Measured groove depth for Si_3N_4

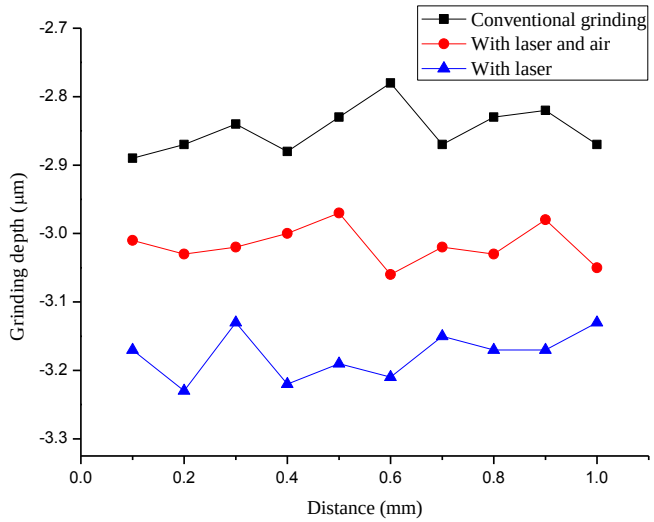

Figure 4-9 Measured groove depth for Al_2O_3

4.5.2 Grinding force

The grinding force on Si_3N_4 was measured using a Kistler dynamometer as shown in Figure 4-10. The grinding force obtained during the conventional grinding process was found to vary less than that obtained using laser assisted grinding. The grinding force for laser assisted grinding without an air coolant was very close to the conventional machining process, especially in the end of the grinding process. The largest grinding force was found when the laser was used with on air coolant with the grinding force varying greatly along the machining distance. This was because when the laser assisted grinding was used, the strength of material was decreased by the rise of the temperatures on the workpiece. Material with lower strength is much easier to be removed. However, the air coolant decreased temperature and the larger grinding force was presented. The average grinding force of conventional grinding process, with laser and with laser and air coolant were 3.51 N, 3.87 N and 9.54 N, respectively.

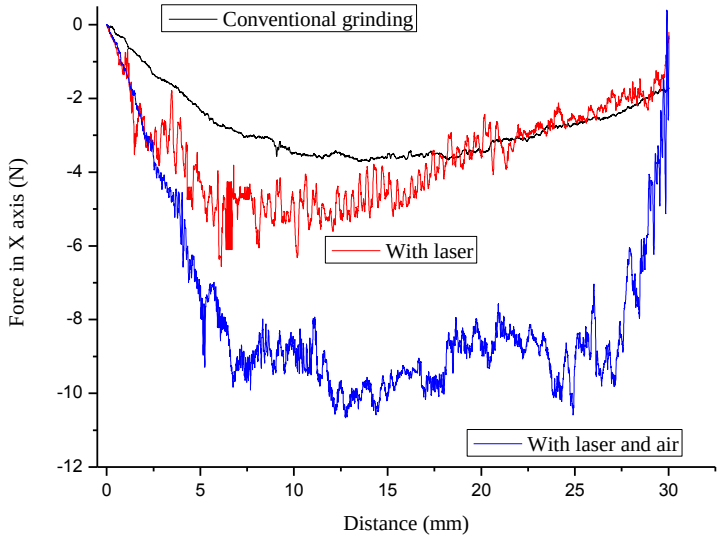

Figure 4-10 The grinding force against cutting distance

4.5.3 Surface roughness and microstructure of the machined surface

The surface roughness Ra on Si_3N_4 is shown in Table 4-3. They were measured by the Zygo white light interferometer and an AFM (DI NanoScope IIIa). The average surface roughness of conventional grinding, laser assisted grindings using air coolant and without using coolant were 202.594 nm, 334.599 nm and 139.923 nm, respectively. These two measured results showed that in terms of surface roughness, the quality of the machined surface can be greatly improved by the laser assisted grinding process.

The microstructure of the machined surface was measured by the AFM. The measured surface topographies are shown in Figure 4-11. and Figure 4-12. Large crests and troughs could be observed on the machined surface obtained using the conventional grinding process. However, a small grain size on the machined surface is observed in both Figure 4-11 (b) and Figure 4-12 (b) when laser assisted grinding was used. The microstructure of the machined surface on both materials showed that smooth surface crest and trough could be obtained when the laser assisted grinding processes was used.

Table 4-3 Surface roughness on Si_3N_4

Surface roughness	White light interferometer (Ra)			AFM (Ra)
Conventional grinding	182.543 nm	225.197 nm	200.041 nm	164.43 nm
Laser assisted grinding with air coolant	353.432 nm	317.939 nm	332.425 nm	294.32 nm
Laser assisted grinding	111.546 nm	173.448 nm	134.776 nm	112.85 nm

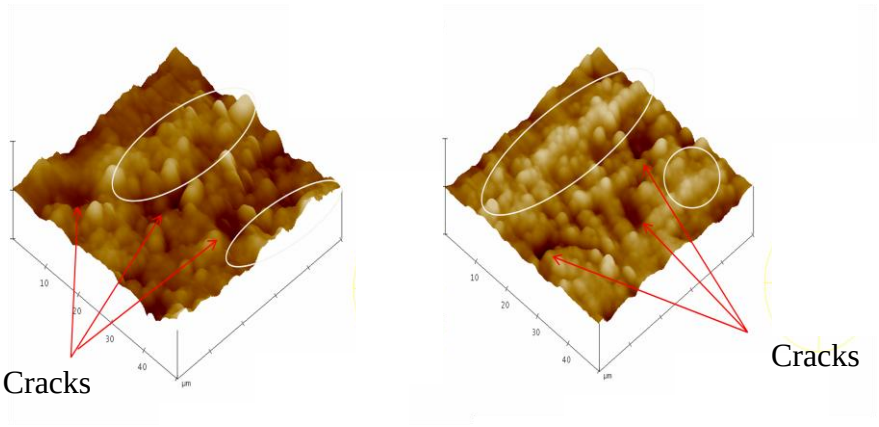

(a) Conventional grinding (b) Laser assisted grinding

Figure 4-11 The 3D structure of Si_3N_4 from AFM

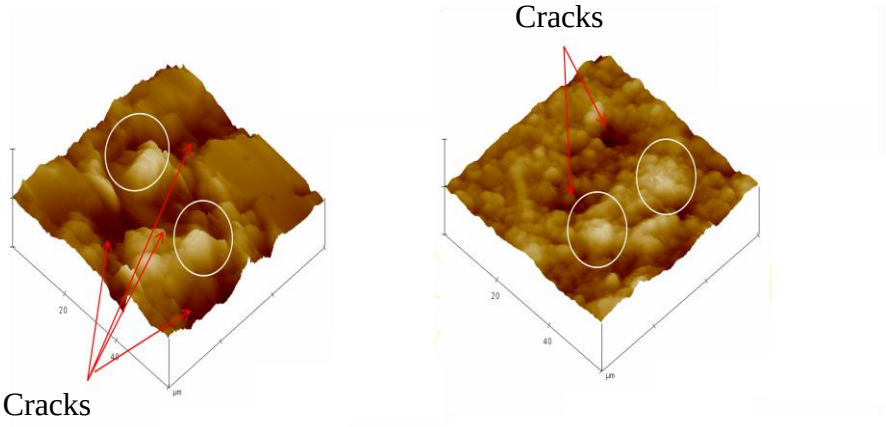

(a) Conventional grinding (b) Laser assisted grinding

Figure 4-12 The 3D structue of Al_2O_3 from AFM

4.5.4 Subsurface damage

The subsurface quality of the machined workpiece was also assessed in this study. The workpiece was coated with a 2 nm thick gold film on the top surface before testing for subsurface damage. The cross sections were obtained on a focused ion beam system (FEI Quanta 3D FEG) and observed using a SEM built inside the FIB system. In each test region, cross sections with dimensions of 5 μm×5 μm×5 μm were milled under a beam current of 7 nA. The subsurface damage on Si_3N_4 after conventional grinding is shown in Figure 4-13(a). It can be seen that the material was compressed and that some small cracks were observed on Si_3N_4 after the laser assisted grinding with air coolant was applied. As shown in Figure 4-14(a) the cracks were about 2 μm long on Al_2O_3 when conventional grinding was used. Some large cracks on Al_2O_3 were also seen when laser assisted grinding with air coolant was used. However, it was difficult to observe subsurface damage on both materials when laser assisted grinding process without using any coolant was used.

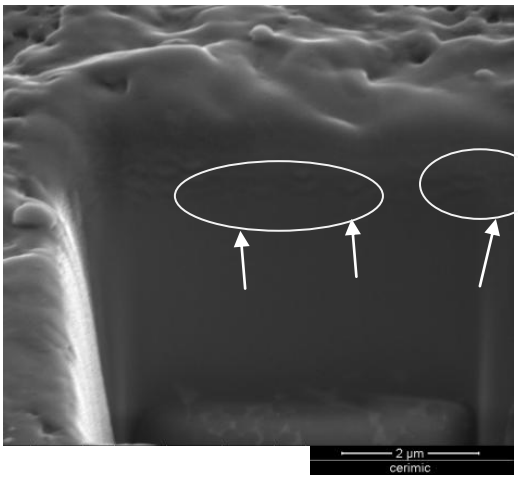

(a)Conventional grinding

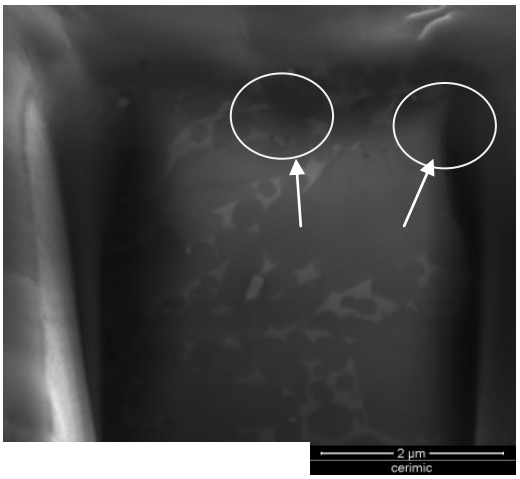

(b) Laser assisted grinding with air coolant

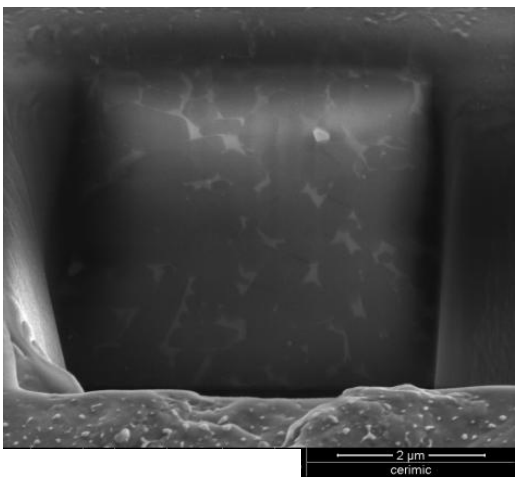

(c) Laser assisted grinding

Figure 4-13 Subsurface damage on Si_3N_4

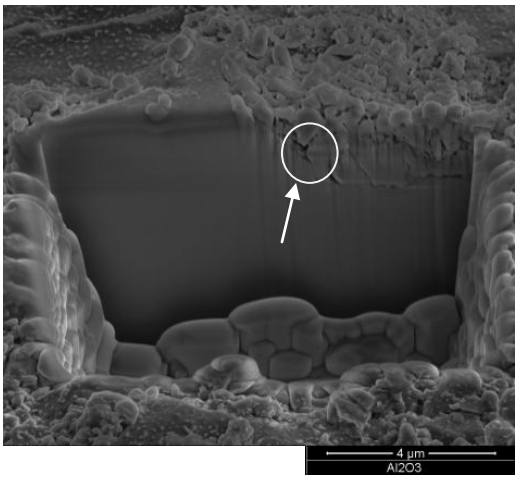

(a)Conventional grinding

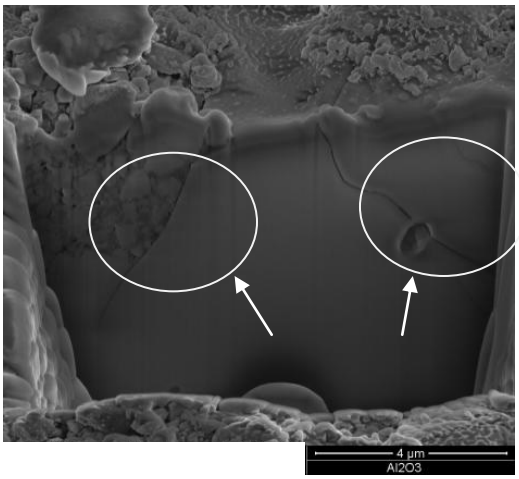

(b) Laser assisted grinding with air coolant

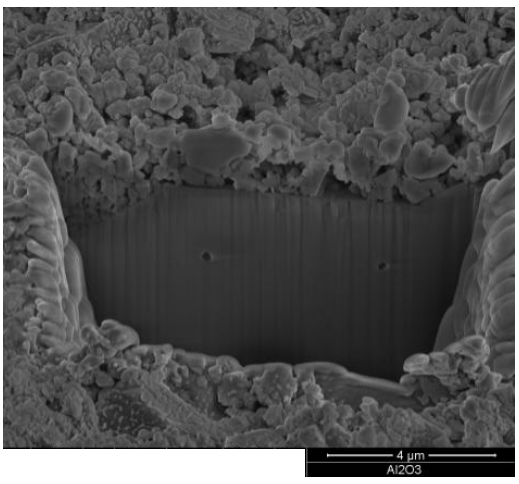

(c) Laser assisted grinding

Figure 4-14 Subsurface damage on Al_2O_3

4.6 Summary

A laser assisted micro grinding approach was developed in this chapter to machine ceramics. The results showed that the laser assisting grinding can achieve almost the same dimensional accuracy as that in conventional grinding process. However, the dimensional errors can be avoided using a compensation program in the controller. Although the grinding force was nearly the same as in conventional grinding, a better surface roughness was achieved when the laser assisted process was applied without coolant; also, there was no subsurface damage, which could make potential bacterial growth on denture. This hybrid machining process would be useful to fabricate many biomedical products that can avoid microorganism breeding. However, this hybrid process has been proven very effective in fabricating ceramics.

Figure 4-15 shows a flowchart of this hybrid machining process, i.e. laser assisted micro grinding. A workpiece is heated by laser radiation and then followed by micro grinding. The temperature needs to be higher than the brittle to ductile transition temperature of the material. High absorption capacity and low thermal conductivity of material with high power, frequency and suitable wavelength of laser radiation can help achieve the high temperature required for the micro grinding process.

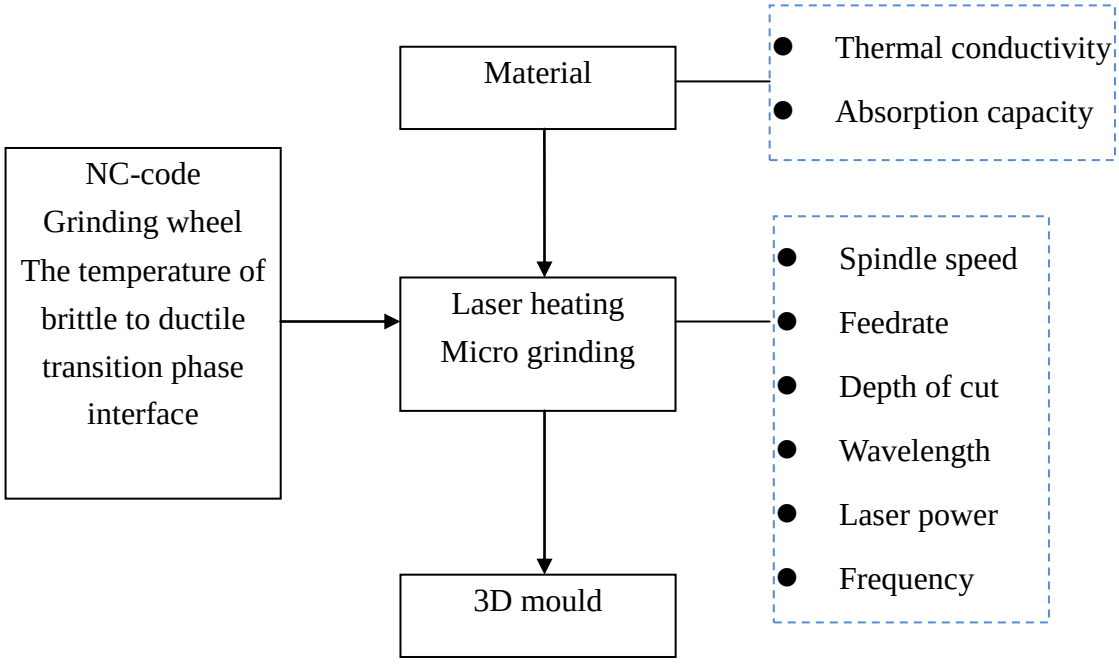

Figure 4-15 Flowchart of laser assisted micro grinding

Chapter 5 A hybrid micro machining approach - micro milling and laser polishing

5.1 Introduction

Replication by pressing and injection moulding is a cost-effective process for producing optical structured elements which are made of glass or polymers [129]. The performance of these elements relies heavily on the quality of the precision moulds or dies. These moulds/dies significantly degrade the performance of optical surfaces. Therefore they have to be polished in order to eliminate any cutting marks produced by pervious processes. However, it is very challenging to polish 3D optical surfaces by the traditional polishing approaches. In the recent years, a newly-developed technique, i.e. laser polishing, appears to be very promising in improving the surface finish of optical components.

Laser polishing is a non-contact and fast speed material removal process. It is particularly suitable for hard-to-machine materials, even compared to diamond which is the hardest material in the world [130, 131]. Ukar et al. [132] obtained up to a 90% surface roughness reduction on tool steel by using two kinds of laser polishing system, a CO_2 laser and a high power diode laser. Tyler et al. [133] investigated pulsed laser micro polishing as a method to reduce the average surface roughness from 206 nm to 70 nm on Ti_6Al_4V. Laser polishing is a complicated thermal dynamic process which is influenced by the laser's parameters, the work material properties and the accuracy of CNC control system of the laser machine, etc. Based on the heat transfer analysis and the consideration of the evaporation of surface asperities, Shao et al. [134] develop a laser surface polishing model to predict the adequate setting of the processing parameters. However, current laser polishing work has only tested to focus on polishing planar workpiece.

In this chapter, the objective is to evaluate a hybrid micro machining approach which combines a high precision milling and nanosecond laser polishing processes for the manufacture of 3D freeform optical surfaces.

5.2 Micro milling solar concentrator moulds

A simplified solar concentrator which was designed using a computer aided design (CAD) system, CATIA, was chosen as a demonstrator part for this study. The dimensions and maximum curvature of this component (shown in Figure 5-1) are 25 mm×25 mm×33.5 mm and 0.435 mm^{-1}, respectively. In manufacturing experiment, a replicated aluminium mould for the solar concentrator was fabricated on a portable milling CNC machine as shown in Figure 5-2. The travelling range of the machine axes is 100 mm × 100 mm × 100 mm. A high speed spindle up to 60,000 rpm is mounted on the Z-axis. Metal carbide ball mill tools with a radius of 1.5 mm were used for rough and finish cutting. For chamfering the edges, metal carbide end mill tools with a diameter of 3 mm and a nose radius of 0.2 mm were used. The 3D part program was generated using computer aided manufacturing (CAM) software, PowerMill. In the experiments, a spindle speed, a feedrate and a cutting depth of 30,000 rev/min, 40 mm/min and 0.2 mm respectively were used to manufacture two samples. After the micro milling process was completed, the edge of the micro channel was observed cutting marks under FEI SEM and the Zygo white light interferometer. The finished solar concentrator mould is shown in Figure 5-3. This was then put through a laser polishing process.

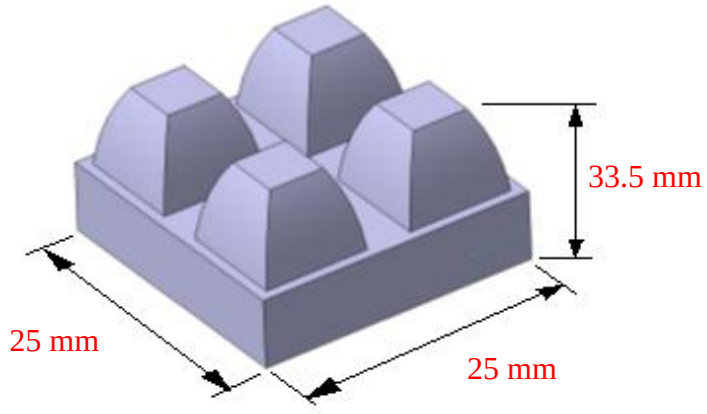

Figure 5-1 CAD model of a simplified solar concentrator mould

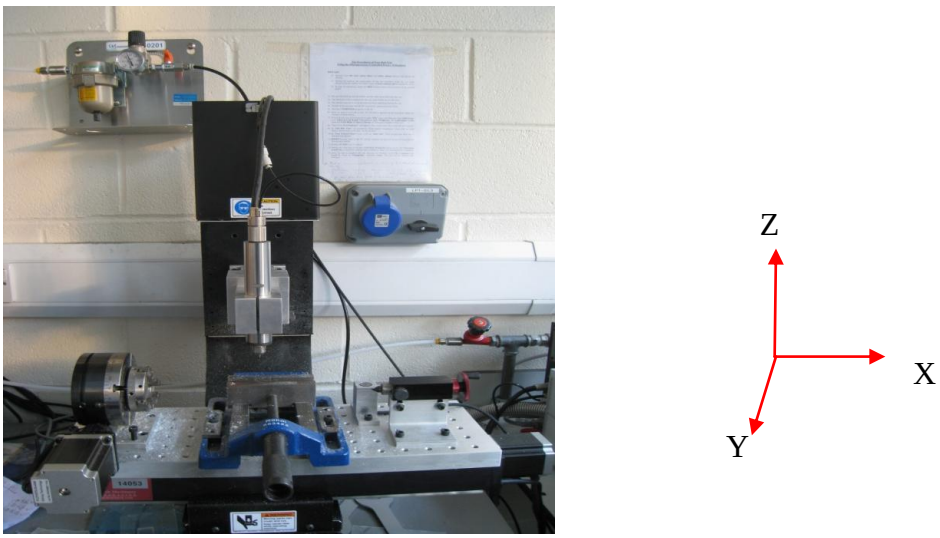

Figure 5-2 A portable milling CNC machine for machining solar concentrator mould

Figure 5-3 The concentrator mould machined after micro milling

5.3 Laser polishing trial

An Nd:YAG nanosecond laser machine was used for laser polishing in this experiment which is shown in Figure 5-4. Its maximum power, wavelength, frequency, pulse duration time and the smallest spot size are 5 W, 533 nm, 15,000 Hz, 65 ns and 20 μm, respectively. The motional stage and laser system are controlled by a computer. A workpiece can be mounted on the work table and a CCD enables to align the datum.

In the polishing experiment, the 3D concentrator mould was fixed on the work table which has a positional resolution of 1 μm. Three laser powers, i.e. 3.5 W, 4 W and 4.5 W, were used in this experiment and the frequency and spot size of the nanosecond laser were setup as 15 kHz and 20 μm, respectively. The feedrate was set at 5 mm/min with the laser scanning path follows the same path as used in the milling process.

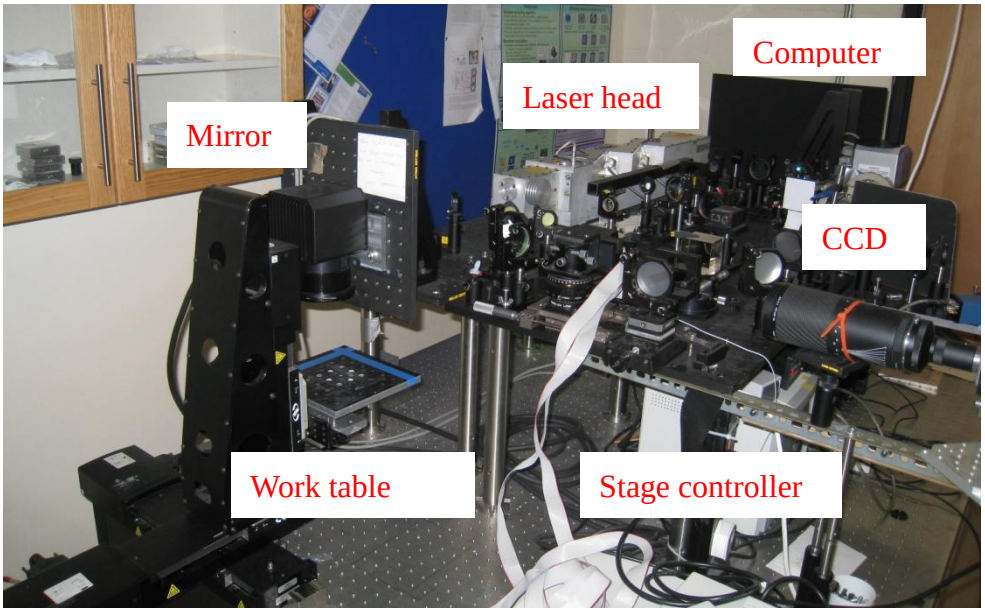

Figure 5-4 A nanosecond YAG laser system for laser polishing

5.4 Results and discussions

The solar concentrator mould was measured using the FEI SEM and the Zygo white light interferometer. Figure 5-5 shows the machined surface of solar concentrator after micro milling process. As shown, cutting marks are found and small particles are deposited on the solar concentrator. These would cause unwanted light reflection thus affecting the performance of the solar cell. Figure 5-6 shows the SEM image of the machined surface after laser polishing when the 3.5W laser power was used. As can be seen, the sharp cutting marks and particles have almost disappeared due to melting on the surface. As shown in Figure 5-6(b), even when using the same laser parameters to polish the same for area a second time on the concentrator mould, the cutting marks and small particles still exist. However, as shown in Figure 5-7 they were completely removed when the laser power was increased to 4.5 W. However, laser polishing did introduce some damage on the surface which can be observed in Figure 5-7(a). The solar concentrator surface polished using a laser power of 4 W is shown in Figure 5-8. It can be seen that most of cutting marks and particles have been removed after one test polishing process. After two polishes, the solar concentrator has very small cutting marks and few particles on the polished surface as shown in Figure 5-8(b).

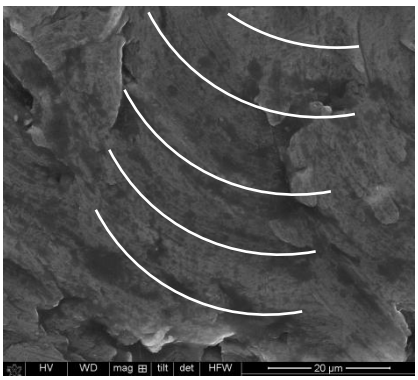

Figure 5-5 SEM image of the machine surface after the micro milling

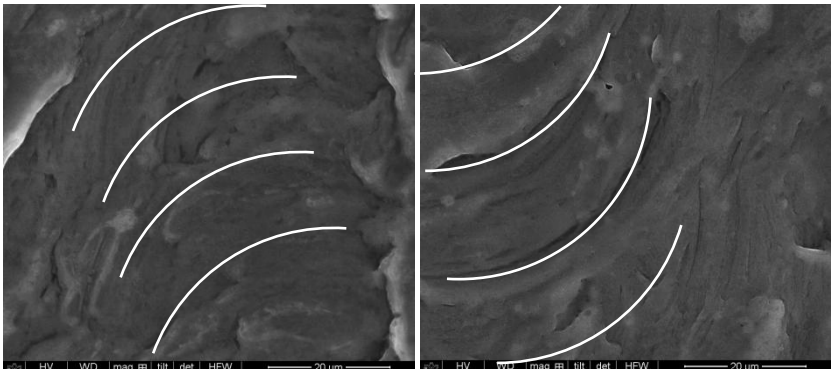

(a) Laser polishing once (b) Laser polishing twice

Figure 5-6 SEM images showing surface after laser polishing with 3.5W power

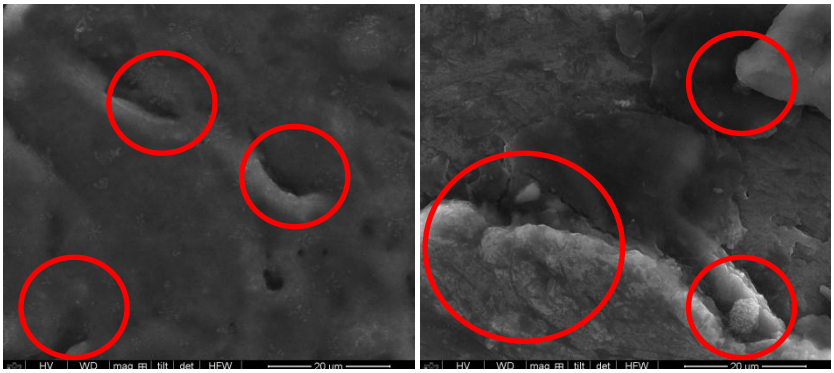

(a) Laser polishing once (b) Laser polishing twice

Figure 5-7 SEM images of the machine surface after laser polishing with 4.5W power

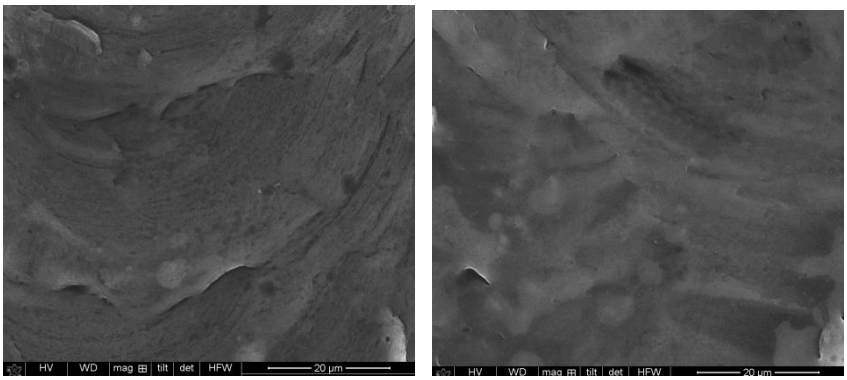

(a) Laser polishing once (b) Laser polishing twice

Figure 5-8 SEM images of machined surface after laser polishing with 4W power

Figure 5-9 shows a comparison of the measured surface roughness (Ra) after the milling process and laser polishing under different processing parameters. The surface roughness Ra after the micro milling is 467 nm. After laser polishing, the measured surface roughnesses are 349 nm, 261nm and 492 nm using laser powers of 3.5 W, 4 W and 4.5 W, respectively. The surface topography measured using white light interferometer was shown in Figure 5-10. A laser power of 4.5 W is proved to be too high for polishing this material as it caused the generation of surface damage as well as discontinuities and unwanted particles on the polish surface which subsequently increased surface roughness. Some sharp cutting marks and small particles can be removed when using a laser power of 3.5 W but there are still a few cutting marks on the surface. The best surface finish is achieved when 4 W laser power were used since the surface roughness (Ra) was reduced from 467 nm to 261 nm. However, these process parameter settings and rejects will be material dependent.

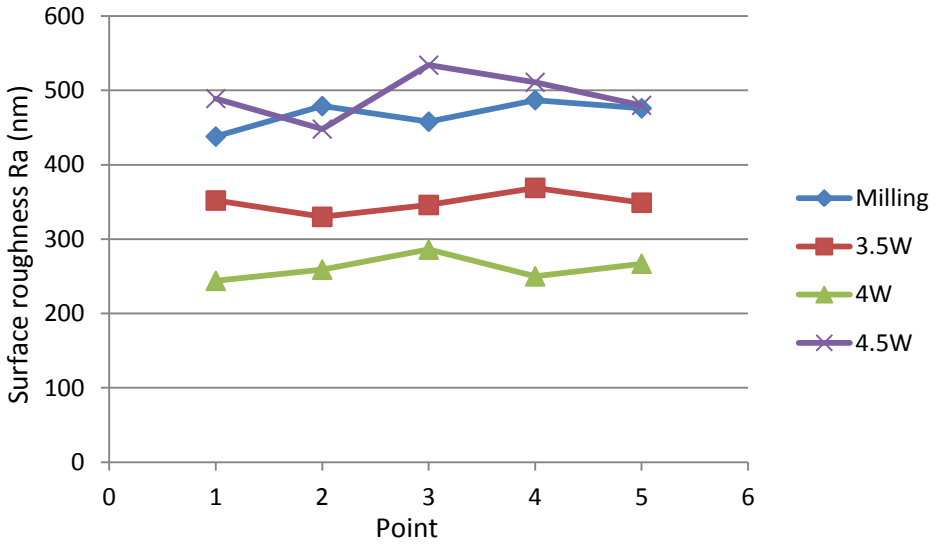

Figure 5-9 Comparisons of surface roughness Ra after micro milling and the use of different laser power

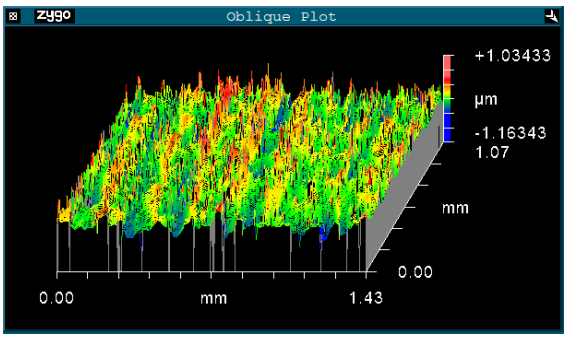

(a) After micro milling process

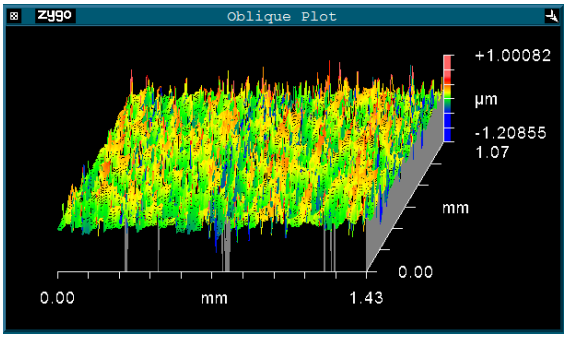

(b) After 3.5 W laser power polishing

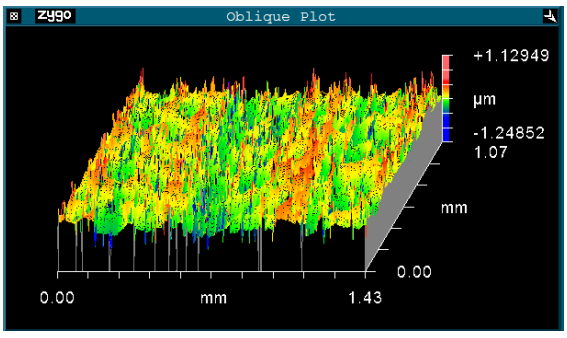

(c) After 4.5 W laser power polishing

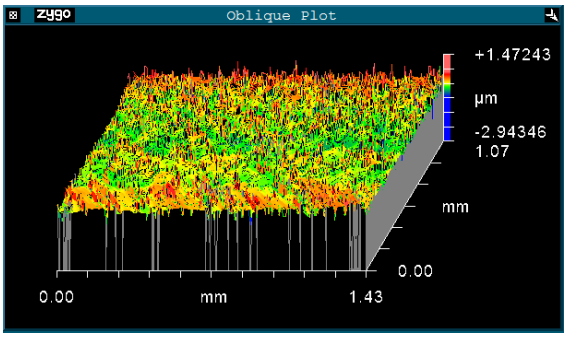

(d) After 4.0 W laser power polishing

Figure 5-10 Surface topography after micro milling and two laser polishing processes

5.5 Summary

A hybrid process which combines micro milling and 3D laser polishing has been evaluated in this chapter towards experimental objectives. The micro milling results in the generation of cutting marks and some particles on the aluminium mould surface. With a higher laser power, i.e. 4.5 W, cutting marks by micro milling were removed while new marks by laser radiation were generated. Using lower laser power, i.e. 3.5 W, can melt sharp marks but cutting marks still exist, even when laser polishing with the same parameters was repeated twice. The laser polishing process is shown to remove most of the cutting marks and particles on the machined surface. Under a laser power of 4 W, 55% improvement in surface finish was achieved demonstrating that it would be beneficial to develop a hybrid micro machining centre which can integrate both micro milling and laser polishing to obtain high quality micro products.

A flowchart of micro milling and laser polishing process is shown in Figure 5-11. Micro milling process is used to fabricate complex 3D shapes on the mould which will then be polished by laser along the same path as milling process. The laser power plays a significant role in affecting cutting marks and surface finish.

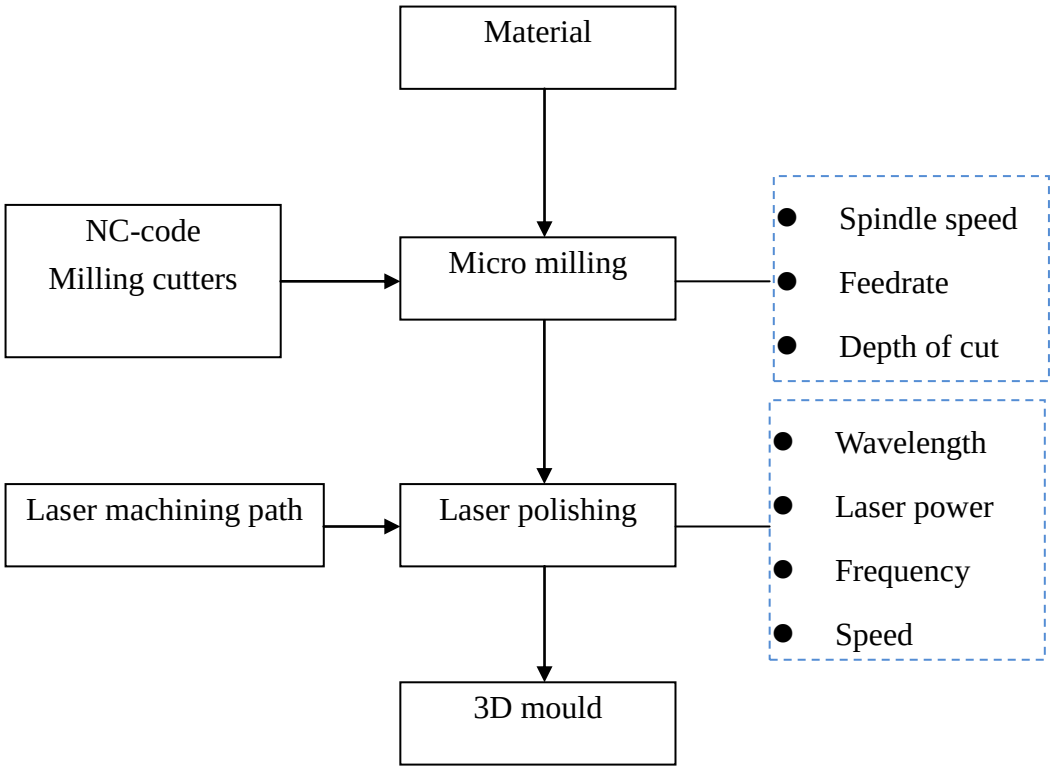

Figure 5-11 Flowchart of micro milling and laser polishing

Chapter 6 Structuring micro milling cutters for deferring tool wear

6.1 Introduction

Micro milling is widely used for manufacturing micro moulds with complex shapes such as metal forming and microinjection moulds. However, tool wear has long been a severe problem in causing degradation in the machined surface finish and dimensional accuracy of micro milled products [135]. A common practice used to defer tool wear in the micro milling industry is to coat hard metal materials on milling cutters [136-138]. Applying optimized cutting path and cutting parameters to reduce cutting forces and increase tool life has also been attempted [139, 140]. Since decreasing the friction force between the chip and the tool rake face can reduce tool wear, Evans et al. [141] investigated functional structured surfaces that could change the chip compression factor and normal force. Kawasegi et al. [142] also investigated the micro-scale and nano-scale structures that could influence tool life in the turning process. However, no work has been carried out on microstructures that can defer tool wear during the micro milling process.

In this chapter, the objective is to explore the novel microstructures on the rake faces of milling cutters using focused ion beam milling and to determine these have an effect on tool wear.

6.2 Structuring micro milling cutter by focused ion beam (FIB)

Three types of microstructures were proposed to defer tool wear in this study. These comprised a number of horizontal grooves, perpendicular grooves and grooves sloping at 45° to the cutting edge of the milling cutter rake faces. The proposed dimensions of each individual microgroove were 4.5 μm (width)×300 μm (length)×7.5 μm (depth). The distance between each groove was 4.5 μm. These microgrooves were fabricated on the rake faces of three identical 1mm diameter carbide end milling cutters using a focused ion beam (FIB) system (FEI Quanta 3D FEG) equipped with liquid gallium ion sources. In the structuring process the milling cutters were firstly mounted on the FIB work stage with the rake face to be structured perpendicular to the ion column so this surface was fully exposed to the incident ion beam. This would make sure that the sidewalls of the microgrooves were perpendicular to the rake face. To reduce the influence of redeposition, multi-pass scanning of the ion beam was used to obtain a smooth microgroove base and uniform milling depth. Once this rake face was structured, the milling cutter was then flipped over 180° and remounted on the work stage. The next rake face to be structured

would be vertical to the ion beam. In the fabrication process, a 30 keV ion beam with a maximum current of 65 nA was applied to obtain maximum the material removal rate afforded by the FIB system. Figure 6-1 shows the Scanning Electron Microscope (SEM) images of the fabricated three microstructured milling cutters and a normal milling cutter with identical geometry (but without microstructures on the rake faces) before the cutting trials. Sharp cutting edges could be observed in all tools. The dimensions of the microgrooves manufactured were consistent with the proposed fabricated dimensions.

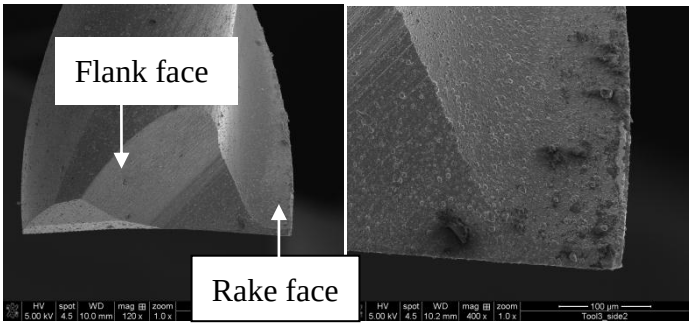

(a) Normal milling cutter

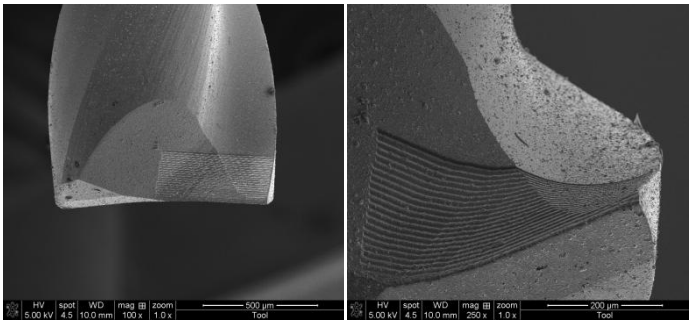

(b) 0° structured cutter

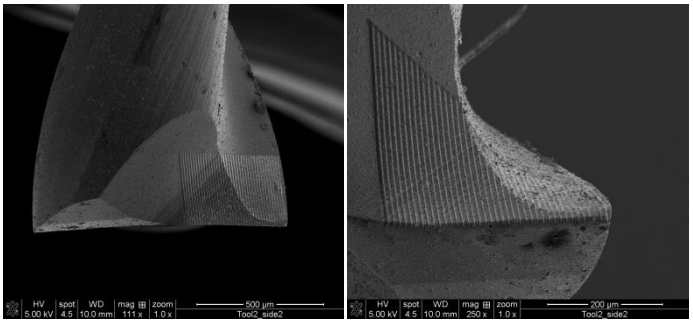

(c) 90° structured cutter

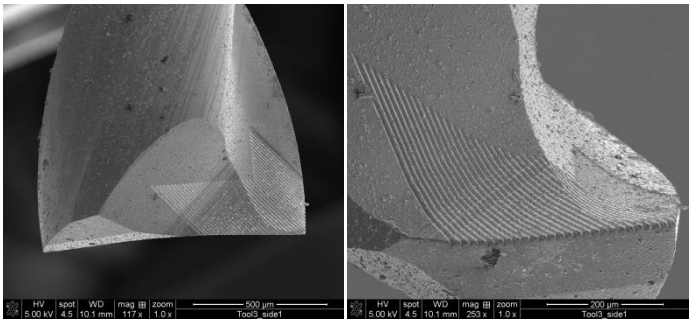

(d) 45° structured cutter

Figure 6-1 SEM images of the microstructured milling cutters and a normal milling cutter

6.3 Evaluation of micro milling trials

The micro milling cutting trials to evaluate the tool wear resistance performance of these milling cutters were carried out on a conventional CNC machining centre (Takang VMC-1020) but using a high speed spindle (SF3060-ST32) instead of the conventional low speed machine spindle. The cutting trial was setup as shown in Figure 6-2. A Kistler Dynamometer 9257BA fixed to the worktable was used to measure the cutting forces. A vise was attached on the Dynamometer to clamp the workpiece. The workpiece was a 80 mm×16 mm×10 mm piece of NAK80 (3.2 % Ni, 1.8 % Mn, 1 % Cu and Al, 0.35 % Si, 0.2 % Mo and 0.12 % C); a hard material commonly used for the fabrication of microinjection moulds. Its hardness is about 40 HRC. The four milling cutters shown in Figure 6-1 (i.e. structured and normal cutter)were used in the machining evaluation trials to cut a number of slots on the NAK80 block.

Each milling cutter was used to cut three slots. In the first and second slot milling trials a coolant comprising 3% soluble cutting oil and 97% water was applied with a cutting distance of 16.5 mm. In the third set of trials no coolant was used but over a longer cutting distance of 495 mm. The spindle speed, feedrate and depth of cut were set at 10,000 revolutions per minute (R.P.M.), 40 mm/min and 0.15 mm, respectively in all trials. The machined surface roughness of the machined slots was measured using a white light interferometer (Zygo Newview5000) and the milling cutters were inspected by a SEM after each slot milling trial.

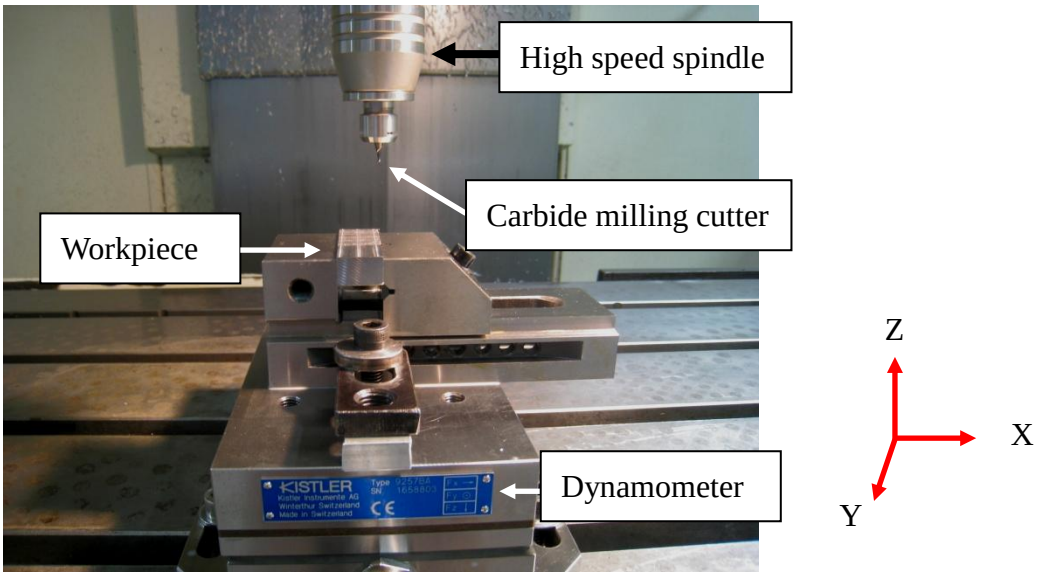

Figure 6-2 Set up of the cutting trial

6.3.1 Cutting force and surface roughness

The cutting forces measured in the first set of slot milling trials are shown in Figure 6-3. It can be seen that they oscillated around an average cutting force value. The average cutting forces when using the normal milling cutter, the microstructured milling tools with structures in the directions of normal horizontal, perpendicular and sloping at 45° to the cutting edges were 1.27 N, 1.16 N, 0.86 N and 1.42 N, respectively. The corresponding cutting forces without coolant were 1.29 N, 1.18 N, 1.03 N and 1.52 N, which were slightly larger than those using coolant. The results showed that the cutting forces when using horizontal and perpendicular microstructured milling cutters were smaller than those using the normal milling cutter. This indicates that these two kinds of microstructured tools might have better tool wear resistance performances than the normal milling cutter and the 45° microstructured cutter.

The surface roughness (Ra) measured in the first and third set of the slot milling trials is shown in Figure 6-4. It can be seen that when using the horizontal and perpendicular microstructured milling cutters without coolant, the surface roughness achieved was better than that with coolant. This was because the perpendicular microstructures could smoothly ease the removal of microchip even without the assistance of coolant. Figure 6-4 shows that the smallest surface roughness Ra value was achieved when using the perpendicular microstructured milling cutter. While using the horizontal structured tool and coolant, the cutting force was stable in the beginning of the cut. After only a cutting

distance of 5 mm, the cutting force increased dramatically and was bigger than that without using coolant (as shown in Figure 6-5). For this reason, when applying coolant the obtained surface roughness (Ra) was higher than that without using coolant.

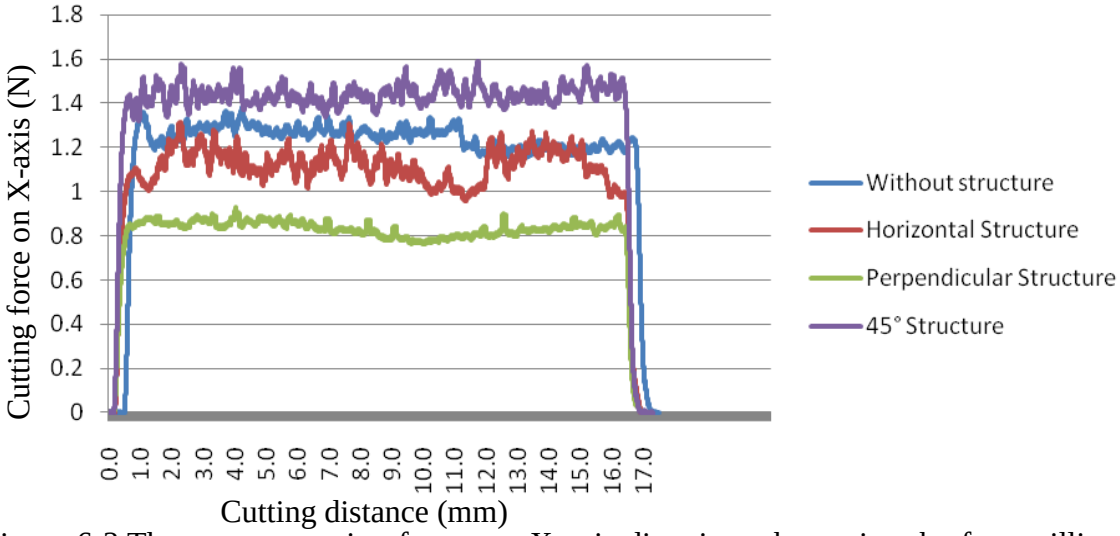

Figure 6-3 The average cutting forces on X-axis direction when using the four milling cutters

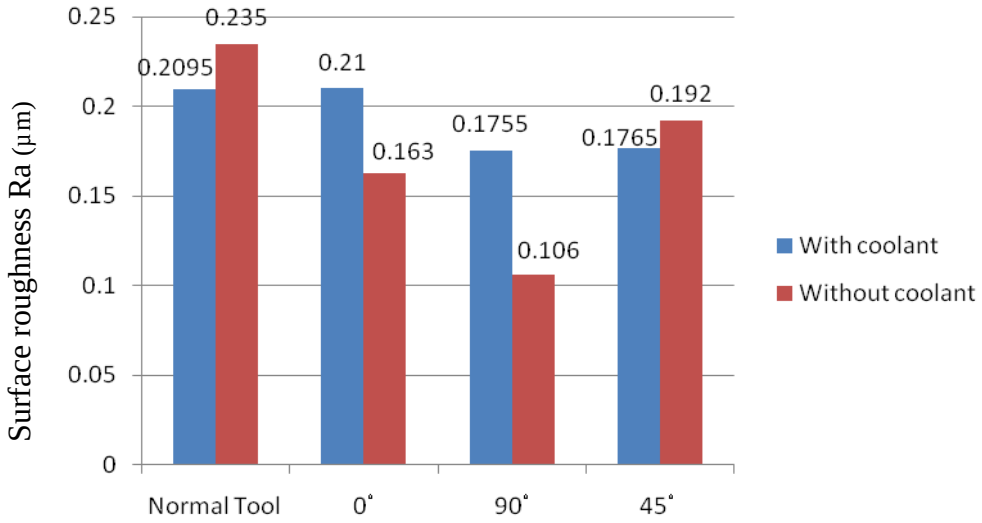

Figure 6-4 Measured surface roughness (Ra) in the first and third set of cutting trials

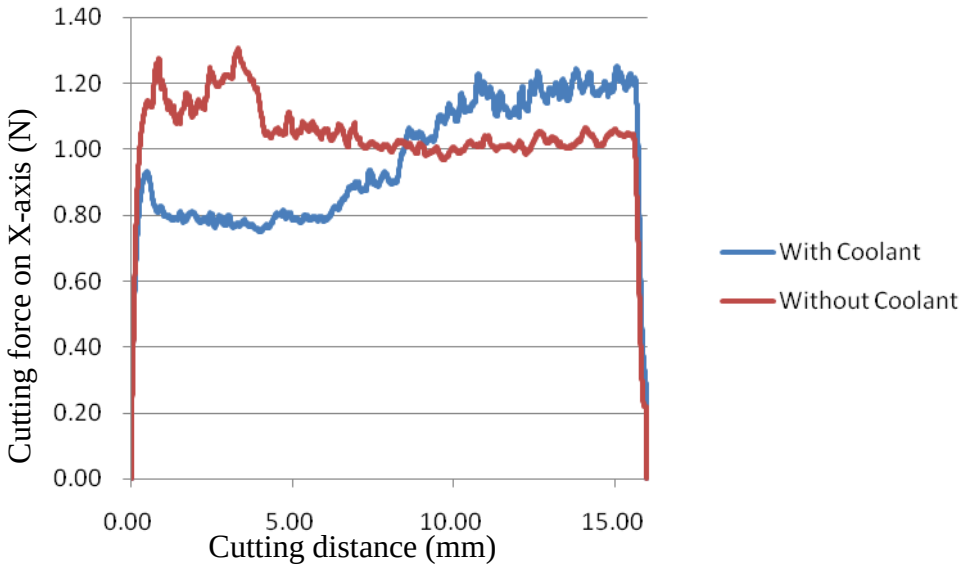

Figure 6-5 The cutting forces on X-axis direction when using horizontal structured tool

6.3.2 Tool wear

The normal milling cutter was broken at a cutting distance of 400 mm in the third set of slot milling trial. Because this tool was broken during the milling process, it was too small to be found in the CNC machine. Only the three microstructured milling cutters were measured using the SEM. The measured depth of microgrooves on the milling cutters was found to remain at 7.5 µm after the third set of slot milling trial. As shown in Figure 6-6, the flank tool wear of the three microstructured milling tools were 0.181 mm, 0.134 mm and 0.17 mm, respectively. Although no tool has reached the end of tool life i.e. 0.3 mm flank wear width as regulated by ISO [143], the microstructured milling cutter with perpendicular structures has shown the best tool wear resistance performance against others. This was evidenced by the smallest flank tool wear compared with the other tools. The rake faces of the milling cutters were also measured using the SEM, which is shown in Figure 6-7. The tool nose radius measured at the cutting edge on the rake face for these three microstructured tools were 0.080 mm, 0.069 mm and 0.075 mm, respectively. This result also indicated that the smallest tool wear was obtained for the microstructured tool with structures in the direction perpendicular to the cutting edge as it still kept its sharpness even after a total cutting distance of 528 mm.

In order to further evaluate the wear resistance performance of these microstructured tools, comparisons of the measured cutting forces in the third slot milling trial were carried out, which are shown in Figure 6-8. It can be seen that the cutting force when using the normal cutter is larger than that when using microstructured milling cutters. A

rapid increase of cutting force was observed before it was broken. When using microstructured tool with microstructures in the perpendicular direction to the cutting edge, the smallest cutting force was obtained. Durazo et al. [144] has reported that the slope of cutting forces against cutting distance would give a correct indication of tool wear resistance performance; the smaller the slope was the longer the tool life. As shown in Figure 6-8, the smallest slope of the cutting force against the cutting distance was observed when the perpendicular microstructured tool was used in the milling process. Therefore, the microstructure in a direction perpendicular to the cutting edge was the best structure which could defer tool wear and obtain prolonged tool life.

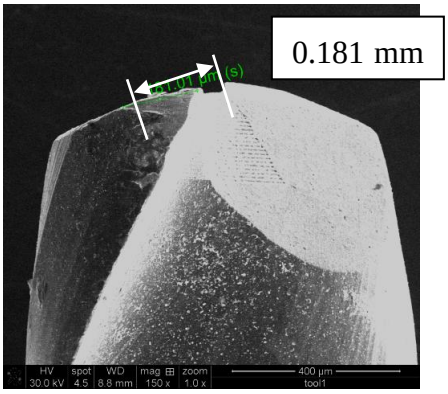

(a) 0°

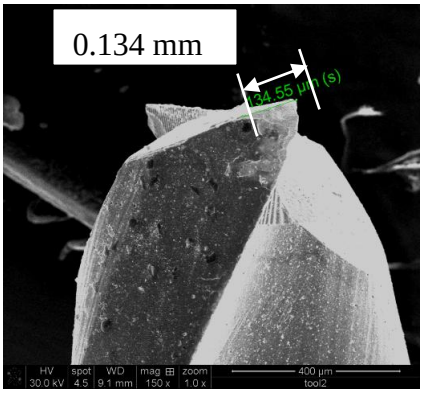

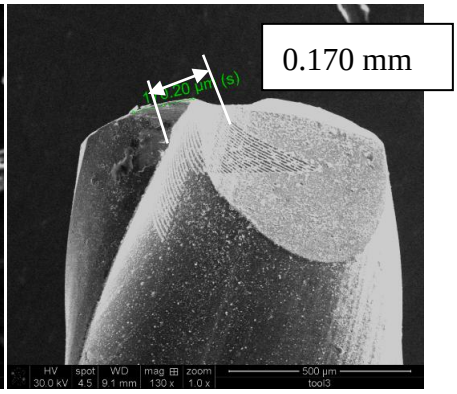

(b) 90° (c) 45°

Figure 6-6 Measured flank tool wear of the microstructured tools after the third set of cutting trials

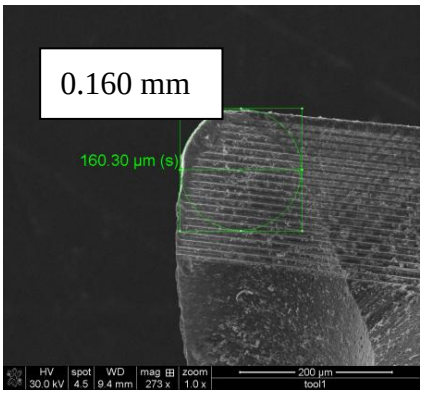

(a) 0°

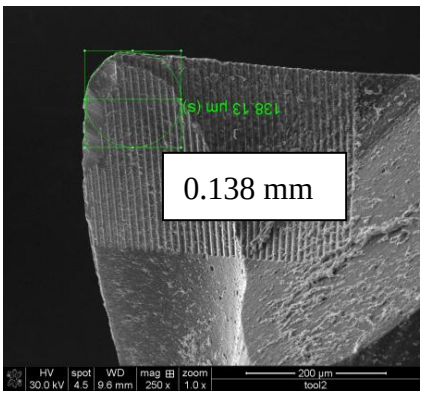

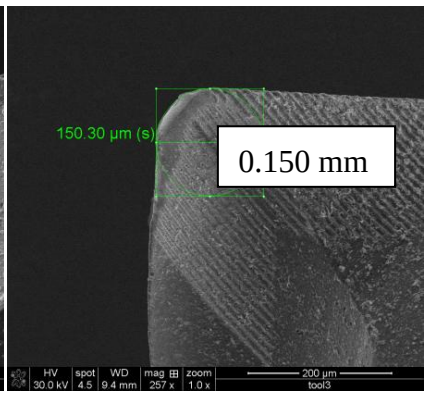

(b) 90° (c) 45°

Figure 6-7 Measured tool nose radius of the microstructured tools after the third set of cutting trials

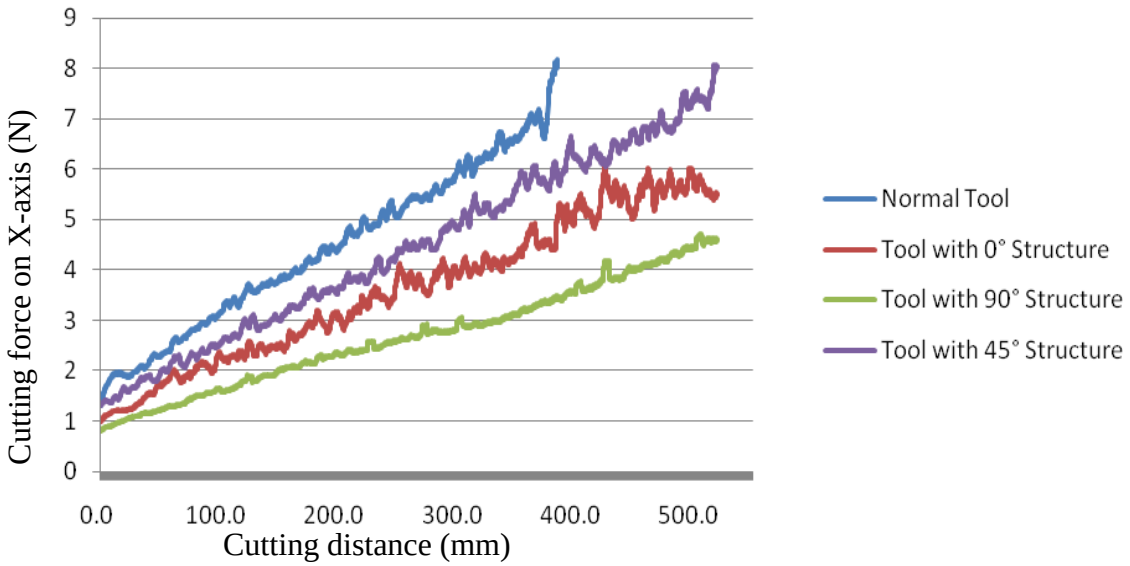

Figure 6-8 Variations of cutting force on X-axis direction against machining distance in the third set of slot milling trial

6.4 Summary

In this chapter, three types of microstructures in the directions of horizontal, perpendicular and sloping at 45° to the cutting edge were fabricated by the FIB on the rake faces of three micro milling cutters. The tool wear resistance performance of these microstructured tools and a normal milling cutter were evaluated through three sets of slot milling trials on a NAK80 specimen. The smallest cutting force was obtained when using the perpendicularly microstructured tool. The smallest flank tool wear of 0.134 mm was also achieved for this tool. Even after a total cutting distance of 528 mm the cutting edge of this microstructrured tool still kept its sharpness. When using this microstructured tool the smallest slope of the cutting force against the cutting distance was observed. These results indicate that microstructured grooves on rake faces of the micro milling cutters can effectively improve their tool wear resistance performance. The microstructure in a direction perpendicular to the cutting edge is the best structure which can defer tool wear and obtain prolonged tool life.

This chapter proves that micro structures can help defer tool wear. However, FIB is very slow machining process and also very expensive to apply in industry. In contrast, laser structuring can be more promising to replace FIB for structuring milling cutters and this method should be investigated in the future.

Chapter 7 Conceptual designs of a hybrid machine

7.1 Introduction

In previous chapters, hybrid micro machining approaches have been shown to be a very cost-effective method in manufacturing micro products. In this chapter, a conceptual design of a hybrid machine tool is presented to implement the hybrid micro machining approach. A hybrid machine tool consists of four major sub-systems which include mechanical structure (machine bed and motional stages), spindle and laser system, control system and a CCD measuring system. The mechanical structure has to hold all machine components and support the forces transmitted from the process in order to achieve its required precision. The stiffness of a machine tool will affect its machining accuracy and the surface finish obtained when the processes are in operation. In this chapter, a mechanical structure analysis has been carried out in order to select a stiffer machine configuration suitable for a proposed hybrid machine tool.

7.2 Proposed hybrid machine specification

The proposed hybrid machine is aimed at manufacturing not only miniature components but also moulds in various engineering materials. The targeted micro products include:

(1) Moulds (high strength steel, Al alloy, and NAK80);

- mould for micro fluidic device; and
- mould for solar concentrator.

(2) Medical components (ceramic and glass);

- ophthalmics (contact lens); and
- dentistry.

(3) Optical components (Glass, polymer, Al);

- complex shape or freeform optical lens; and
- lens shutters, light guiding microstructures.

(4) Mechanical components (Al, steel);

- micro sensors (pressure, flow, gas); and
- fibre optic-mechanical components (filter, wave-plates) [145].

In order to machine micro products with complex shapes, a five-axis (3 linear and 2 rotational) configuration has been recommended for the proposed hybrid machine. The strokes of the X, Y and Z axes are 200 mm×200 mm×50 mm to cope with the largest

product scale, i.e. a solar concentrator mould. The three types of machining process are proposed for incorporation i.e. micro milling, grinding and laser machining into this machine. These will cover a range of various engineering materials, i.e. micro milling, grinding and laser machining.

In order to achieve the required precision, a high damping ratio and low thermal distortion are necessary. The structure of machine tool has to hold all the machined components and withstand the various forces from the processes. The high precision machines introduced in chapter 2 are commonly based around a horizontal lathe and a vertical milling machine configuration. The lathe configuration is open-loop with the spindle work horizontal to the machine base. A closed-loop gantry is common for vertical machining. These configurations are advised for the proposed hybrid machine. The machine bed and structural components are required to be stiff and lightweight with low thermal deformation and easy to manufacture. Granite is commonly used as a bed structure for such a high precision machine because of its high stiffness and low thermal expansion coefficient. Aluminium alloy is a lightweight and an easy to be manufactured material which can be used to make rotary tables and the linear stages.

7.3 Conceptual design

Three machine layouts have been proposed in the conceptual design stage. The first conceptual design is a closed loop gantry structure which is shown in Figure 7-1. A rotary table (C-axis) is used to carry workpiece and the other rotary head used to fix spindle is attached on the Z axis. The strokes of X and Y axes are 200 mm and the strokes of Z axis is 100 mm. In order to achieve high stiffness, the width and thinness of gantry is 500 mm $\times$ 130 mm, respectively. The cutting tools, such as milling cutter and grinding wheel, can be changed automatically by Automatic Tool Changing system (ATCs). For this kind of layout, laser head can be easily placed on the top of the machine and guided by reflected mirrors.

The second conceptual design is a kind of horizontal machine which adopts a diamond turning machine concept as shown in Figure 7-2. The spindle, diamond cutter and laser lens are fixed on the C axis. A laser head is placed on the top of the Y stage. The strokes of the X and Z axes are 200 mm. The Y axis is only 50 mm because this is an open-loop

structure. When the large stage is used, the stiffness rapidly decreases.

The third conceptual design proposed is an open-loop vertical machine configurations as shown in Figure 7-3. Both rotary axes (A and C) are based on the Y axis. The dimension of gantry is 800 mm×600 mm×150 mm which is used to hold the X and Z axes stages and support cutting forces coming from machining process. The travel range of the X and Y axes are 200 mm and the Z axis is 100 mm. The laser head is also placed on the top of the gantry with the laser light guided by reflections mirrors

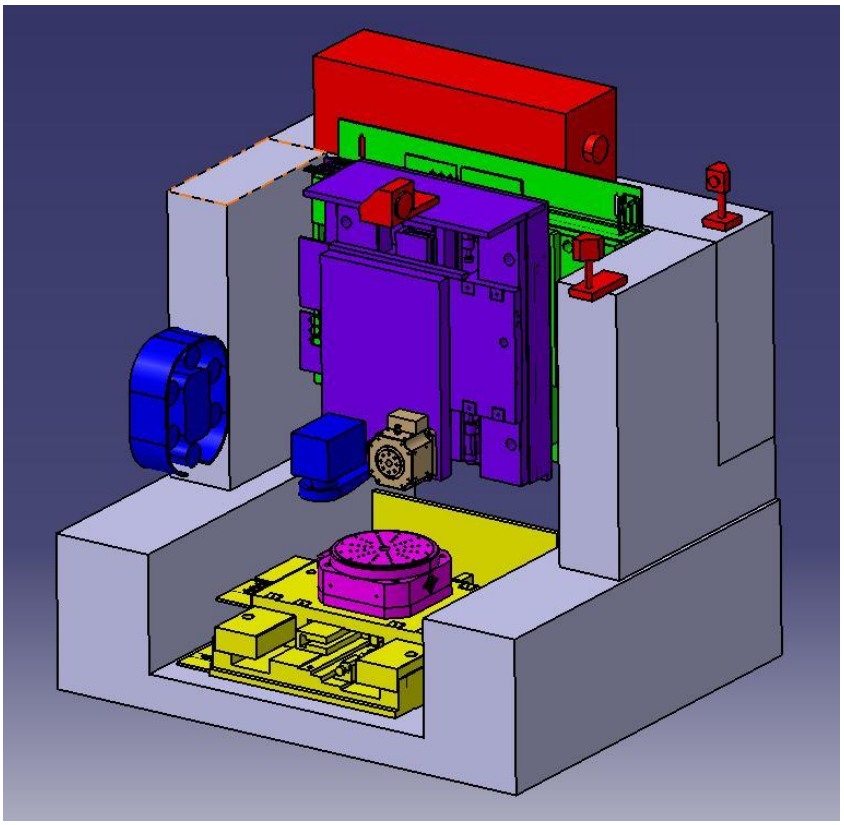

Figure 7-1 Conceptual design 1

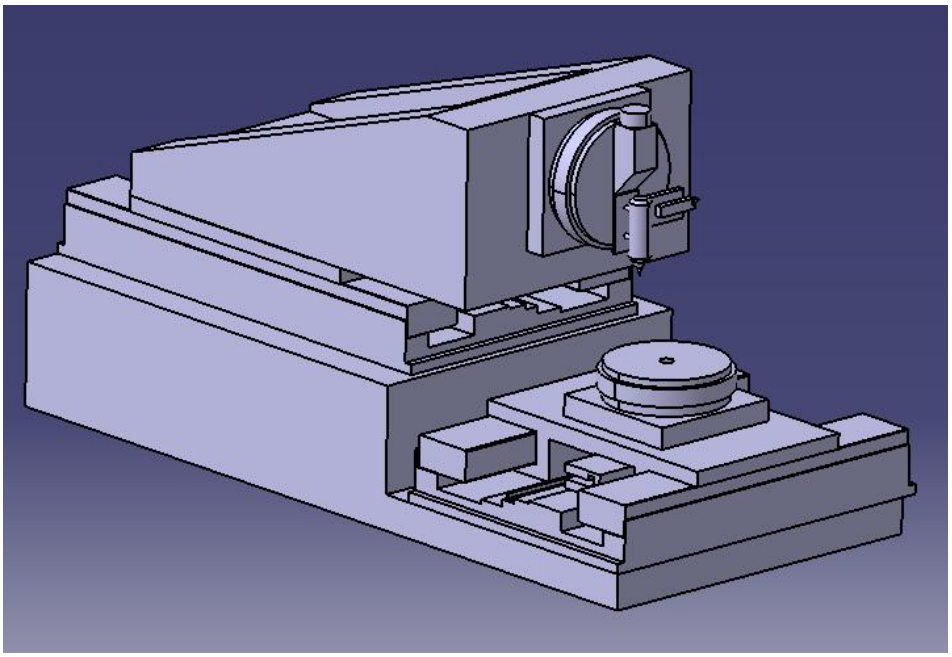

Figure 7-2 Conceptual design 2

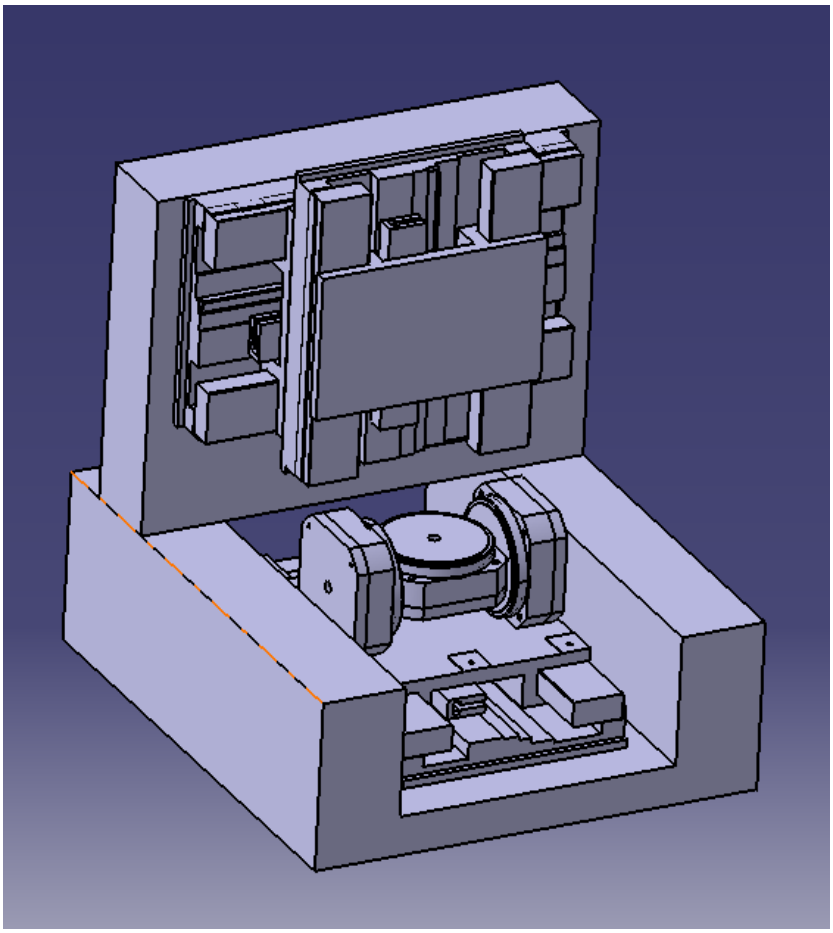

Figure 7-3 Conceptual design 3

7.4 Finite element analysis of the proposed hybrid machines' mechanical structures

7.4.1 Finite element analysis procedure

The finite element analysis (FEA) software, CATIA, was used to analyze the proposed hybrid machine tool structure. It enables simulation of the deformation, stress and natural frequencies when the loads, pressures and gravity act on the spindles and are transmitted onto the main body of the 5-axis hybrid machining centre. The FEA follows three main steps: pre-processing, solution and post-processing as shown in Figure 7-4.

In the pre-processing stage, the machine structure has to be simplified in order to reduce the simulating time. All threads, holds, fillets and chamfers are removed for the sake of simplicity. After that the simplified model is then imported into the FEA program. The material properties including elasticity, Poisson's ratio and density are applied and the structures of the machine tools will be mesh. In the CATIA system, the deformation and von Mises stress of the machine tool structure is calculated in the static analysis process. Natural frequency of the machine tools are calculated in dynamic analysis process. Initial condition includes constrain and the connect property. Boundary condition contains the applied force, pressure and gravity.

Implicit solution in CATIA is used in the solution stage.

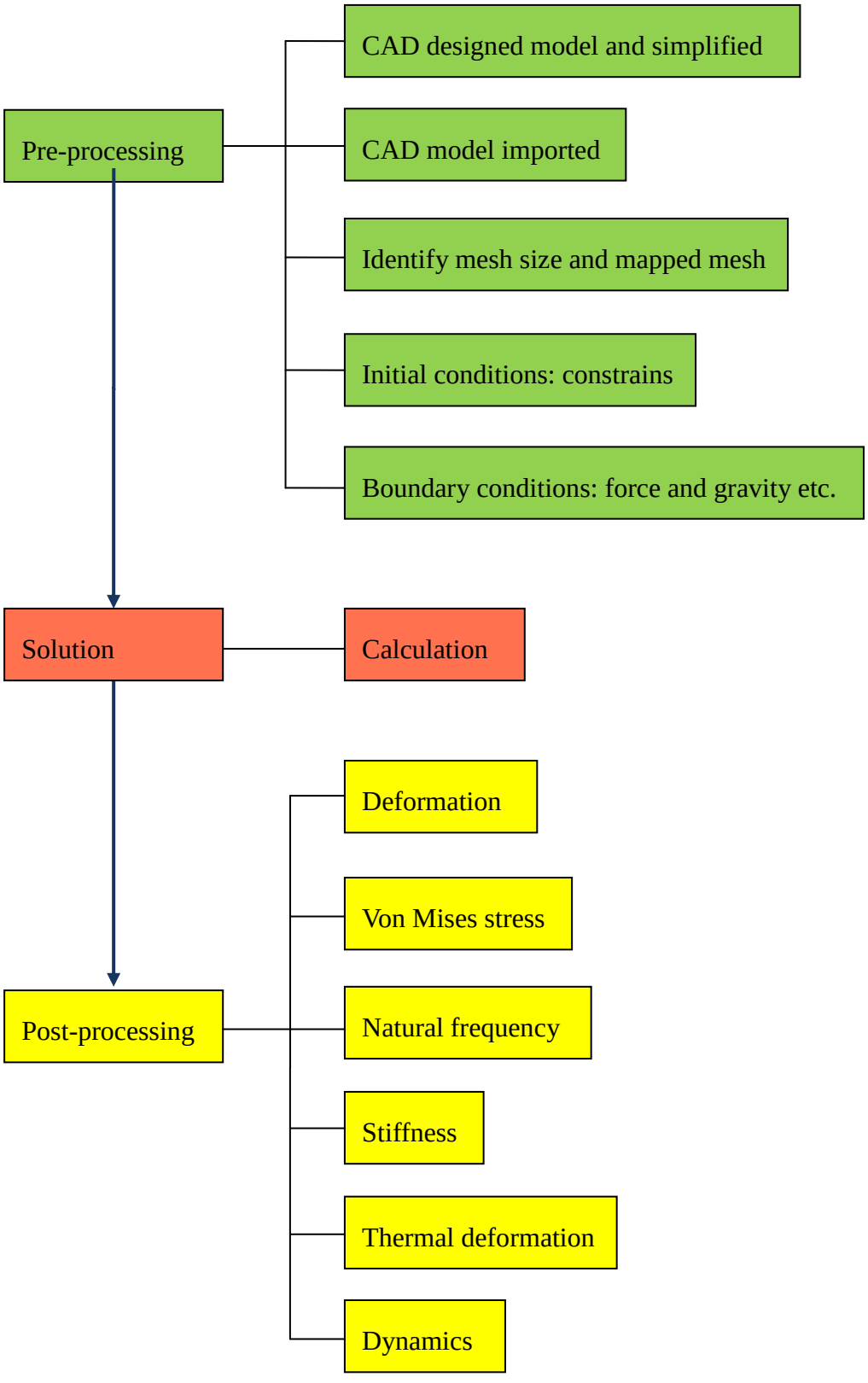

Figure 7-4 Illustration of finite element analysis procedure

During the post-processing stage, the machine deformation and stress under static force will be calculated. The deformation presents the machining error when the machining process is operated. The von Mises stress provides a prediction of the failure area and it also allows designers to improve the machine. Natural frequency will be calculated through dynamic analysis and provides the values of frequency that have to be avoided when the machine is in operation.

7.4.2 Finite element analysis of the proposed hybrid machine mechanical structures

The simplified machine structure for concept 1 is shown in Figure 7-5. In the analysis, the material of main structure was assumed to be granite and the slides aluminium alloy. Their material properties are shown in Table 7-1. The TE4 mesh shown in Figure 7-6 was used in this finite element analysis and numbers of elements on each machine were shown in Table 7-2. The boundary conditions are shown in Figure 7-7. Six degrees of freedom are fixed on the lowest surface of machine and in the static analysis, gravity is applied on all structures.

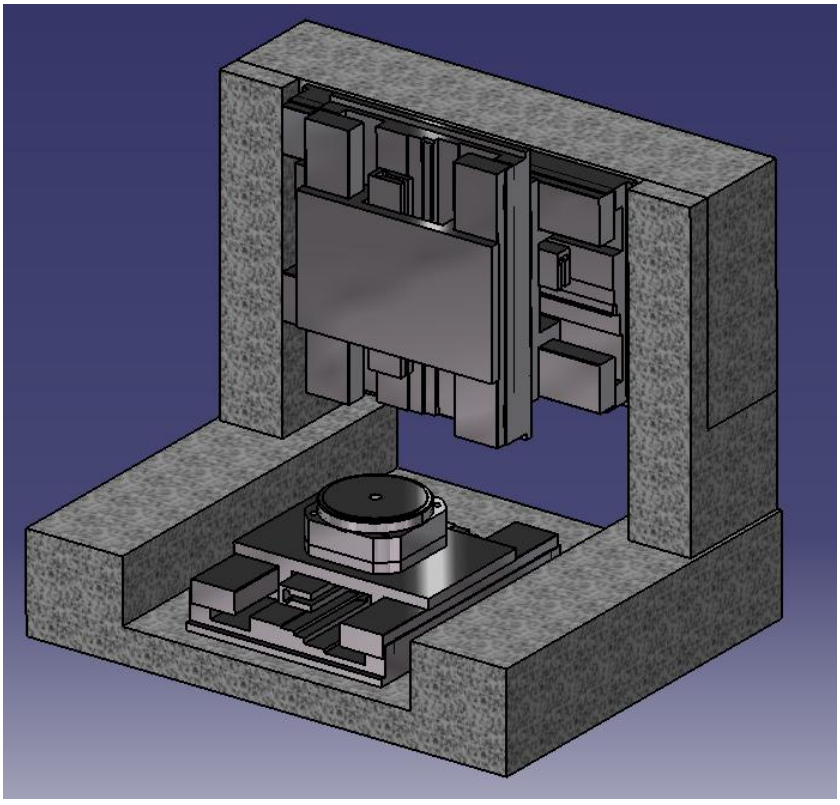

Figure 7-5 Simplified structure of conceptual design 1

Table 7-1 Design data of granite and Al alloy used in the machine

Item	Granite	Aluminium alloy
Elasticity	5×10^{10} N-m^2	7×10^{10} N-m^2
Poisson ratio	0.27	0.346
Density	2770 kg/m^3	2710 kg/m^3

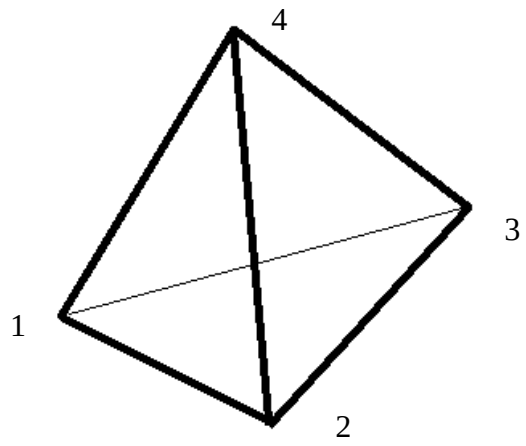

Figure 7-6 Illustration of TE4 element type

Table 7-2 Numbers of elements for three conceptual design

	Number of elements
Conceptual design 1	103923
Conceptual design 2	99283
Conceptual design 3	98322

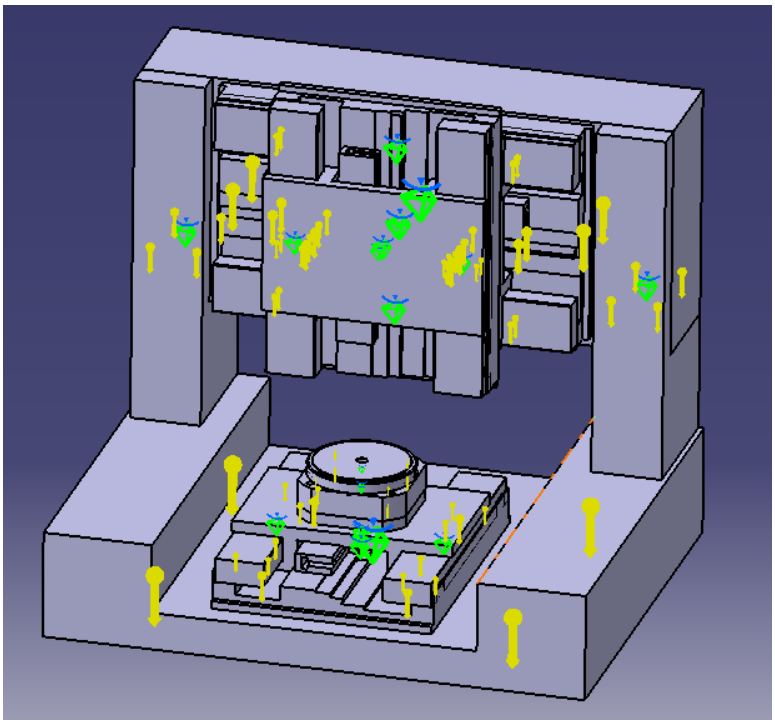

Figure 7-7 Boundary conditions of 5 axes hybrid machine type 1

The results of displacement and von Mises stress are shown in Figure 7-8 and Figure 7-9, respectively. The maximum displacement found was 2.5 μm on the Z axis slide. The maximum von Mises stress is 1.69×10^5 N/m^2 found on the bottom of the stud. Three major vibration modes of natural frequency mode are shown in Figure 7-10, Figure 7-11 andFigure 7-12. These are 184.34, 251.73 and 450.29 Hz, respectively.

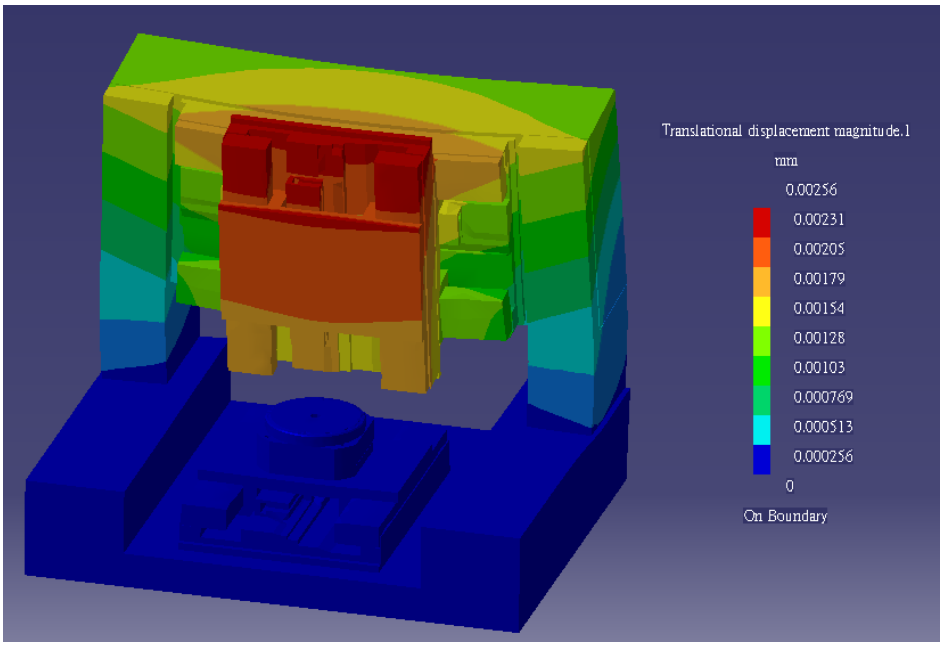

Figure 7-8 Displacement of the machine structure of conceptual design 1

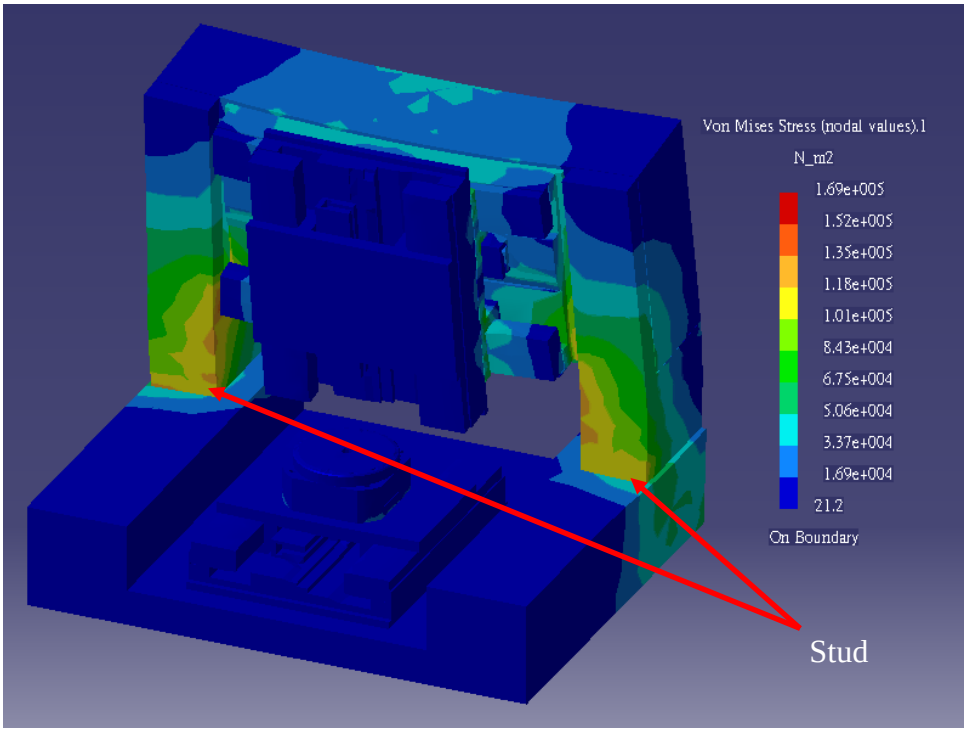

Figure 7-9 Stress of the machine structure of conceptual design 1

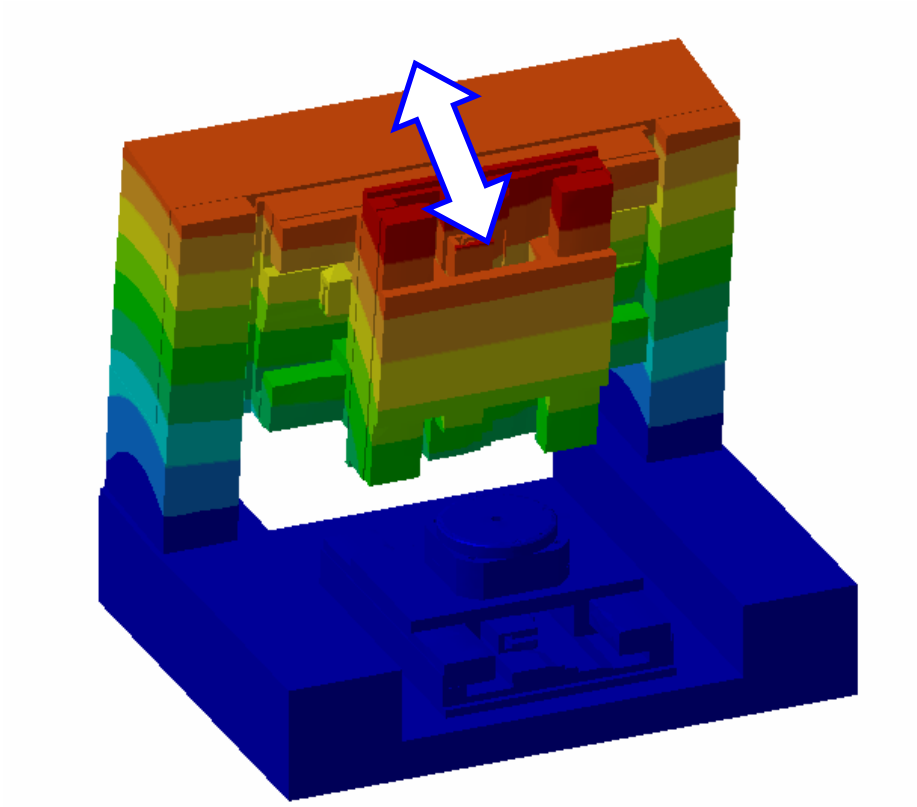

Figure 7-10 Mode 1 of natural frequency of conceptual design 1

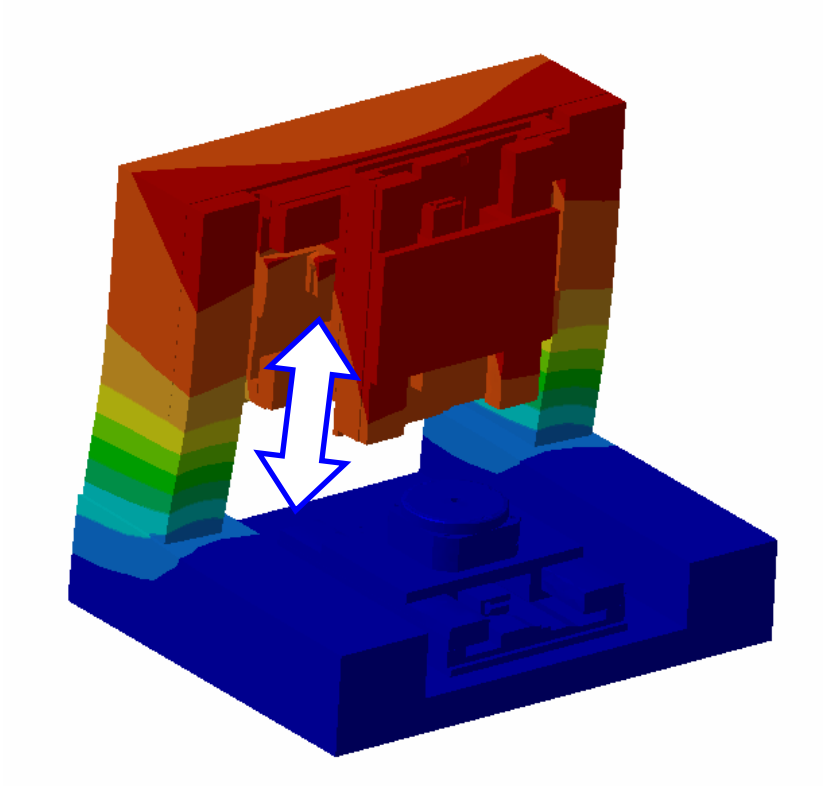

Figure 7-11 Mode 2 of natural frequency of conceptual design 1

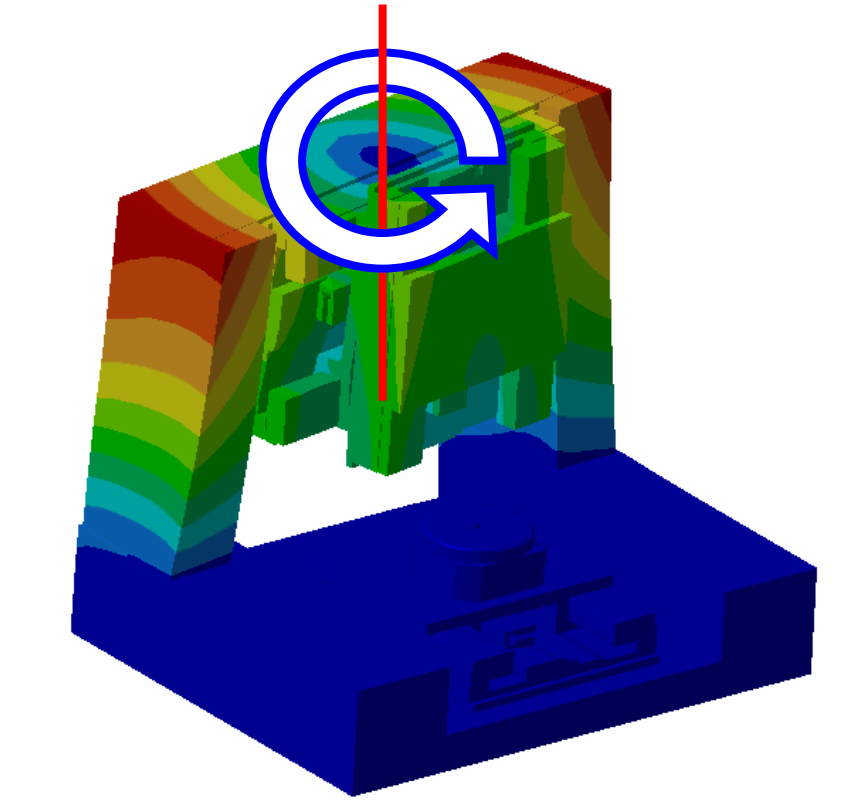

Figure 7-12 Mode 3 of natural frequency of conceptual design 1

For conceptual design 2, the displacement and von Mises stress are shown in Figure 7-13 and Figure 7-14. The maximum displacement is 2.19 μm which is found at the spindle. The maximum von Mises stress is 5.09×10^5 N/m^2 to be found on the Y axis. The three modes of natural frequency are shown in Figure 7-15, Figure 7-16 and Figure 7-17. These are 176.53, 207.16 and 412.31 Hz, respectively.

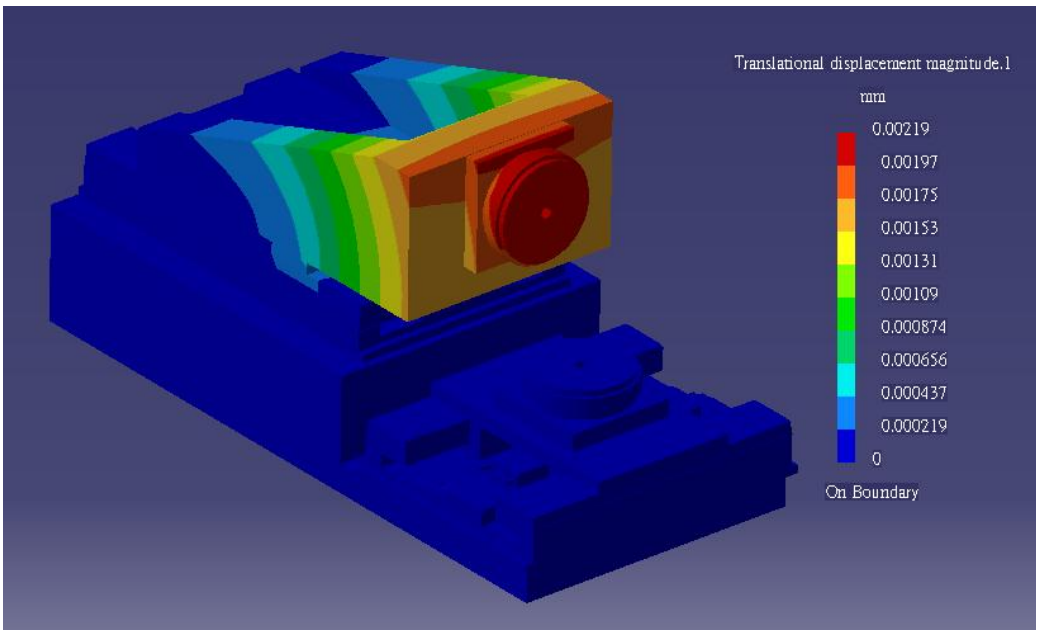

Figure 7-13 Displacement of the machine structure of conceptual design 2

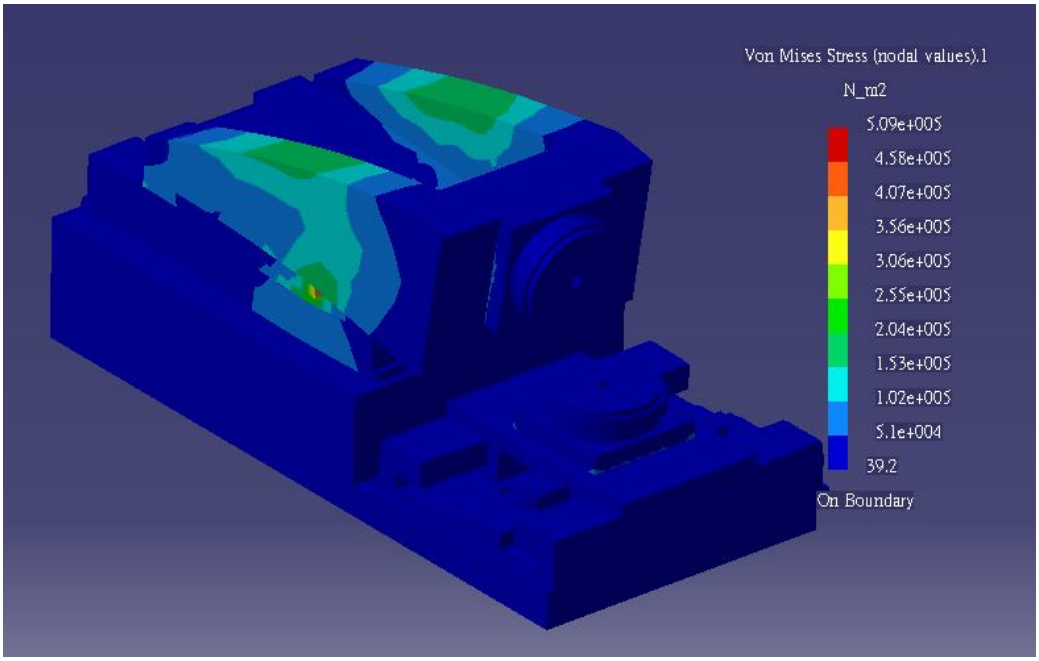

Figure 7-14 Stress of the machine structure of conceptual design 2

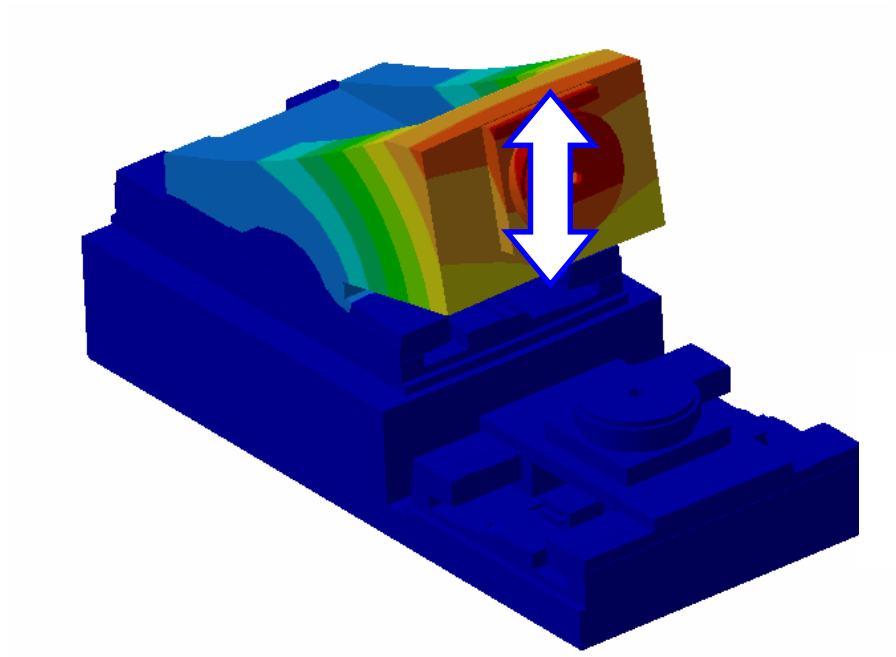

Figure 7-15 Mode 1 of natural frequency of conceptual design 2

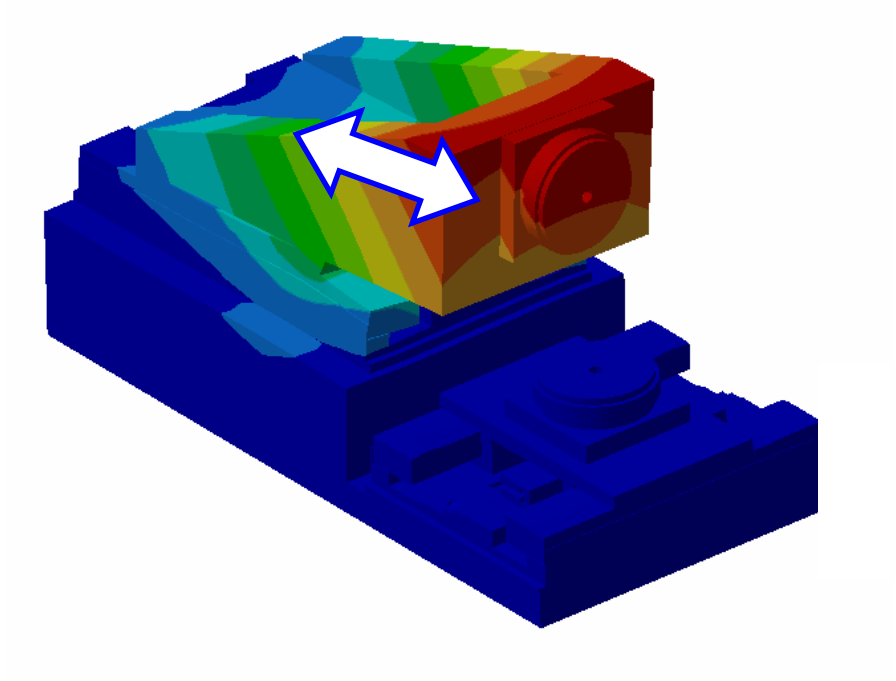

Figure 7-16 Mode 2 of natural frequency of conceptual design 2

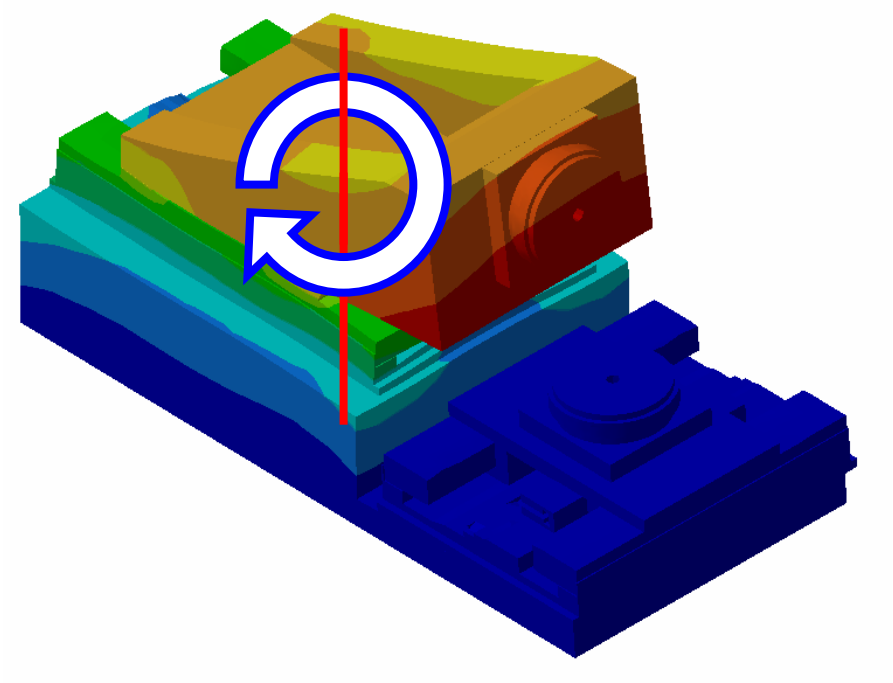

Figure 7-17 Mode 3 of natural frequency of conceptual design 2

For conceptual design 3, the results of the displacement and von Mises stress are shown in Figure 7-18 and Figure 7-19. The maximum displacement is 4.51 μm which is found on the Z axis slide. The maximum von Mises stress is 2.19×10^5 N/m^2 found at the base of the back plate. The three modes of natural frequency mode are shown in Figure 7-20, Figure 7-21 and Figure 7-22 and these natural frequencies are 176.53, 231.26 and 407.71 Hz, respectively.

.

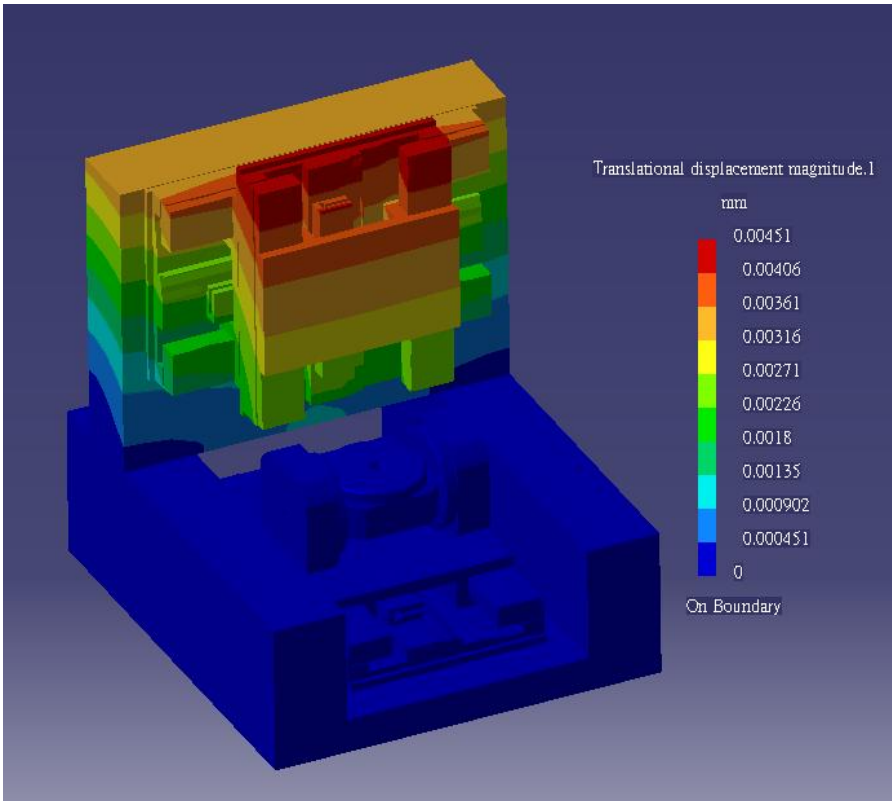

Figure 7-18 Displacement of the machine structure of conceptual design 3

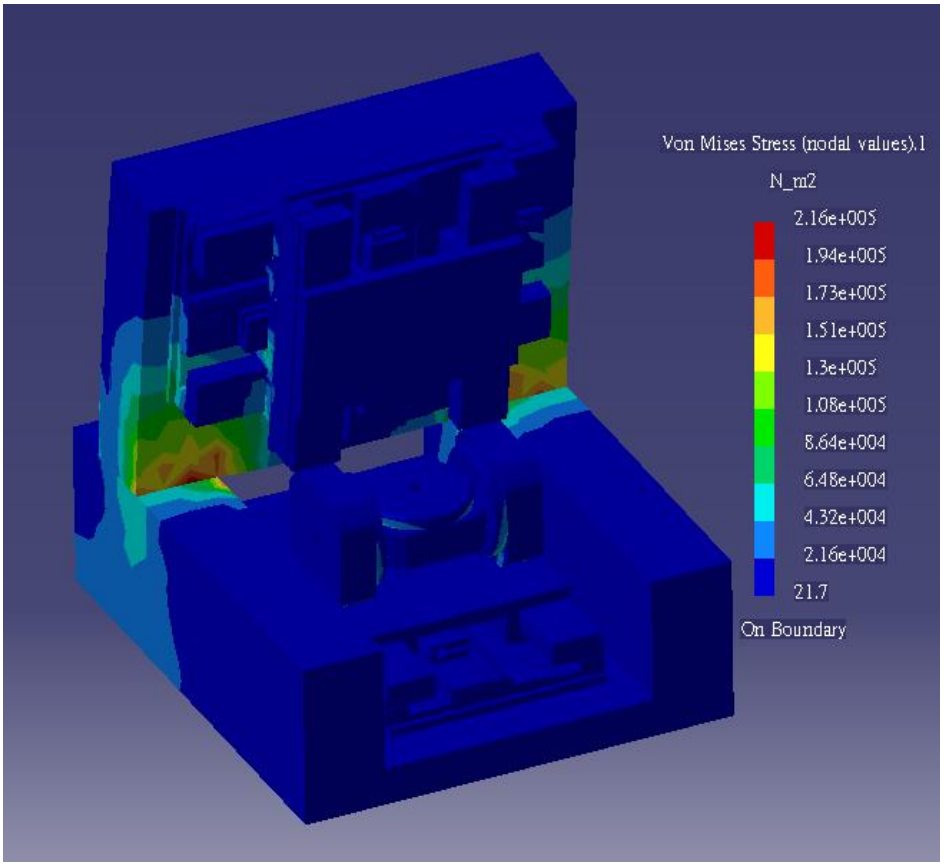

Figure 7-19 Stress of the machine structure of conceptual design 3

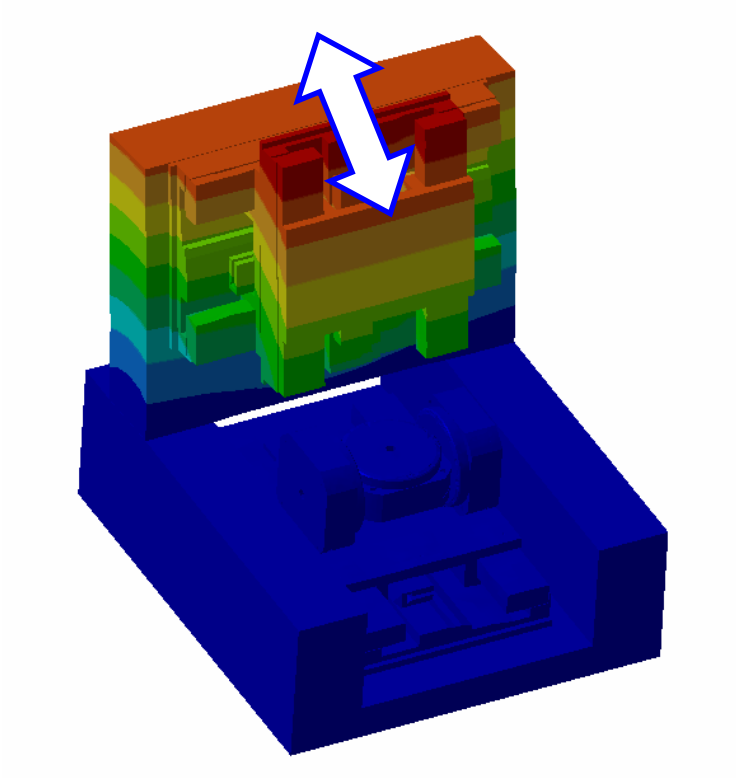

Figure 7-20 Mode 1 of natural frequency of conceptual design 3.

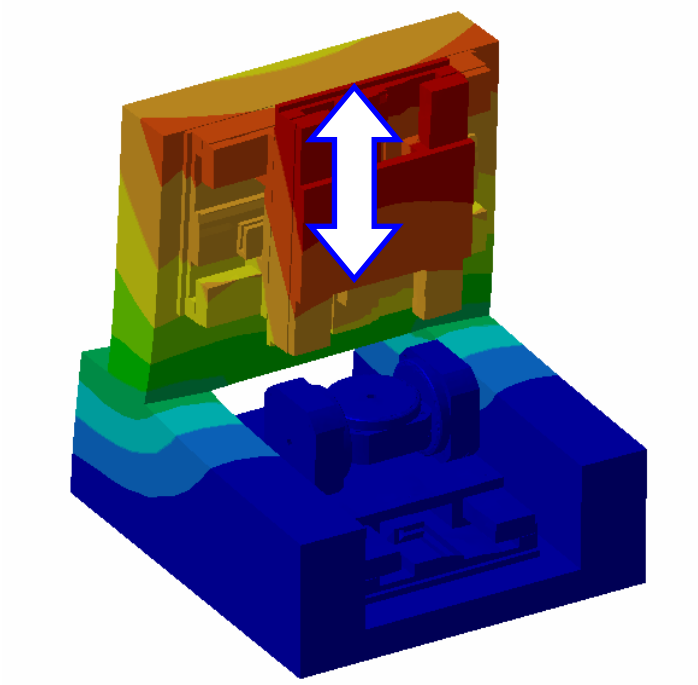

Figure 7-21 Mode 2 of natural frequency of conceptual design 3

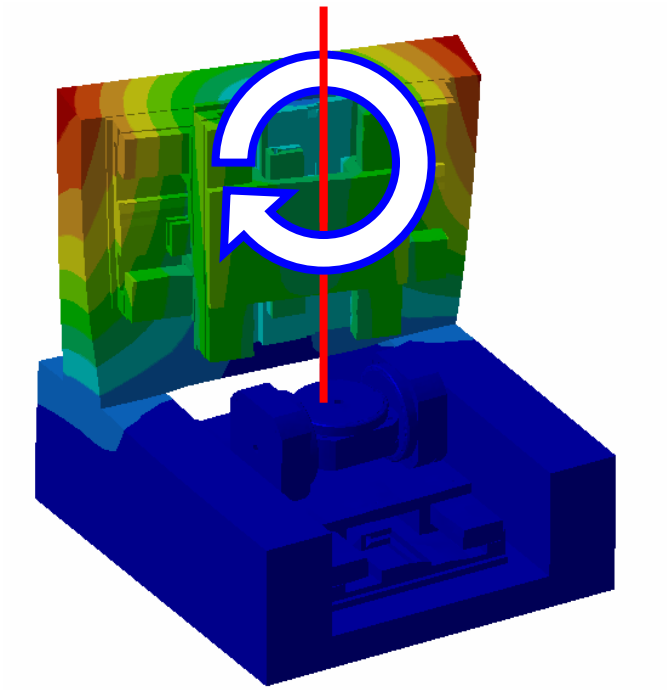

Figure 7-22 Mode 3 of natural frequency of conceptual design 3

The results of conceptual design and finite element analysis of the various concept machine tools are summarized in Table 7-3. In order to machine complex shape micro products, the three designs are 5-axis hybrid machine tools. The strokes of three linear axis are larger than 200 mm, 200 mm and 50 mm which can cope with large products. In the FEA results, the deformations of three machines are 2.5 µm, 2.1 µm and 4.5 µm. The conceptual design 1 and 2 are very close in the deformation results. The maximum von Mises stress of three machines are 1.69×10^5 N/m^2, 5.09×10^5 N/m^2 and 2.19×10^5 N/m^2, respectively. The lathe configuration has the highest maximum von Mises stress and it needs to be modified, especially at the stage of Y axis. Natural frequency results show that the closed-loop gantry configuration is the optimal design.

Table 7-3 Summary of these three finite element analysis machines

	Conceptual design 1	Conceptual design 2	Conceptual design 3
X axis stroke	200 mm	200 mm	200 mm
Y axis stroke	200 mm	50 mm	200 mm
Z axis stroke	100 mm	200 mm	100 mm
Rotary stage 1	C axis: 360°	C axis: 360°	C axis: 360°
Rotary stage 2	B axis: 360°	B axis: 360°	A axis: 120°
Deformation	2.5 μm	2.1 μm	4.5 μm
Von Mises stress (maximum)	1.69×10^5 N/m^2	5.09×10^5 N/m^2	2.19×10^5 N/m^2
Natural frequency: mode 1	184.34 Hz	176.53 Hz	145.91 Hz
Natural frequency: mode 2	251.73 Hz	207.16 Hz	231.26 Hz
Natural frequency: mode 3	450.29 Hz	412.31 Hz	407.71 Hz

7.5 Summary

In this chapter, three types conceptual designs for a 5-axis hybrid machine tool are proposed and FEA was used to find out the optimal hybrid machine tool which achieve the smallest deformation, von Mises stress and highest natural frequency. According to the numerical results, the closed-loop hybrid machine tool has the lowest maximum von Mises stress of 1.69×10^5 N/m^2. In the first three modes of natural frequency, the closed-loop gantry of conceptual design 1 also achieves a higher natural frequency in the hybrid machines. The deformation of the conceptual design 1 under gravity is 2.5 μm. It is very similar to the smallest deformation of conceptual design 2. However, these deformation errors can be solved by using mechanism, benchwork or error compensation via the controller. According to the above results, the closed-loop gantry is the best conceptual design for a 5-axis hybrid machine tools for this combination of processes and products.

Although the result shows that conceptual design 1 is the best structure in these three types of 5-axis hybrid machine tools, it also can be optimized such as changing geometry to avoid stress concentration or using different joints between two components. In the future study, thermal analysis also needs to be investigated in the micro machining process.

Chapter 8 Conclusions & recommendations for future work

8.1 Assessment of the research

The initial objective of this research was to develop hybrid machining approaches and test-bed for cost-effectively manufacturing micro products such as micro fluidic devices, denture, solar cell concentrators and in-suit structured cutter system. With this aim the thesis has provided a thorough investigation on process development of hybrid machining processes to achieve better surface finish and higher machining efficiency than traditional machining process. This study also provides a useful conceptual design of 5 axes hybrid machines which can be used as a start-point to implement the test-bed for hybrid micro machining.

8.2 Conclusions

The major results met with the research objectives can be summarised as follows:

(a) The burrs generation in the micro milling process can be simplified as a micro cutting process. The height of burrs which were generated on the edge can be assumed to be equal to the height of the top burrs generated using milling process.

(b) The micro burrs generated in micro milling were completely removed by the developed laser deburring approach in which an Nd:YAG nanosecond laser is used. The surface roughness was also improved after adopting the laser deburring process on NAK80.

(c) Micro fluidic moulds were successfully manufactured by using this novel hybrid machining approaches with promising surface roughness.

(d) Laser assisted micro grinding approach will slightly influence the dimensional accuracy of the machined micro products due to the thermal expansion of the workpiece. However, this error can be compensated by adjusting the depth of cut.

(e) The average grinding force in laser assisted grinding without coolant was very close to that in conventional grinding process where coolant is applied.

(f) In terms of surface roughness, the quality of the machined surface can be greatly improved using laser assisted grinding process.

(g) Conventional grinding and laser assisted grinding with air coolant may lead to subsurface damage on ceramics like Si_3N_4 or Al_2O_3 but it was barely to find subsurface damage when the laser assisted grinding was used without coolant.

(h) By adopting proper laser processing parameters, cutting marks generated in micro milling process can be removed.

(i) In the laser polishing process, increasing laser power can remove cutting marks but also lead to surface damage. Applying lower laser power may result in better cutting marks removal, even after the surface was polished twice with the same laser power.

(j) The microstructure in the direction perpendicular to the cutting edge is the best structure which can defer tool wear and obtain prolonged tool life.

(k) The finite element analysis showed the closed-loop vertical machine is the optimal machine configuration which can offer high stiffness and good dynamic characteristics for the propose hybrid machine.

In light of the research development shown above, the contributions to knowledge in this study can be summarised as:

- To implement different micro machining approaches for various industrial products and materials.
- To observe that Nd:YAG laser machine not only removes micro burrs completely but greatly improves machined surface finish.
- To prove that the laser assisted grinding can relieve subsurface damage on brittle materials.
- To provide a novel idea for *in-situ* structuring micro cutters to defer tool wear.

8.3 Recommendations for future work

Regarding the recommendations for future work of this research, the following is suggested:

(a) Fundamental understanding of hybrid machining processes. Study on influence of hybrid machining processes on surface integrity of micro product is critical for commercialisation of microproducts.

(b) Laser assisted repairing approach: Cracks or damages will be generated on the surface or subsurface of brittle materials when using traditional machining process. Laser may be used to repair these cracks or damages through recrystallisation.

(c) A further finite element analysis of thermal deformations, stresses and cutting force during machining process for investigation of 5 axes hybrid CNC structures. The machining accuracy may be further improved by thermal and force compensation.

(d) Integration of control system. Development of novel control system which can effectively integrate mechanical machining with laser modules. Such integration will be of critical importance in the development of the hybrid machine.

References

1 Ehmann, K.F. International assessment of research and development in micromanufacturing. (DTIC Document, 2005).

2 Huo, D., Cheng, K. and Wardle, F. Design of a five-axis ultra-precision micro-milling machine—UltraMill. Part 1: holistic design approach, design considerations and specifications. *The International Journal of Advanced Manufacturing Technology*, 2010, **47**(9), 867-877.

3 Liu, X., DeVor, R., Kapoor, S. and Ehmann, K. The mechanics of machining at the microscale: assessment of the current state of the science. *Journal of Manufacturing Science and Engineering*, 2004, **126**, 666-679.

4 Chae, J., Park, S. and Freiheit, T. Investigation of micro-cutting operations. *International Journal of Machine Tools and Manufacture*, 2006, **46**(3-4), 313-332.

5 Filiz, S., Conley, C.M., Wasserman, M.B. and Ozdoganlar, O.B. An experimental investigation of micro-machinability of copper 101 using tungsten carbide micro-endmills. *International Journal of Machine Tools and Manufacture*, 2007, **47**(7-8), 1088-1100.

6 Taniguchi, N. Current status in, and future trends of, ultraprecision machining and ultrafine materials processing. *CIRP Annals-Manufacturing Technology*, 1983, **32**(2), 573-582.

7 Melkote, S., Kumar, M., Hashimoto, F. and Lahoti, G. Laser assisted micro-milling of hard-to-machine materials. *CIRP Annals-Manufacturing Technology*, 2009, **58**(1), 45-48.

8 Sun, S., Brandt, M. and Dargusch, M. Thermally enhanced machining of hard-to-machine materials--A review. *International Journal of Machine Tools and Manufacture*, 2010, **50**(8), 663-680.

9 Li, Z., Treadwell, C. and Pei, Z. Drilling small holes in hard-to-machine materials by rotary ultrasonic machining. *Technical paper of Society of Manufacturing Engineering*, 2004.

10 Lim, H., Wong, Y., Rahman, M. and Edwin Lee, M. A study on the machining of high-aspect ratio micro-structures using micro-EDM. *Journal of Materials Processing Technology*, 2003, **140**(1), 318-325.

11 Brinksmeier, E., Mutlugünes, Y., Klocke, F., Aurich, J., Shore, P. and Ohmori, H. Ultra-precision grinding. *CIRP Annals-Manufacturing Technology*, 2010, **59**(2), 652-671.

12 Moriwaki, T. Multi-functional machine tool. *CIRP Annals-Manufacturing Technology*, 2008, **57**(2), 736-749.

13 McKeown, P. From micro-to nano-machining–towards the nanometre era. *Sensor Review*, 1996, **16**(2), 4-10.

14 Ikawa, N., Donaldson, R., Komanduri, R., König, W., Mckeown, P., Moriwaki, T. and Stowers, I. Ultraprecision metal cutting--the past, the present and the future. *CIRP Annals-Manufacturing Technology*, 1991, **40**(2), 587-594.

15 Cheung, C.F. and Lee, W. *Surface Generation in Ultra-precision Diamond Turning: Modelling and Practices*. (Wiltshire, UK, 2003).

16 Stephenson, D.J., Veselovac, D., Manley, S. and Corbett, J. Ultra-precision grinding of hard steels. *Precision Engineering*, 2001, **25**(4), 336-345.

17 Liang, S.Y., Hecker, R.L. and Landers, R.G. Machining process monitoring and control: the state-of-the-art. *Journal of Manufacturing Science and Engineering*, 2004, **126**, 297-311.

18 Lin, Y.C., Yan, B.H. and Chang, Y.S. Machining characteristics of titanium alloy (Ti-6Al-4V) using a combination process of EDM with USM. *Journal of Materials Processing Technology*, 2000, **104**(3), 171-177.

19 Bissacco, G., Hansen, H.N. and De Chiffre, L. Size effects on surface generation in micro milling of hardened tool steel. *CIRP Annals-Manufacturing Technology*, 2006, **55**(1), 593-596.

20 Sriyotha, P., Nakamoto, K., Sugai, M. and Yamazaki, K. Development of 5-axis linear motor driven super-precision machine. *CIRP Annals-Manufacturing Technology*, 2006, **55**(1), 381-384.

21 Takeuchi, Y., Sakaida, Y., Sawada, K. and Sata, T. Development of a 5-axis control ultraprecision milling machine for micromachining based on non-friction servomechanisms. *CIRP Annals-Manufacturing Technology*, 2000, **49**(1), 295-298.

22 Bang, Y., Lee, K. and Oh, S. 5-axis micro milling machine for machining micro parts. *The International Journal of Advanced Manufacturing Technology*, 2005, **25**(9), 888-894.

23 Newby, G., Venkatachalam, S. and Liang, S.Y. Empirical analysis of cutting force constants in micro-end-milling operations. *Journal of Materials Processing Technology*, 2007, **192**, 41-47.

24 Jun, M.B.G., Liu, X., DeVor, R.E., Fellow, A. and Kapoor, S.G. Investigation of the dynamics of microend milling—Part I: model development. *Journal of Manufacturing Science and Engineering*, 2006, **128**, 893-900.

25 Lu, Z. and Yoneyama, T. Micro cutting in the micro lathe turning system. *International Journal of Machine Tools and Manufacture*, 1999, **39**(7), 1171-1183.

26 Woronko, A., Huang, J.I.N. and Altintas, Y. Piezoelectric tool actuator for precision machining on conventional CNC turning centers. *Precision Engineering*, 2003, **27**(4), 335-345.

27 MCT5000. http://www.novatechonline.com/. (accessed on 24/12/2010).

28 Bifano, T.G., Dow, T.A. and Scattergood, R.O. Ductile-regime grinding: a new technology for machining brittle materials. *Journal of Engineering for Industry*, 1991, **113**(2), 184-189.

29 Ohmori, H., Ebizuka, N., Morita, S., Yamagata, Y. and Kudo, H. Ultraprecision micro-grinding of germanium immersion grating element for mid-infrared super dispersion spectrograph. *CIRP Annals-Manufacturing Technology*, 2001, **50**(1), 221-224.

30 Namba, Y., Kobayashi, H., Suzuki, H., Yamashita, K. and Taniguchi, N. Ultraprecision surface grinding of chemical vapor deposited silicon carbide for X-ray mirrors using resinoid-bonded diamond wheels. *CIRP Annals-Manufacturing Technology*, 1999, **48**(1), 277-280.

31 Knowles, M.R.H., Rutterford, G., Karnakis, D., Dobrev, T., Petkov, P. and Dimov, S. Laser micro-milling of ceramics, dielectrics and metals using nanosecond and picosecond lasers. *Proceedings of the 4M*, 2006.

32 Rizvi, N.H. and Apte, P. Developments in laser micro-machining techniques. *Journal of Materials Processing Technology*, 2002, **127**(2), 206-210.

33 Chryssolouris, G. *Laser Machining-Theory and Practice*. (Springer-Verlag, New York, 1991).

34 Wei, P.S. and Chiou, L.R. Molten metal flow around the base of a cavity during a high-energy beam penetrating process. *Journal of Heat Transfer*, 1988, **110**, 918-924.

35 Wei, P.S. and Ho, J.Y. Energy considerations in high-energy beam drilling. *International Journal of Heat and Mass Transfer*, 1990, **33**(10), 2207-2217.

36 Geiger, M. Laser cutting of steel sheets. *Laser Assisted Processing, SPIE*, 1988, **1022**, 20-33.

37 Pham, D.T., Dimov, S.S., Petkov, P.V. and Petkov, S.P. Laser milling. *Proceedings of the Institution of Mechanical Engineers, Part B: Journal of Engineering Manufacture*, 2002, **216**(5), 657-667.

38 Petkov, P.V., Dimov, S.S., Minev, R.M. and Pham, D.T. Laser milling: pulse duration effects on surface integrity. *Proceedings of the Institution of Mechanical Engineers, Part B: Journal of Engineering Manufacture*, 2008, **222**(1), 35-45.

39 Klimt, B. New tool for the toolbox. *Industrial Laser Solutions*, 2006, **21**(12), 9-11.

40 Cheng, X., Nakamoto, K., Sugai, M., Matsumoto, S., Wang, Z.G. and Yamazaki, K. Development of ultra-precision machining system with unique wire EDM tool fabrication system for micro/nano-machining. *CIRP Annals-Manufacturing Technology*, 2008, **57**(1), 415-420.

41 Li, L., Diver, C., Atkinson, J., Giedl-Wagner, R. and Helml, H.J. Sequential laser and EDM micro-drilling for next generation fuel injection nozzle manufacture. *CIRP Annals-Manufacturing Technology*, 2006, **55**(1), 179-182.

42 Heinz Jr, K.G. Fundamental study of magnetic field-assisted micro-EDM for non-magnetic materials. (University of Illinois, 2010).

43 Thoe, T., Aspinwall, D. and Wise, M. Review on ultrasonic machining. *International Journal of Machine Tools and Manufacture*, 1998, **38**(4), 239-255.

44 Tseng, F.G., Chuang, Y.J. and Lin, W. A novel fabrication method of embedded micro channels employing simple UV dosage control and antireflection coating. *Presented at Technical Digest. MEMS 2002 IEEE Int. Conf. 15th IEEE Int. Conf. on Micro Electro Mechanical Systems*, 69-72, 2002.

45 Tian, W.C. *Microfluidics for Biological Applications*. (Springer, 2008).

46 Jo, B.H., Van Lerberghe, L.M., Motsegood, K.M. and Beebe, D.J. Three-dimensional micro-channel fabrication in polydimethylsiloxane (PDMS) elastomer. *Journal of Microelectromechanical Systems*, 2000, **9**(1), 76-81.

47 Ho, C.M. and Tai, Y.C. Micro-electro-mechanical-systems (MEMS) and fluid flows. *Annual Review of Fluid Mechanics*, 1998, **30**(1), 579-612.

48 Yun, D.J., Seo, T.I. and Park, D.S. Fabrication of biochips with micro fluidic channels by micro end-milling and powder blasting. *Sensors*, 2008, **8**(2), 1308-1320.

49 Lee, S.H. Precision laser deburring. *Journal of Manufacturing Science and Engineering*, 2001, **123**, 601-609.

50 Ramachandran, N., Pande, S.S. and Ramakrishnan, N. The role of deburring in manufacturing: A state-of-the-art survey. *Journal of Materials Processing Technology*, 1994, **44**(1-2), 1-13.

51 Jung, W.C., Heo, Y.M., Yoon, G.S., Shin, K.H., Chang, S.H., Kim, G.H. and Cho, M.W. Micro machining of injection mold inserts for fluidic channel of polymeric biochips. *Sensors*, 2007, **7**(8), 1643-1654.

52 Chang, C., Lee, M. and Wang, S. Digital denture manufacturing-An integrated technologies of abrasive computer tomography, CNC machining and rapid prototyping. *The International Journal of Advanced Manufacturing Technology*, 2006, **31**(1), 41-49.

53 Denture image. http://www.newimagedentallab.com. (accessed on 21/05/2010).

54 Kugler MICROMASTER machine. http://www.kugler-precision.com. (accessed on 13/11/2011).

55 Ultra NANO 100 machine. http://www.sodick.com/ (accessed on 24/05/2009).

56 Brinksmeier, E., Grimme, D. and Preuss, W. Generation of freeform surfaces by diamond machining. (2002).

57 Freeform 700 machine. http:www.precitech.com/. (accessed on 20/05/2009).

58 She, C.H. and Chang, C.C. Development of a five-axis postprocessor system with a nutating head. *Journal of Materials Processing Technology*, 2007, **187**, 60-64.

59 Takino, H., Kawai, T. and Takeuchi, Y. 5-axis control ultra-precision machining of complex-shaped mirrors for extreme ultraviolet lithography system. *CIRP Annals-Manufacturing Technology*, 2007, **56**(1), 123-126.

60 Karnakis, D., Knowles, M., Petkov, P., Dobrev, T. and Dimov, S. Surface integrity optimisation in ps-laser milling of advanced engineering materials, *Proceedings of 4th International WLT-Conference on Lasers in Manufacturing 2007, Munich, Germany*, 2007, 619-623.

61 PL10100 machine. http://www.ekspla.com/en/. (accessed on 21/05/2009).

62 FANUC Robonano machine. http://www.fanuc.co.jp/. (accessed on 20/05/2009).

63 Kurita, T. and Hattori, M. Development of new-concept desk top size machine tool. *International Journal of Machine Tools and Manufacture*, 2005, **45**(7-8), 959-965.

64 AIST's hybrid machine. http://www.wtec.org. (accessed on 10/11/2011).

65 Rahman, M., Asad, A.B.M.A., Masaki, T., Saleh, T., Nath, C., Wong, Y.S., Kumar, A.S. and Lin, H.S.. Compound Micro/Nano Machining – A Tool-Based Innovative and Integrated Approach. *4M/ICOMM*, 2009, 59-72.

66 Kurita, T., Kasashima, N. and Mishima, N. Development of a laser/ECM complex machining system for small diameter tube and rod. *ICOMM*, 2008, 228-232.

67 Takashima's hybrid machine. http://www.takashima.co.jp. (accessed on 10/11/2011).

68 Chung, Y., Chou, C.P., Chien, K.Y., Hu, P.C., Tsai, C.L., Wu, W.C., Hung, J.C., Huang, K.M., Lin, Y.C. and Wu, C.F. The Development of a compact, high efficiency micro/meso machining system with multiple machining modules. *The 7th International Workshop on Micro Facturies*Daejeon, Korea, 2010.

69 Shin, H.M., Choi, H.W. and Kim, S.D. Hybrid (Laser+ CNC) process for lubricant groove on linear guides. *The International Journal of Advanced Manufacturing Technology*, 2010, **46**(9), 1001-1008.

70 Chung, Y., Hu, P.C., Chien, K.Y., Chou, C.P., Tsai, C.L., Lu, Y.T. and Wu, C.F. The Development of a reconfigurable micro/meso machining system with multiple machining modules *6th International Conference on Micro-Manufacturing, ICOMM*, Tokyo, 2011.

71 MikroTool's hybrid machine. http://www.mikrotools.com. (accessed on 11/07/2011).

72 De Souza, A.M., Sales, W.F., Ezugwu, E.O., Bonney, J. and Machado, A.R. Burr formation in face milling of cast iron with different milling cutter systems. *Proceedings of the Institution of Mechanical Engineers, Part B: Journal of Engineering Manufacture*, 2003, **217**(11), 1589-1596.

73 Huang, B.W., Cai, J.Z. and Hsiao, W.L. Cutting force estimation in a micromilling process. *Proceedings of the Institution of Mechanical Engineers, Part B: Journal of Engineering Manufacture*, 2011, **224**(10), 1615-1619.

74 Lee, S.H. and Asme, D. Precision laser deburring. *Journal of Manufacturing Science and Engineering*, 2001, **123**, 601-609.

75 DeLitizia, A.T. Mechanical deburring with centrifugal blast equipment. *Advancement in Surface Treatment Technology*, 1986, **2**, 241-254.

76 Ferrara, A.K. Vibratory finishing equipment. (Google Patents, 1976).

77 Sonego, R.A. Electrolyte deburring. *Products Finishing*, 1988, **53**(2), 57-62.

78 Jeong, Y.H., HanYoo, B., Lee, H.U., Min, B.K., Cho, D.W. and Lee, S.J. Deburring microfeatures using micro-EDM. *Journal of Materials Processing Technology*, 2009, **209**(14), 5399-5406.

79 Alwerfalli, D.R. Deburring metal parts. *American Machinist*, 1975, 55-62.

80 Ko, S.L., Baron, Y.M. and Park, J.I. Micro deburring for precision parts using magnetic abrasive finishing method. *Journal of Materials Processing Technology*, 2007, **187**, 19-25.

81 Yeo, S.H., Ngoi, B.B.K.A. and Chua, L.Y. Ultrasonic deburring. *International Journal of Advanced Manufacturing Technology*, 1997, **13**(5), 333-341.

82 Jun, M.B.G., Liu, X., DeVor, R.E., Fellow, A. and Kapoor, S.G. Investigation of the dynamics of microend milling Part I: model development. *Journal of Manufacturing Science and Engineering*, 2006, **128**, 893-900.

83 Ko, S.L. and Dornfeld, D.A. A study on burr formation mechanism. *Journal of Engineering materials and technology*, 1991, **113**, 75-88.

84 Gillespie, L.K. and Blotter, P.T. The formation and properties of machining burrs. *Journal of Engineering for Industry- Transaction of ASME*, 1976, **98**, 66-74.

85 Aurich, J.C., Dornfeld, D., Arrazola, P.J., Franke, V., Leitz, L. and Min, S. Burrs--Analysis, control and removal. *CIRP Annals-Manufacturing Technology*, 2009, **58**(2), 519-542.

86 Park, J.B., Wie, K.H., Park, J.S. and Ahn, S.H. Evaluation of machinability in the micro end milling of printed circuit boards. *Proceedings of the Institution of Mechanical Engineers, Part B: Journal of Engineering Manufacture*, 2009, **223**(11), 1465-1474.

87 Zhou, L., Wang, C.Y. and Qin, Z. Tool wear characteristics in high-speed milling of graphite using a coated carbide micro endmill. *Proceedings of the Institution of Mechanical Engineers, Part B: Journal of Engineering Manufacture*, 2009, **223**(3), 267-277.

88 Lee, K. and Dornfeld, D.A. Micro-burr formation and minimization through process control. *Precision Engineering*, 2005, **29**(2), 246-252.

89 Stein, J.M. and Dornfeld, D.A. Burr formation in drilling miniature holes. *CIRP Annals-Manufacturing Technology*, 1997, **46**(1), 63-66.

90 Heisel, U., Luik, M., Eisseler, R. and Schaal, M. Prediction of parameters for the burr dimensions in short-hole drilling. *CIRP Annals-Manufacturing Technology*, 2005,

54(1), 79-82.

91 Fang, F.Z. and Liu, Y.C. On minimum exit-burr in micro cutting. *Journal of Micromechanics and Microengineering*, 2004, **14**, 984-988.

92 Dornfeld, D. Strategies for preventing and minimizing burr formation. Berkeley, 2004.

93 Ko, S.L. and Dornfeld, D.A. A study on burr formation mechanism. *Journal of Engineering materials and technology*, 1991, **113**, 75-88.

94 Ko, S.L. and Dornfeld, D.A. Burr formation and fracture in oblique cutting. *Journal of Materials Processing Technology*, 1996, **62**(1-3), 24-36.

95 Fang, F., Wu, H., Liu, Y. and Ng, S. Burr Formation in Fly-cutting. (Citeseer, 2003).

96 Dubey, A.K. and Yadava, V. Laser beam machining--A review. *International Journal of Machine Tools and Manufacture*, 2008, **48**(6), 609-628.

97 Glass, J.M. Heat transfer in metallic glasses during laser cutting. *Heat Transfer in Manufacturing and Materials Processing*, 1977, **13**, 31-38.

98 Rajaram, S. and Coyle, R.J. Numerical modeling of laser material processing. *Proc. of the Materials Processing Symp. ICALEO 83*, 1983, **38**, 216-223.

99 Smith, R.N., Surprenant, R.T. and Kaminshki, D. Fracture characteristics of an aluminum oxide ceramic during continuous wave carbon dioxide laser cutting. *Journal of Laser Applications*, 1992, **4**(2), 25-32.

100 Cline, H.E. and Anthony, T.R. Heat treating and melting material with a scanning laser or electron beam. *Journal of Applied Physics*, 1977, **48**(9), 3895-3900.

101 Wellershoff, S.S., Hohlfeld, J., G de, J. and Matthias, E. The role of electron-phonon coupling in femtosecond laser damage of metals. *Applied Physics A: Materials Science & Processing*, 1999, **69**(7), 99-107.

102 Mannion, P., Magee, J., Coyne, E., O'Connor, G. and Glynn, T. The effect of damage accumulation behaviour on ablation thresholds and damage morphology in ultrafast laser micro-machining of common metals in air. *Applied Surface Science*, 2004, **233**(1), 275-287.

103 Schaffer, C.B. Interaction of femtosecond laser pulses with transparent materials. (Harvard University, 2001).

104 Allor, R.L. and Jahanmir, S. Current problems and future directions for ceramic machining. *American Ceramic Society Bulletin*, 1996, **75**(7), 40-43.

105 Konig, W. and Zaboklicki, A. Laser-assisted hot machining of ceramics and composite materials. *NIST Special Publication*, 1993, **847**(6), 455-463.

106 Wiedenmann, R., Langhorst, M. and Zaeh, M. Computerized optimization of the process parameters in laser-assisted milling. *Physics Procedia*, 2011, **12**, 607-616.

107 Jung, J. and Lee, C. Cutting temperature and laser beam temperature effects on cutting tool deformation in laser-assisted machining. *Proceedings of the International MultiConference of Engineers and Computer Scientists*, 2009.

108 Chang, C.W. and Kuo, C.P. Evaluation of surface roughness in laser-assisted machining of aluminum oxide ceramics with Taguchi method. *International Journal of Machine Tools and Manufacture*, 2007, **47**(1), 141-147.

109 Shen, X. and Lei, S. Experimental study on operating temperature in laser-assisted milling of silicon nitride ceramics. *The International Journal of Advanced Manufacturing Technology*, 2011, **52**(1), 143-154.

110 Dumitrescu, P., Koshy, P., Stenekes, J. and Elbestawi, M. High-power diode laser assisted hard turning of AISI D2 tool steel. *International Journal of Machine Tools and Manufacture*, 2006, **46**(15), 2009-2016.

111 Steen, W.M. *Laser Material Processing*. (Springer, New York, 2003).

112 Steen, W.M. and Mazumder, J. *Laser material processing*. (Springer Verlag, 2010).

113 Yang, B. Experimental and numerical investigation of laser assisted milling of silicon nitride ceramics. (Kansas State University, 2009).

114 Chang, C.W. and Kuo, C.P. An investigation of laser-assisted machining of Al2O3 ceramics planing. *International Journal of Machine Tools and Manufacture*, 2007, **47**(3-4), 452-461.

115 Rozzi, J.C., Pfefferkorn, F.E., Shin, Y.C. and Incropera, F.P. Experimental evaluation of the laser assisted machining of silicon nitride ceramics. *Journal of Manufacturing Science and Engineering*, 2000, **122**, 666-671.

116 Rozzi, J.C., Pfefferkorn, F.E., Incropera, F.P. and Shin, Y.C. Transient, three-dimensional heat transfer model for the laser assisted machining of silicon nitride: I. Comparison of predictions with measured surface temperature histories. *International Journal of Heat and Mass Transfer*, 2000, **43**(8), 1409-1424.

117 Shelton, J.A. and Shin, Y.C. Experimental Evaluation of Laser-Assisted Micromilling in a Slotting Configuration. *Journal of Manufacturing Science and*

Engineering, 2010, **132**, 021008.

118 Anderson, M., Patwa, R. and Shin, Y.C. Laser-assisted machining of Inconel 718 with an economic analysis. *International Journal of Machine Tools and Manufacture*, 2006, **46**(14), 1879-1891.

119 Ding, H. and Shin, Y.C. Laser-assisted machining of hardened steel parts with surface integrity analysis. *International Journal of Machine Tools and Manufacture*, 2010, **50**(1), 106-114.

120 Jeon, Y. and Pfefferkorn, F. Effect of laser preheating the workpiece on micro end milling of metals. *Journal of Manufacturing Science and Engineering*, 2008, **130**, 011004.

121 Yang, B. and Lei, S. Laser-Assisted Milling of silicon nitride ceramic: a machinability study. *International Journal of Mechatronics and Manufacturing Systems*, 2008, **1**(1), 116-130.

122 Brecher, C., Emonts, M., Rosen, C.J. and Hermani, J.P. Laser-assisted milling of advanced materials. *Physics Procedia*, 2011, **12**, 599-606.

123 Singh, R. and Melkote, S.N. Hybrid laser-assisted mechanical micromachining (LAMM) process for hard-to-machine materials. *Journal of Laser Micro/Nanoengineering*, 2007, **2**(2), 156-161.

124 Kim, J.D., Lee, S.J. and Suh, J. Characteristics of laser assisted machining for silicon nitride ceramic according to machining parameters. *Journal of Mechanical Science and Technology*, 2011, **25**(4), 995-1001.

125 Kumar, M., Melkote, S. and Lahoti, G. Laser-assisted microgrinding of ceramics. *CIRP Annals-Manufacturing Technology*, 2011, **60**(1), 367-370.

126 http://info.coatings.hc360.com. (accessed on 09/01/2009).

127 Prokhorov, A.M., Konov V.I., Ursu I., Mihailescu I.N. *Laser Heating of Metals*. (IOP Publishing Ltd, 1990).

128 James, T.L. and David, E.P. *Industrial Lasers and Their Applications*. (Prentice-Hall international London, 1992).

129 Brinksmeier, E. and Riemer, O. Deterministic production of complex optical elements. *Production Engineering and Computers*, 2002, **4**(5), 63-72.

130 Pimenov, S., Kononenko, V., Ralchenko, V., Konov, V., Gloor, S., Lüthy, W., Weber, H. and Khomich, A. Laser polishing of diamond plates. *Applied Physics A: Materials Science & Processing*, 1999, **69**(1), 81-88.

131 Ozkan, A.M., Malshe, A.P. and Brown, W.D. Sequential multiple-laser-assisted polishing of free-standing CVD diamond substrates. *Diamond and Related Materials*, 1997, **6**(12), 1789-1798.

132 Ukar, E., Lamikiz, A., López de Lacalle, L., del Pozo, D. and Arana, J. Laser polishing of tool steel with CO2 laser and high-power diode laser. *International Journal of Machine Tools and Manufacture*, 2010, **50**(1), 115-125.

133 Perry, T.L., Werschmoeller, D., Li, X., Pfefferkorn, F.E. and Duffie, N.A. Pulsed laser polishing of micro-milled Ti6Al4V samples. *Journal of Manufacturing Processes*, 2009, **11**(2), 74-81.

134 Shao, T., Hua, M., Tam, H. and Cheung, E.H.M. An approach to modelling of laser polishing of metals. *Surface and Coatings Technology*, 2005, **197**(1), 77-84.

135 Benardos, P.G. and Vosniakos, G.C. Prediction of surface roughness in CNC face milling using neural networks and Taguchi's design of experiments. *Robotics and Computer-Integrated Manufacturing*, 2002, **18**(5-6), 343-354.

136 Li, H.Z., Zeng, H. and Chen, X.Q. An experimental study of tool wear and cutting force variation in the end milling of Inconel 718 with coated carbide inserts. *Journal of Materials Processing Technology*, 2006, **180**(1-3), 296-304.

137 Manna, I., Chattopadhyay, P.P., Banhart, F., Croopnick, J. and Fecht, H.J. Microstructural evolution of wear-resistant FeCrB and FeCrNiCoB coating alloys during high-energy mechanical attrition. *Wear*, 2008, **264**(11-12), 940-946.

138 Yao, S.H., Su, Y.L., Kao, W.H. and Cheng, K.W. A wear-resistant coating--Oxidized graded multilayer TiN/W coating. *Materials Letters*, 2010, **64**(1), 99-101.

139 Merdol, S.D. and Altintas, Y. Virtual cutting and optimization of three-axis milling processes. *International Journal of Machine Tools and Manufacture*, 2008, **48**(10), 1063-1071.

140 Toh, C.K. Cutter path strategies in high speed rough milling of hardened steel. *Materials & Design*, 2006, **27**(2), 107-114.

141 Evans, C.J. and Bryan, J.B. "Structured" "textured" or "engineered" surfaces. *CIRP Annals-Manufacturing Technology*, 1999, **48**(2), 541-556.

142 Kawasegi, N., Sugimori, H., Morimoto, H., Morita, N. and Hori, I. Development of cutting tools with microscale and nanoscale textures to improve frictional behavior. *Precision Engineering*, 2009, **33**(3), 248-254.

143 ISO 8688-2. Tool-life testing in milling — Part 2: end milling. 1989.

144 Durazo-Cardenas, I., Shore, P., Luo, X., Jacklin, T., Impey, S. and Cox, A. 3D characterisation of tool wear whilst diamond turning silicon. *Wear*, 2007, **262**(3-4), 340-349.

145 Luo, X., Cheng, K., Webb, D. and Wardle, F. Design of ultraprecision machine tools with applications to manufacture of miniature and micro components. *Journal of Materials Processing Technology*, 2005, **167**(2-3), 515-528.

Appendix 1

Key Engineering Materials Vol. 496 (2012) pp 44-49
Online available since 2011/Dec/22 at www.scientific.net

doi:10.4028/www.scientific.net/KEM.496.44

Laser assisted micro grinding of high strength materials

W Chang[1, a], X Luo[1,b], Q Zhao[2,c] J Sun[1,d] and Y Zhao[2,e]

[1]Heriot-Watt University, Edinburgh EH14 4AS, UK

[2]Center for precision Engineer, Harbin Institute of Technology, China

[a]wc129@hw.ac.uk, [b]xl90@hw.ac.uk, [c]zhaoqingliang@hit.edu.cn,

[d]js173@hw.ac.uk, [e]luobo4423362@163.com

Keywords: Laser assisted grinding, Hybrid process, Micro grinding, Subsurface damage

Abstract.
This paper aims to develop a laser assisted grinding process capable of manufacturing micro features in high strength materials. A diode laser with wavelength 808 nm was set on a precision grinding machine. Micro grooves were fabricated on high strength materials including silicon nitride and aluminium oxide by using the laser assisted grinding process, i.e. laser pre-heat workpiece flowed by micro grinding. The experimental results showed that the laser assisted grinding process resulted in deeper grooves due to thermal expansion of workpiece materials caused by laser heating. However, the machined surface roughness was more consistently better than that obtained using solo grinding process and applying coolant. No subsurface damage was observed in the SEM images of cross sections of the machined workpieces when laser assisted grinding process was used.

Introduction

High strength materials, including silicon nitride (Si_3N_4) and aluminium oxide (Al_2O_3), are widely used in the application of highly stressed components. Due to high hardness of such workpiece materials, conventional machining approached such as grinding and milling suffer from low machining efficiency and high tool wear which will affect the attainable fine surface quality. Yang [1] found the laser heating could improve the machinability of silicon nitride ceramics through reducing cutting force, increasing tool life and reducing workpiece edge chipping. Melkote [2] and Brecher [3] presented laser assisted milling which can obtain much better surface roughness. Singh [4] investigated the impact of laser power, spot size and speed to reduce cutting force and tool deflections when fabricating hard-to-machine materials. Laser assisted milling/turning processes have been studied in many researches but very limited work has been reported on laser assisted grinding processes [5].

This paper presents an experimental study of the laser assisted micro grinding process. A diode laser system has been integrated into a grinding machine. Experiments have been carried out on the machine to investigate laser assisted micro grinding process on materials including Si_3N_4 and Al_2O_3. The grooves dimension, grinding force, surface roughness, microstructure of machined surface and subsurface damage are also discussed in this study.

Experiment setup

The experimental equipments of laser assisted micro grinding are shown in Fig 1. The grinding machine (MUGK7120X5) consists of servo motors on the X and Z axes and a linear motor on the Y axis. A variable high speed spindle (SF3060-ST32) with rotational speeds up to 60,000 rpm and laser focus lens were fixed on the grinding machine. A 3 mm diameter grinding cutter with grit size of 70 - 80 μm was used in the experiment. The thickness of diamond layer was about 0.3 mm and the length was 15 mm. The diode laser power was up to 120 W and wavelength was 808 nm. The spot size was near 3.2 mm on the focus point and the distance between the focus point and the grinding cutter was about 10 mm. The workpiece was fixed on a small vice which was attached on a Kistler dynamometer (9256C). Two kinds of materials, Si_3N_4 and Al_2O_3, were investigated in this experiment. A nozzle with air assisting was used to blow grinding cutter on the Y axis.

In the experiments, three grooves were machined on each material. First groove was fabricated by traditional grinding approach with soluble oil coolant. Second groove was machined by using laser assisted grinding and air coolant on the grinding cutter. Final groove was manufactured by laser assisted grinding without applying any coolant. The spindle speed, feedrate and cutting depth were 10,000 rpm, 10 mm/min and 3 μm, respectively. The laser power was set to 45 W, 70 W on material of Si_3N_4 and Al_2O_3.

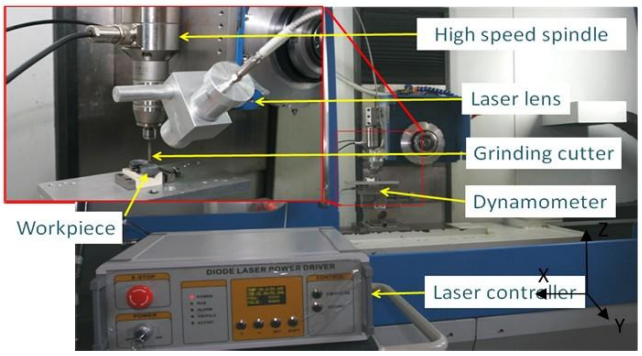

Fig 1. Experiment system of laser assisted grinding

Results and discussions

Groove depth

The variation in groove depth measured by a Form Talysurf (Taylor-Hobson Talysurf 4-120) is shown in Fig 2. It shows that the groove depth is relatively close to the set depth 3 μm. When laser assisted process was used, the groove depth was higher due to thermal expansion. In addition, the thermal expansion of the tool and the workpiece during laser heating affect the accuracy of the groove depth. The grinding depth manufactured by using laser assisted grinding with air coolant

was between the cutting depth machined by using conventional grinding process and laser assisted process. The workpiece was heated by laser assisted process but the air coolant counteracted such an effect and kept the temperature constant.

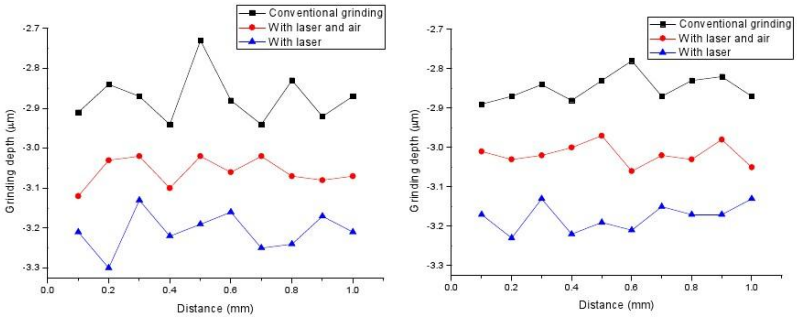

(a) Si_3N_4 (b) Al_2O_3

Fig 2. Groove depth on the middle surface cross the machining direction

Grinding force

The grinding force on Si_3N_4 measured by Kistler dynamometer is shown in Fig 3. The grinding force in conventional grinding process was smoother than that by using laser assisting grinding. The grinding force of laser assisted grinding without air coolant was very close to the conventional machining process, especially in the end of the grinding process. The largest grinding force was found when both the laser and air coolant were used. Under this circumstance, the grinding force varied greatly along the machining distance. This was because when the laser assisted grinding was used, the strength of material was decreased by the rise of the temperatures on the workpiece. Material with lower strength is much easier to be removed. However, the air coolant decreased temperature and the larger grinding force was presented. The average grinding force of conventional grinding process, with laser and with laser and air coolant were 3.51 N, 3.87 N and 9.54 N, respectively.

Surface roughness and microstructure of the machined surface

The surface roughness Ra on Si_3N_4 is shown in Table 1. They were measured by both a white light interferometer (Zygo New View 5000) and an AFM (DI NanoScope IIIa). The average surface roughness of conventional grinding, laser assisted grindings using air coolant and without using coolant were 202.594 μm, 334.599 μm and 139.923 μm, respectively. These two measured results showed that in terms of surface roughness, the quality of the machined surface can be greatly improved by the laser assisted grinding process.

The microstructure of the machined surface was measured by the AFM. The measured surface topographies are shown in Fig 4. and Fig 5. Large crest and trough could be observed on the machined surface obtained by using conventional grinding process. However, small grain size on the machine surface is observed in both Fig 4 (b) and Fig 5 (b) when laser assisted grinding was used. The microstructure of the machined surface on both materials showed that smooth surface crest and trough could be obtained when the laser assisted grinding processes was used.

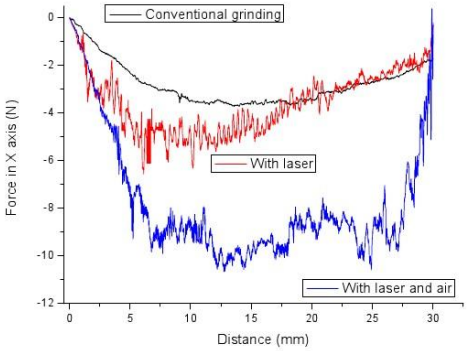

Fig 3. The grinding force against cutting distance

Table 1 Surface roughness on Si_3N_4

Surface roughness Ra	White light interferometer [μm]			AFM [μm]
Conventional grinding	182.543	225.197	200.041	164.43
Laser assisted grinding and air coolant	353.432	317.939	332.425	294.32
Laser assisted grinding	111.546	173.448	134.776	112.85

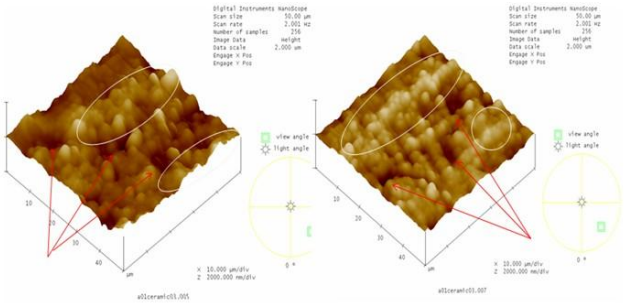

(a)Conventional grinding (b)Laser assisted grinding

Fig 4. The 3D structure of Si_3N_4

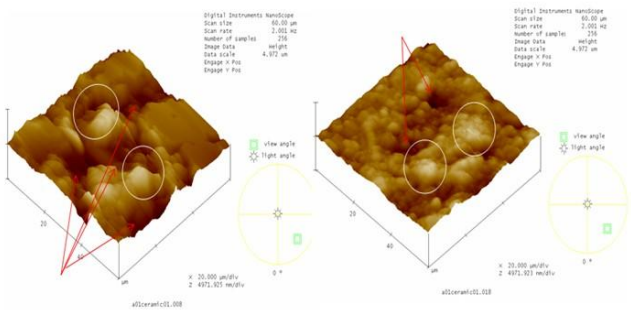

(a)Conventional grinding (b)Laser assisted grinding

Fig 5. The 3D structure of Al_2O_3

Subsurface damage

The workpiece was coated 2 nm gold on the top surface before testing subsurface damage. The cross sections were obtained on a focused ion beam system (FEI Quanta 3D FEG) and observed by a SEM built inside the FIB system. In each test region, cross sections with dimensions of 5 μm × 5 μm × 5 μm were milled under a beam current of 7 nA. The subsurface damage on Si_3N_4 after conventional grinding is shown in Fig 6(a). It could be seen that the material was compressed. Some small cracks were observed on Si_3N_4 after laser assisted grinding with air coolant applied. As shown in Fig 7 (a) the cracks were about 2 μm long on Al_2O_3 when conventional grinding was used. Some large cracks on Al_2O_3were also seen when laser assisted grinding with air coolant was used. However it was barely to see subsurface damage on both materials when the laser assisted grinding process without using any coolant was used.

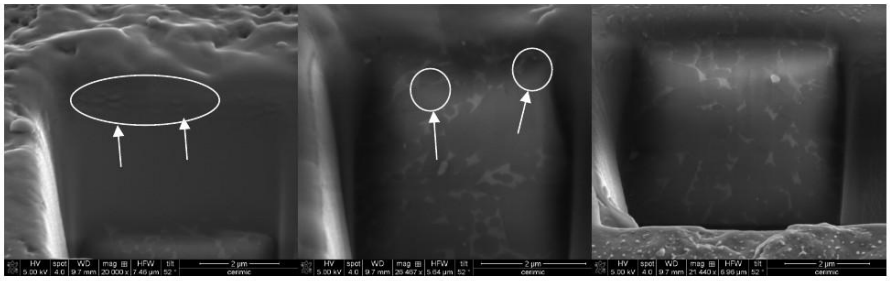

(a)Conventional grinding (b) Laser assisted grinding with air coolant (c) Laser assisted grinding

Fig 6. Subsurface damage on Si_3N_4

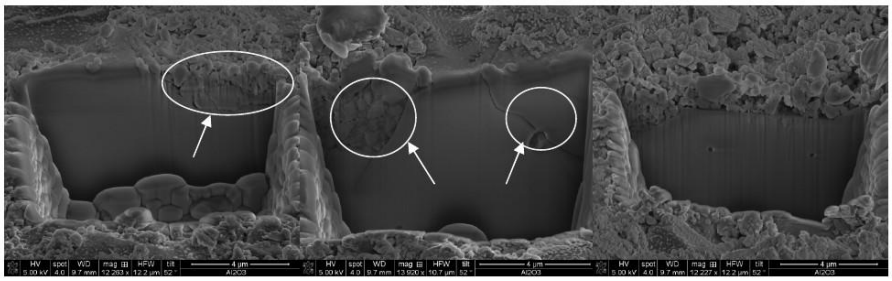

(a)Conventional grinding (b) Laser assisted grinding with air coolant (c) Laser assisted grinding

Fig 7. Subsurface damage on Al_2O_3

Conclusion

This research carried out experimental study on laser assisted grinding approach to machine hard-to-machine materials. The results showed that the laser assisting grinding achieved almost the same grinding depth as that in conventional grinding process. Although the grinding force were nearly the same as that in conventional grinding better surface roughness was achieved when the laser assisted process was applied. There was no subsurface damage obtained by using laser assisted grinding approach. This hybrid process will be very useful to fabricate brittle materials such as Si_3N_4 and Al_2O_3.

References

[1] B. Yang and S. Lei, in: Int. J. Mechatronics and Manufacturing System. Vol. 1 (2008), p. 116

[2] S. Melkote, M. Kumar, F. Hashimoto and G. Lahoti, in: CIRP annals - Manufacturing Technology. Vol. 58 (2009), p. 45

[3] C. Brecher, M. Emonts, C.J. Rosen and J.P. Hermani, in: Physics Procedia. Vol. 12 (2011), p. 599

[4] R. Singha and S.N. Melkote, in: Int. J. of Machine Tools and Manufacture. Vol. 47 (2007), p. 1139

[5] E. Westkamper, in: CIRP annals - Manufacturing Technology. Vol. 44 (1995), p. 317

Precision Machining VI
10.4028/www.scientific.net/KEM.496

Laser Assisted Micro Grinding of High Strength Materials
10.4028/www.scientific.net/KEM.496.44

DOI References

[1] B. Yang and S. Lei, in: Int. J. Mechatronics and Manufacturing System. Vol. 1 (2008), p.116.
doi:10.1504/IJMMS.2008.018282

[3] C. Brecher, M. Emonts, C.J. Rosen and J.P. Hermani, in: Physics Procedia. Vol. 12 (2011), p.599.
doi:10.1016/j.phpro.2011.03.076

Appendix 2

Proceedings of the Institution of Mechanical Engineers, Part B: Journal of Engineering Manufacture
http://pib.sagepub.com/

Fabrication of microfluidic injection moulds by a hybrid micromachining process

W-L Chang, X-C Luo, J M Ritchie, J-N Sun and C Mark

Proceedings of the Institution of Mechanical Engineers, Part B: Journal of Engineering Manufacture 2011 225: 458
DOI: 10.1177/2041297510394059

The online version of this article can be found at:
http://pib.sagepub.com/content/225/3/458

Published by:
SAGE
http://www.sagepublications.com

On behalf of:
Institution of MECHANICAL ENGINEERS
Institution of Mechanical Engineers

Fabrication of microfluidic injection moulds by a hybrid micromachining process

W-L Chang, X-C Luo*, J M Ritchie, J-N Sun, and **C Mark**
School of Engineering and Physical Sciences, Heriot-Watt University, Edinburgh, UK

The manuscript was received on 11 May 2010 and was accepted after revision for publication on 2 June 2010.

DOI: 10.1177/2041297510394059

Abstract: In this paper a hybrid micromachining approach was developed for the fabrication of microfluidic injection moulds. A micro injection mould with 500 μm wide and 200 μm high channels was machined by high-speed micromilling. The microchannels inside the mould were then processed by a Nd:YAG laser to remove the burrs generated in the micromilling process. The measurement results confirmed the effectiveness of this hybrid micromachining process in obtaining high-quality microproducts.

Keywords: microfluidic mould, micro burrs, micromilling, laser deburring, hybrid micromachining

1 INTRODUCTION

Today, low cost and disposable microfluidic chips are becoming very popular microproducts for disease diagnostic and chemical analysis [1]. Normally, these microfluidic chips are made of poly(methyl methacrylate) and the widths of the microchannels are restricted to be between 100 and 500 μm. Both good edge quality and fine surface roughness of the microchannel are crucial to carry the laminar flow within the microfluidic devices [2]. In the past, microfluidic chips have usually been fabricated using etching and photolithography. However, these two approaches face difficulties in producing the three-dimensional shape channels required for the advanced functionality of microfluidic chips. Therefore, a microinjection moulding approach has been developed to overcome this deficiency [3].

Micromilling is commonly used to machine moulds for injection moulding. However, the burrs or particles generated on the edge of channels in the mould will be replicated on the fabricated microfluidic chip and results in catastrophic flow turbulence in the microfluidic devices [4].

In this paper, a hybrid micromachining process is developed that is able to produce high-quality micro injection moulds through a combination of micromilling and laser deburring. The machined surface roughness and burrs generated before and after laser deburring are measured using a Form Talysurf and a coordinate measuring machine (CMM). The measurement results confirm the effectiveness of this hybrid process.

*Corresponding author: School of Engineering and Physical Sciences, Heriot-Watt University, Edinburgh, EH14 4AS, UK.
email: X.Luo@hw.ac.uk

2 A HYBRID MICROMACHINING PROCESS

Due to the increased complexity of the design and surface quality required for moulded micro-based products, the majority of micro injection moulds have to be manufactured using several production processes, including operations such as milling, turning, grinding, electro-discharge machining etc. Moving the workpiece between different stand-alone machine tools introduces machining errors due to workpiece repositioning and also increases the lead time. The development of multifunctional machining centres is a promising approach at the micro level since they will integrate several operations into a one-machine solution. Micro-milling is an efficient process with which to manufacture microfluidic moulds. However, the burrs inevitably generated by this process create problems in that burrs on the edge of a channel are replicated on the associated fabricated microchip resulting in catastrophic turbulent flow within the microfluidic devices [5, 6]. Therefore, a deburring process has to be carried out after micro milling.

In recent years, several deburring methods have been developed, including tumbling, electrochemical deburring, abrasive jet machining, water jet machining, and vibratory finishing [7]. However, these methods are either expensive or difficult to integrate onto a micromilling machine. In this study, an accurate laser deburring method was developed in order to compliment the micromilling process. Indeed, the laser system was relatively easy to integrate onto a micromachining centre which helps demonstrate the effectiveness of a hybrid machining process.

2.1 Micromilling process

Micro milling is a process that removes material with a sub-micron depth of cut when feeding a workpiece to a rotating tool. The cutting action of many teeth around the milling tool produces a fast machining method [8–11]. However, micromilling often fails to produce smooth or well finished edges on parts due to the generation of burrs [12, 13]. Poisson burrs and tear burrs are two kinds of burr generated during the micromilling of microproducts. The Poisson burr is the result of the workpiece bulging to one side when it is compressed by a milling cutter until permanent plastic deformation occurs. Tear burrs appear when a chip is torn from the workpiece rather than it shearing away [14, 15].

2.2 Laser deburring process

Laser machining is a non-contact material removal process that uses a laser focused on the surface of the workpiece [16, 17]. A key parameter of laser machining is the energy density (F). This can be predicted based on Beer's law

$$F = F_0 e^{-\alpha I_f} \tag{1}$$

where F_0, α, and I_f are the ablation threshold, optical penetration depth, and ablation rate, respectively. The ablation threshold and optical penetration depth are workpiece-dependent parameters. The ablation rate can be assumed to be equal to the height of the burrs to be removed per pulse. Therefore, the energy density can be obtained using equation (1).

The power of the laser system to be used in laser deburring can be obtained as

$$F = F \times F_r \times A \tag{2}$$

where P, F_r, and A are the laser power, laser frequency, and area of the laser spot, respectively.

3 MACHINING TRIALS

A microfluidic injection mould (made of NAK80) with channels 500 μm wide and 200 μm high was fabricated using the proposed hybrid machining approach.

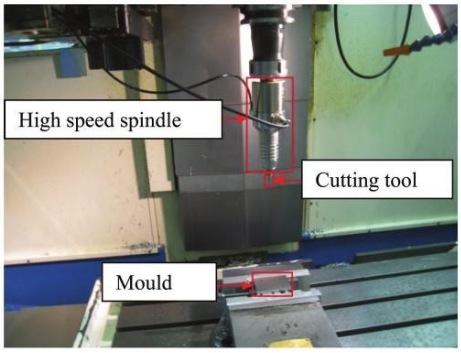

Fig. 1 Set-up for micromilling microfluidic mould using a high-speed spindle

The milling process was carried out on a conventional Takang VMC-1202 CNC machining centre equipped with a high-speed spindle (SF3060-ST32). This was followed by laser deburring using a Nd:YAG laser.

3.1 Micromilling

Two metal carbide end-mill tools with diameters of 2 mm and 500 μm were used for face milling and profiling, respectively. Both of them were two-flute long-neck end mills made from 93 per cent WC and 7 per cent Co. The cutter surface was coated with Mugen Coating Premium to improve tool life. The machining set-up is shown in Fig. 1. In the face milling and roughing profiling process, a spindle speed, feed rate, and depth of cut of 20 000 rev/min, 300 mm/min, and 0.05 mm were applied, respectively. In finish profiling milling, a 0.5 mm diameter milling cutter was used and a spindle speed of 30 000 rev/min, feed rate of 400 mm/min, and depth of cut of 0.2 mm were adopted. The surface roughness of the microfluidic channel and generated burrs were measured by a Taylor-Hobson Form Talysurf 4-120 and a Wenzel LH-65 CMM, respectively. The machined microfluidic mould is shown in Fig. 2.

3.2 Laser deburring

A Nd:YAG laser with a maximum power of 30 W and minimum frequency of 15 kHz was used in the deburring process after micromilling. The optical penetration depth and ablation threshold of NAK80 are 0.3 μm^{-1} and 2.5 J/cm^2 , respectively [18, 19] and the ablation rate was 10 μm/pulse. The energy density calculated using equation (1) was 50 J/cm^2. A laser power of 2.5 W was applied in the laser deburring process at a laser frequency of 15 kHz and a spot size of 20 μm in diameter. The laser cutting path followed the edge

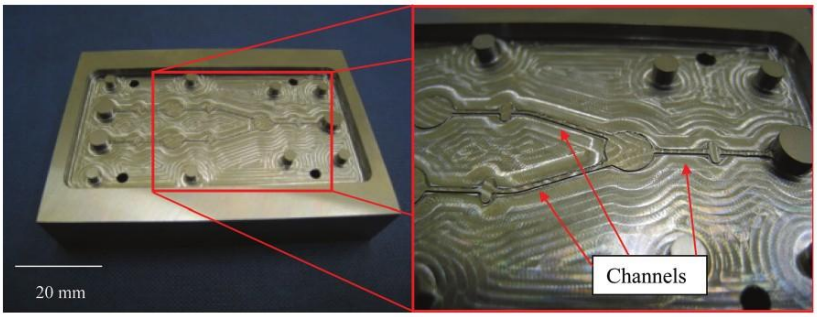

Fig. 2 The microfluidic mould machined using a high-speed spindle

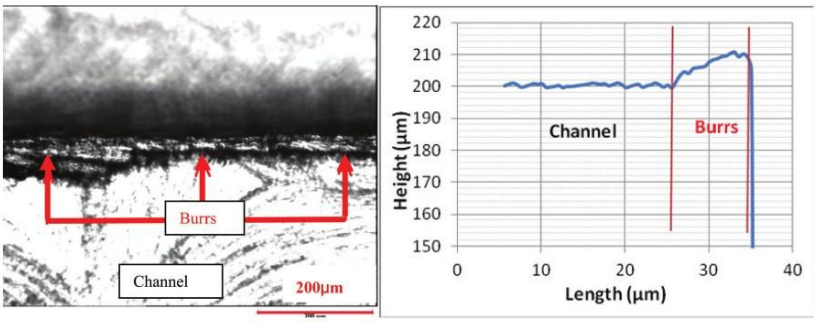

Fig. 3 The burrs on the edge of the microfluidic channels (a) the burrs observed on the edge of the channel and (b) the profile of the channel

of the microfluidic channel but with an offset of 5 μm on the surface in order to keep the laser focus point on the burrs of the microfluidic channel during laser processing.

4 RESULTS AND DISCUSSIONS

4.1 Generation of micro-sized burrs in micromilling

Figure 3(a) and (b) shows the burrs generated on the top surface of the micro-fluidic mould channel after the micromilling process. The optical micrograph was obtained using a Nikon Optophod microscope. All the burrs are observed to extend along the edge of the channel and to have a measured average width of about 10 μm. The heights of the burrs are between 8 and 10 μm. Thus, burrs with dimensions of 10 μm (width) × 10 μm (height) were generated when micromilling a channel with dimension of 500 μm (width) × 200 (height) μm. The cross-sectional profile of the microchannels on the mould is shown in Fig. 3(b).

The average measured surface roughness (R_a) on the top surface of the microfluidic channel (in an area without burrs) is 0.357 μm (the average of readings of 0.355, 0.348, and 0.367 μm). Taking into account the height of the burrs, the value of surface roughness R_a on the top surface of the microfluidic channel is in the order of several micrometres.

4.2 Laser deburring

Figure 4(a) shows an image of the edge of the microfluidic mould channel after the laser deburring process. It can be seen that the burrs generated in the micromilling process are completely removed by the laser deburring process. The quality of the micro-fluidic mould channel has been dramatically improved. The profile of the cross-section on the edge is shown in Fig. 4(b). The surface roughness R_a on

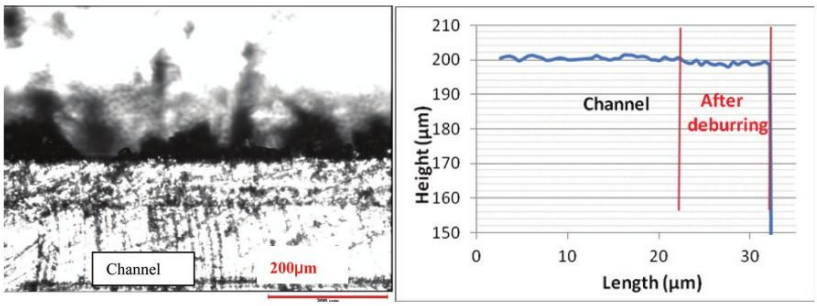

Fig. 4 The edge of the microfluidic channel after laser deburring (a) the burrs removed on the edge of the channel and (b) the profile of the channel after deburring

the top of the microfluidic channel after laser deburring is 0.417 μm (the average of readings of 0.408, 0.441, and 0.403 μm), very close to the value of the clear top surface machined surface (0.357 μm); therefore, the effectiveness of laser deburring is clearly demonstrated.

5 CONCLUSIONS

In this paper, a hybrid micromachining approach was developed to fabricate a microinjection mould. The micro fluidic channels, 500 μm (width) × 200 μm (depth), were micromilled using a high-speed spindle with a speed of 30 000 rev/min and a feed rate of 300 mm/min. The micro-sized burrs, inevitably formed at the channel edges during the micromilling process, were completely removed by using a Nd:YAG laser. The presented results demonstrate that high-quality microinjection moulds can be obtained by applying this hybrid micromachining approach. Future work will involve the development of a multifunctional micromachining centre which will integrate both micromilling and laser machining to obtain high-quality, repeatable microproducts.

ACKNOWLEDGEMENT

This work is supported by Jonathan P Parry and Professor Duncan P Hand at Heriot-Watt University.

REFERENCES

1 **Tseng, F. G., Chuang, Y. J.,** and **Lin, W.** A novel fabrication method of embedded micro channels employing simple UV dosage control and antireflection coating. In Proceedings of the 15th IEEE Conference on *Micro-electromechanical systems*, Las Vegas, Nevada, 20–24 January 2002, pp. 69–72 (IEEE Press, Piscataway, New Jersey).

2 **Tian, W. C.** *Microfluidics for biological applications*, 2008 (Springer, New York).

3 **Yun, D. J., Seo, T. I.,** and **Park, D. S.** Fabrication of biochips with micro fluidic channels by micro end-milling and powder blasting. *Sensors*, 2008, **8**(2), 1308–1320.

4 **Ko, S. L.** and **Dornfeld, D. A.** A study on burr formation mechanism. *J. Engng Mater. Technol.*, 1991, **113**, 75–87.

5 **de Souza, A. M., Sales, W. F., Ezugwu, E. O., Bonney, J.,** and **Machado, A. R.** Burr formation in face milling of cast iron with different milling cutter systems. *Proc. IMechE, Part B: J. Engineering Manufacture*, 2003, **217**(11), 1589–1596. DOI: 10.1243/095440503771909962.

6 **Huang, B. W., Cai, J. Z.,** and **Hsiao, W. L.** Cutting force estimation in a micromilling process. *Proc. IMechE, Part B: J. Engineering Manufacture*, 2010, **224**(10), 1615–1619. DOI: 10.1243/09544054JEM1960SC.

7 **Lee, S. H.** and **Asme, D.** Precision laser deburring. *J. Mfg Sci. Engng*, 2001, **123**, 601–608.

8 **Bang, Y., Lee, K.,** and **Oh, S.** 5-axis micro milling machine for machining micro parts. *Int. J. Adv. Mfg Technology*, 2005, **25**(9), 893–900.

9 **Takeuchi, Y., Sakaida, Y., Sawada, K.,** and **Sata, T.** Development of a 5-axis control ultraprecision milling machine for micromachining based on non-friction servomechanisms. *CIRP Ann.-Mfg Technol.*, 2000, **49**(1), 295–298.

10 **Newby, G., Venkatachalam, S.,** and **Liang, S. Y.** Empirical analysis of cutting force constants in micro-end-milling operations. *J. Mater. Process. Technol.*, 2007, **192**, 41–47.

11 **Jun, M. B. G., Liu, X., de Vor, R. E., Fellow, A.,** and **Kapoor, S. G.** Investigation of the dynamics of microend milling. Part I: model development. *J. Mfg Sci. Engng*, 2006, **128**, 893–900.

12 **Park, J. B., Wie, K. H., Park, J. S.,** and **Ahn, S. H.** Evaluation of machinability in the micro end milling

of printed circuit boards. *Proc. IMechE, Part B: J. Engineering Manufacture*, 2009, **223**(11), 1465–1474. DOI: 10.1243/09544054JEM1427.

13 **Zhou, L., Wang, C. Y.,** and **Qin, Z.** Tool wear characteristics in high-speed milling of graphite using a coated carbide micro endmill. *Proc. IMechE, Part B: J. Engineering Manufacture*, 2009, **223**(3), 267–277. DOI: 10.1243/09544054JEM1326.

14 **Gillespie, L. K.** and **Blotter, P. T.** Formation and properties of machining burrs. *Trans. ASME B, J. Engng Ind.*, 1976, **98**(1), 66–74.

15 **Lee, K.** and **Dornfeld, D. A.** Micro-burr formation and minimization through process control. *Precis. Engng*, 2005, **29**(2), 246–252.

16 **Denkena, B., Leon, L.,** and **Kästner, J.** Burr formation in microstructuring processes. In *Burrs-analysis, control and removal*, 2010, pp. 55-62 (Springer, Berlin).

17 **Dornfeld, S.** Precision laser deburring and acoustic emission feedback. *J. Mfg Sci. Engng*, 2001, **123**(2), 356–364.

18 **18 Mannion, P. T., Magee, J., Coyne, E., O'Connor, G. M.,** and **Glynn, T. J.** The effect of damage accumulation behaviour on ablation thresholds and damage morphology in ultrafast laser micro-machining of common metals in air. *Appl. Surf. Sci.*, 2004, **233**(1-4), 275–287.

19 **Schaffer, C.** *Interaction of femtosecond laser pulses with transparent materials.* PhD Thesis, Department of physics, Harvard University, 2001.

APPENDIX 1

Notation

A	area of spot size
F	energy density
F_0	ablation threshold
F_r	frequency
I_f	ablation rate
P	laser power
α	optical penetration depth

Appendix 3

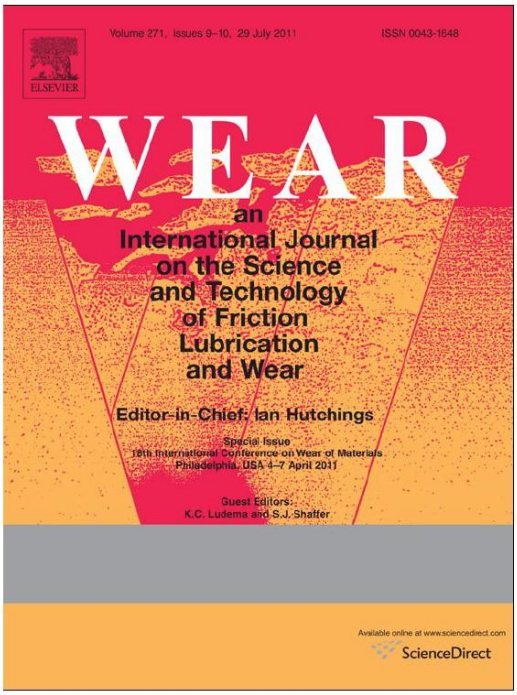

Wear 271 (2011) 2433–2437

Contents lists available at ScienceDirect

Wear

journal homepage: www.elsevier.com/locate/wear

Short communication

Investigation of microstructured milling tool for deferring tool wear

Wenlong Chang, Jining Sun, Xichun Luo*, James M. Ritchie, Chris Mack

School of Engineering and Physical Sciences, Heriot-Watt University, Edinburgh EH14 4AS, UK

ARTICLE INFO

Article history:
Received 1 September 2010
Received in revised form
15 December 2010
Accepted 15 December 2010

Keywords:
Microstructured tool
Flank tool wear
Cutting force
Micromilling

ABSTRACT

An approach to defer tool wear in the micromilling process is investigated in this paper. Three different microstructure patterns, i.e. a number of micro-scale grooves which are in the directions of horizontal (0°), perpendicular (90°) and sloping at 45° to the cutting edge of the rake face, are generated by focused ion beam on three identical end mill cutters. The effects of these microstructures on tool wear resistance performance are investigated through three sets of slot milling trials on a NAK80 by using a CNC milling machine. Cutting forces are measured by a Kistler dynamometer. The machined surface roughness (Ra) is obtained by a white light interferometer. The milling cutters are inspected by a Scanning Electron Microscope (SEM) after each set of slot milling trial. The measurement results show that low cutting force is achieved when the microstructures are in the perpendicular direction rather than in the horizontal direction to the cutting edge is used. The tool with perpendicular microstructures to its cutting edge possesses the best tool wear resistance performance against other tested microstructured tools and the normal tool.

1. Introduction

Micromilling is widely used for manufacturing complex shapes micromoulds such as metal forming mould and microinjection mould. However, tool wear has long been a severe problem to cause the degradation of the machined surface roughness and dimensional accuracy of the micro milled products [1]. A common practice in the micromilling industry to defer tool wear is to coat hard metal materials on the milling cutters [2–4]. Applying optimized cutting path and cutting parameters to reduce cutting force and increase tool life was also attempted by some researchers [5,6]. As decreasing friction force between the chip and the tool rake face can reduce tool wear, Evans and Bryan have investigated functional structured surfaces that could change the chip compression factor and normal force [7]. Kawasegi et al. have also investigated the micro-scale and nano-scale structures that could influence tool life in the turning process [8]. But no work has been carried out on the microstructures that can defer tool wear in the micromilling process.

In this study, an approach is developed to generate microstructures on the rake faces of the milling cutters by using focused ion beam milling. The effects of the fabricated microstructures on tool wear resistance performance are evaluated by machining trials.

2. Micro structuring milling cutter

Three types of microstructures, i.e. a number of grooves in the directions of horizontal, perpendicular and sloping at 45° to the cutting edge on the milling cutter rake faces were proposed in this study. The proposed dimension of each individual microgroove was 4.5 μm (width) by 300 μm (length) by 7.5 μm (depth). The distance between each groove was 4.5 μm. These microgrooves were fabricated on the rake faces of three identical carbide end milling cutters (1 mm diameter) by using a Focused Ion Beam (FIB) system (FEI Quanta 3D FEG) equipped with liquid gallium ion sources. In the structuring process the milling cutters were firstly mounted on the FIB work stage with the rake face to be structured perpendicular to the ion column so this surface was fully exposed to the incident ion beam. This would make sure the sidewalls of the microgrooves fabricated were perpendicular to the rake face. To reduce the influence of redeposition, multi-pass scanning of ion beam approach was used to obtain smooth microgroove bottom and uniform milling depth. Once this rake face was structured, the milling cutter was then flipped over 180° and remounted on the work stage. Therefore, another rake face to be structured would be vertical to the ion beam. Multi-pass scanning of ion beam approach was also used to fabricate microstructures on this rake face. 30 keV ion beam with the highest current of 65 nA were applied to obtain maximum material removal rate afforded by the FIB system. Fig. 1 shows the Scanning Electron Microscope (SEM) images of the fabricated three microstructured milling cutters and a normal milling cutter with identical geometry (but without microstructures on the rake faces) before the cutting trials. Sharp cutting edges could be

* Corresponding author. Tel.: +44 131 451 3197; fax: +44 131 4513129.
E-mail address: x.luo@hw.ac.uk (X. Luo).

0043-1648/$ – see front matter © 2011 Elsevier B.V. All rights reserved.
doi:10.1016/j.wear.2010.12.026

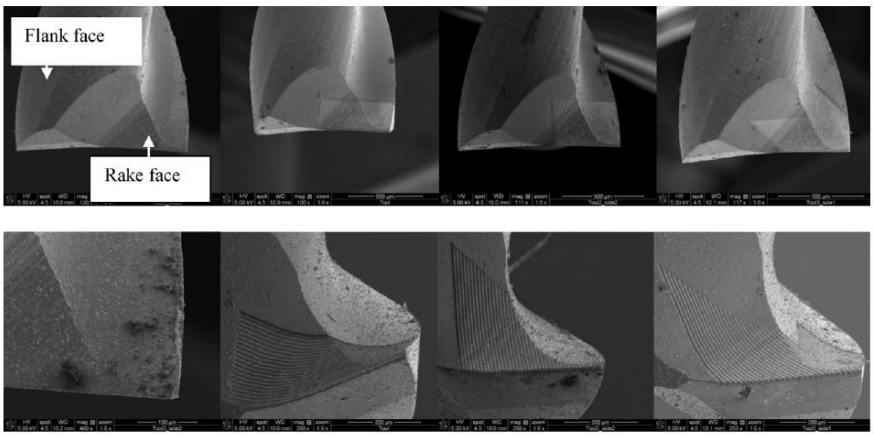

Fig. 1. SEM images of the microstructured milling cutters and a normal milling cutter.

observed in all tools. The measured dimensions of the microgrooves were consistent with the proposed fabricated dimensions.

3. Machining trials

The micromilling cutting trials to evaluate the tool wear resistance performance of these milling cutters were carried out on a conventional CNC machining centre (Takang VMC-1202), but using a high speed spindle (SF3060-ST32) instead of the conventional low speed machine spindle. The carbide end mill cutters (ø 2 mm and length 10 mm) were used. The cutting trial setup is shown in Fig. 2. A Kistler Dynamometer 9257BA which was fixed on the worktable was used to measure the cutting forces. A vise was attached on the Dynamometer. It was used to clamp the workpiece- a block of NAK80 which dimension was 80 mm × 16 mm × 10 mm. NAK80 (3.2% Ni, 1.8% Mn, 1% Cu and Al, 0.35% Si, 0.2% Mo and 0.12% C) is a material commonly used for fabrication of microinjection mould. Its hardness is 40 HRC. Four milling cutters shown in Fig. 1 were used in the evaluation machining trials to cut a number of slots on the NAK80 block. The evaluation trials included three sets of slot millings. In the first and second slot milling trials coolant (3% of soluble cutting oil and 97% water) were applied with a cutting distance of 16.5 mm. In the third set of slot milling trial no coolant was used but with a long cutting distance of 495 mm. A spindle speed, a feedrate and a depth of cut were set at 10,000 revolutions per minute (R.P.M.), 40 mm/min and 0.15 mm, respectively in all sets of slot milling trials. The machined surface roughness of the machined slots was measured by a white light interferometer (Zygo Newview5000). The milling cutters were inspected by a SEM after each set of slot milling trial.

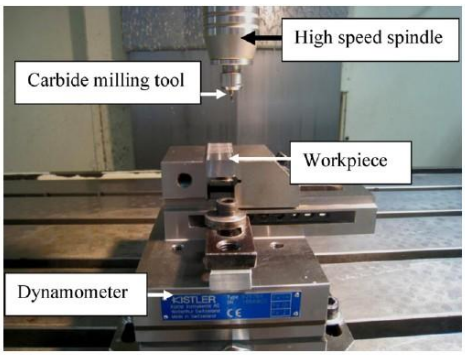

Fig. 2. Set up of the cutting trial.

4. Results and discussions

4.1. Cutting force and surface roughness

The measured cutting forces in the first set of slot milling trial are shown in Fig. 3. It can be seen that they oscillated around an average cutting force value. The average cutting forces when using the normal milling cutter, the microstructured milling tools with structures in the directions of normal horizontal, perpendicular and sloping at 45° to the cutting edges were 1.27 N, 1.16 N, 0.86 N and 1.42 N, respectively. The corresponding cutting forces without coolant were 1.29 N, 1.18 N, 1.03 N and 1.52 N, which were slightly larger than those using coolant. The results showed that the cutting forces when using horizontal and perpendicular microstructured milling cutters were smaller than those using the normal milling cutter. This indicated that these two kinds of microstructured tools might have better tool wear resistance performances than the normal milling cutter and the 45° microstructured cutter.

The measured surface roughness (Ra) in the first and third set of the slot milling trials is shown in Fig. 4. It can be seen that when using the horizontally and perpendicularly microstructured milling cutters without coolant, the achieved surface roughness was better than that with coolant. This was because the perpendicular microstructures could ease the removal of microchip smoothly even without the assistant of coolant. Fig. 4 shows that the smallest surface roughness Ra value was achieved when using the perpendicularly microstructured milling cutter. While using the horizontal

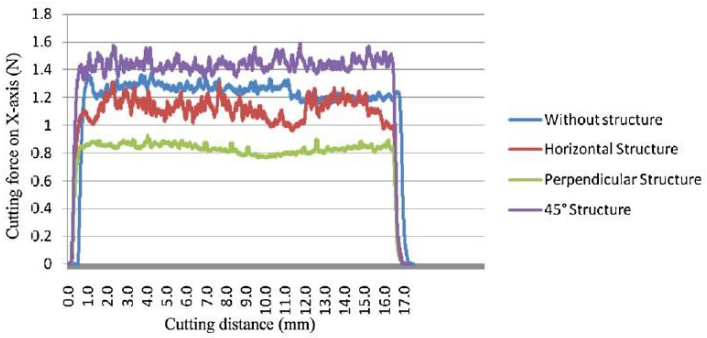

Fig. 3. The average cutting forces on X-axis when using the four milling cutters.

structured tool and applying coolant, the cutting force was stable in the beginning of the cut. After only a cutting distance of 5 mm, the cutting force increased dramatically and was bigger than that without using coolant (as shown in Fig. 5). For this reason, when applying coolant the obtained surface roughness (Ra) was higher than that without using coolant.

4.2. Tool wear

The normal milling cutter was broken at a cutting distance of 400 mm in the third set of slot milling trial. As this broken tool was too small to be found only the three microstructured milling cutters were measured by the SEM. The measured depth of microgrooves on the milling cutters was found to remain at 7.5 μm after the third set of slot milling trial. As shown in Fig. 6, the flank tool wear of the three microstructured milling tools were 0.181 mm, 0.134 mm and 0.17 mm, respectively. Although no tool has reached the end of tool life, i.e. 0.3 mm flank wear width as regulated by ISO [9], the microstructured milling cutter with perpendicular structures has shown the best tool wear resistance performance against other tools. This was evidenced by the smallest flank tool wear compared with other tools. The rake faces of the milling cutters were also measured by the SEM, which is shown in Fig. 7. The measured tool nose radius at the cutting edge on the rake face for these three microstructured tools were 0.080 mm, 0.069 mm and 0.075 mm, respectively. This result also indicated that the smallest tool wear was obtained for the microstructured tool with structures in the direction of perpendicular to the cutting edge as it still kept its sharpness even after a total cutting distance of 528 mm.

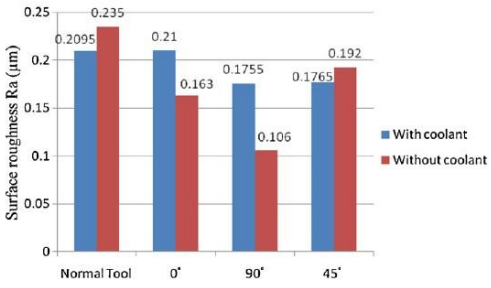

Fig. 4. Measured surface roughness (Ra) in the first and third set of cutting trials.

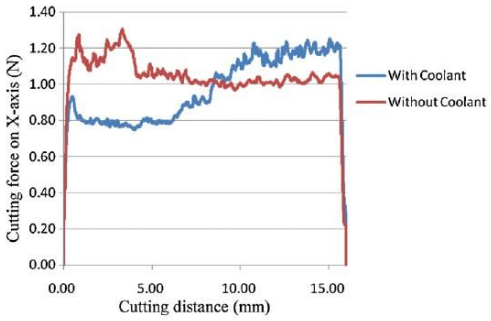

Fig. 5. The cutting forces on X-axis when using horizontal structured tool.

In order to further evaluate the wear resistance performance of these microstructured tools, comparisons of the measured cutting forces in the third slot milling trial was carried out. The results are shown in Fig. 8. It can be seen that the cutting force when using the normal cutter is larger than that when using microstructured milling cutters. A rapid increase of cutting force was observed before it was broken. When using microstructured tool with microstructures in the direction perpendicular to the cutting edge, the smallest cutting force was obtained. Durazo-Cardenas et al. have reported that the slope of cutting forces against cutting distance would give a correct indication of tool wear resistance performance. The smaller the slope was the longer the tool life was [10]. As shown in Fig. 8, the smallest slope of the cutting force against the cutting distance was observed when the perpendicularly microstructured tool was used in the milling process. Therefore, the microstructure in the direction of perpendicular to the cutting edge was the best structure which could defer tool wear and obtain prolonged tool life.

5. Summary of results

In this paper, three types of microstructures which are in the directions of horizontal, perpendicular and sloping at 45° to the cutting edge are fabricated by the FIB on the rake faces of three micromilling cutters. The tool wear resistance performances of these microstructured tools and a normal milling cutter are evaluated through three sets of slot milling trials on a NAK80 specimen. The smallest cutting force was obtained when using the perpen-

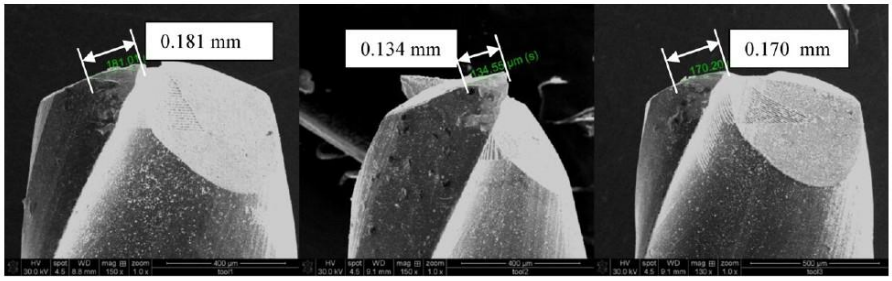

Fig. 6. Measured flank tool wear of the microstructured tools after the third set of cutting trial.

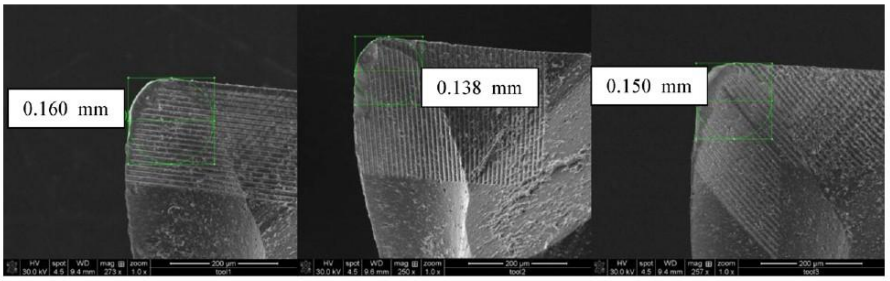

Fig. 7. Measured tool nose radius of the microstructured tools after the third set of cutting trial.

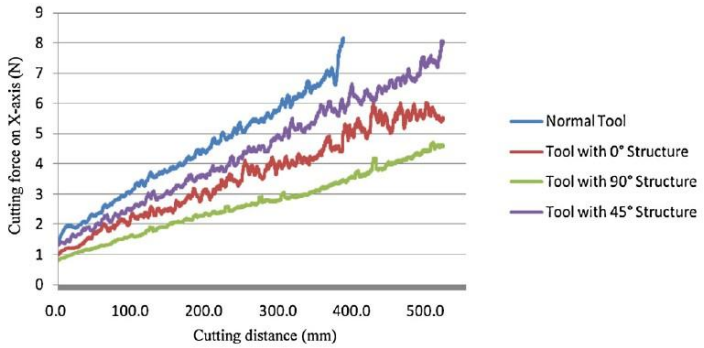

Fig. 8. Variations of cutting force on X-axis against machining distance in the third set of slot milling trial.

dicularly microstructured tool. The smallest flank tool wear of 0.134 mm was also achieved for this tool. Even after a total cutting distance of 528 mm the cutting edge of this microstructrured tool can still keep its sharpness. When using this microstructured tool the smallest slope of the cutting force against the cutting distance was observed. The above results indicate that microstructuring rake faces of the micromilling cutters can effectively improve their tool wear resistance performance. The microstructure in the direction of perpendicular to the cutting edge is the best structure which can defer tool wear and obtain prolonged tool life.

References

[1] P.G. Benardos, G.C. Vosniakos, Prediction of surface roughness in CNC face milling using neural networks and Taguchi's design of experiments, Robotics and Computer-Integrated Manufacturing 18 (2002) 343–354.

[2] H.Z. Li, H. Zeng, X.Q. Chen, An experimental study of tool wear and cutting force variation in the end milling of Inconel 718 with coated carbide inserts, Journal of Materials Processing Technology 180 (2006) 296–304.
[3] I. Manna, P.P. Chattopadhyay, F. Banhart, J. Croopnick, H.J. Fecht, Microstructural evolution of wear-resistant FeCrB and FeCrNiCoB coating alloys during high-energy mechanical attrition, Wear 264 (2008) 940–946.
[4] S.H. Yao, Y.L. Su, W.H. Kao, K.W. Cheng, A wear-resistant coating—oxidized graded multilayer TiN/W coating, Materials Letters 64 (2010) 99–101.
[5] W.Y.H. Liew, X. Ding, Wear progression of carbide tool in low-speed end milling of stainless steel, Wear 265 (2008) 155–166.
[6] C.K. Toh, Cutter path strategies in high speed rough milling of hardened steel, Materials & Design 27 (2006) 107–114.
[7] C.J. Evans, J.B. Bryan, "Structured" "textured" or "engineered" surfaces, CIRP Annals-Manufacturing Technology 48 (1999) 541–556.
[8] N. Kawasegi, H. Sugimori, H. Morimoto, N. Morita, I. Hori, Development of cutting tools with microscale and nanoscale textures to improve frictional behavior, Precision Engineering 33 (2009) 248–254.
[9] ISO 8688-2:1989, Tool-life testing in milling—Part 2: end milling.
[10] I. Durazo-Cardenas, P. Shore, X. Luo, T. Jacklin, S. Impey, A. Cox, 3D Characterisation of tool wear while diamond turning silicon, Wear 262 (2007) 340–349.

Appendix 4

Int. J. Nanomanufacturing, Vol. 7, Nos. 3/4, 2011 327

Laser deburring process for structured edges on precision moulds

Wenlong Chang, Xichun Luo*,
James M. Ritchie, Jining Sun and
Christopher Mack

Department of Mechanical Engineering,
School of Engineering and Physical Sciences,
Heriot-Watt University,
Edinburgh EH14 4AS, UK
Fax: 44-131-4513129
E-mail: wc129@hw.ac.uk
E-mail: xl90@hw.ac.uk
E-mail: J.M.Ritchie@hw.ac.uk
E-mail: js173@hw.ac.uk
E-mail: C.A.Mack@hw.ac.uk
*Corresponding author

Abstract: In this paper a laser deburring process is developed to remove micro burrs generated by micromilling processes in order to obtain high quality micro fluidic injection mould. A two-temperature model (TTM) is used to determine the critical laser machining parameters such as the laser energy density and laser power. The laser deburring experiment is carried on by using an Nd:YAG nanosecond laser source with frequency of 15 Hz and a spot size of 5 μm. The edge quality and the machined surface of micro channels in the micro fluidic mould are measured by a SEM and a white light interferometer. The measurement results show that the micro burrs on the micro channels in the micro fluidic mould have been completely removed. The average surface roughness (Ra) was only 0.114 μm after the laser deburring process. Therefore, laser deburring process cannot only remove micro burrs on the micro fluidic channel but also help to achieve good surface finish on the mould.

Keywords: laser deburring; micro fluidics; micromilling; precision mould; hybrid process.

Reference to this paper should be made as follows: Chang, W., Luo, X., Ritchie, J.M., Sun, J. and Mack, C. (2011) 'Laser deburring process for structured edges on precision moulds', *Int. J. Nanomanufacturing*, Vol. 7, Nos. 3/4, pp.327–335.

Biographical notes: Wenlong Chang is doing his PhD in Department of Mechanical Engineering at Heriot-Watt University since 2008. His research is about hybrid machining processes which is including micro milling, micro turning, micro grinding and laser machining. He worked in Metal Industry Research and Development Centre in Taiwan in September 2005. In the centre, he handles the investigations about the ultra short pulse pico-second laser machine and he is good at micro manufacturing and CAD/CAE/CAM software system. He joined an international collaboration project with Georgia Tech in USA on topic of spatial error compensation.

Xichun Luo is a Lecturer in Ultra Precision Machining and Nanomanufacturing at Heriot-Watt University. He obtained his PhD in Ultra Precision Manufacturing at Harbin Institute of Technology in 2002 and second PhD in Precision Engineering at Leeds Metropolitan University in 2004. From 2004 to 2007, he worked at Cranfield University as a Research Officer and is involved in several world leading research projects in ultra precision diamond grinding, diamond turning of freeform optics and machine tool development. In September 2007, he joined the School of Engineering and Physical Science of Heriot-Watt University as a Lecturer. He has published one book chapter and more than 40 papers in peer-reviewed journals and international conferences.

James M. Ritchie is a Professor in Manufacturing Sciences and the Head of Mechanical Engineering Department at Heriot-Watt University. He has an international reputation in precision engineering, micromachining, haptics manufacturing and virtual manufacturing. He has published three books and more than 100 journal papers. He currently held more than £1 M research grants from EPSRC grant challenge and EPSRC IMRC.

Jining Sun is a PhD in Heriot-Watt University. He obtained his Bachelor degree and Master degree in Peking University, China. His research is mainly focused on micro/nano fabrication of three dimensional freeform structured surfaces by focused ion beam lithography and nanoimprint lithography. He is also interested in Monte Carlo simulation and topography simulation algorithms.

Christopher Mack is a Professional Mechanical Engineer working in the Advanced Manufacturing Unit at Heriot-Watt University. He has been employed there for 23 years and during this time has been involved in imparting his knowledge and experience to assist many researches, undergraduate and commercial projects. He is one of the most experienced CNC programmer/operators within the university and works daily with the industry standard equipment the unit houses.

This paper is a revised and expanded version of a paper entitled 'Laser deburring process for structured edges on precision moulds' presented at The 2nd International Conference on Nanomanufacturing (nanoMan2010), Tianjin, China, 24–26 September 2010.

1 Introduction

Micro biochips, such as micro fluidic devices, are becoming the most popular biomedical products (Tseng et al., 2002). These micro fluidic chips are usually made of PDMS and PMMA and the width of micro channels in them is restricted within several μms to few hundred μms. Both good edge quality and fine surface roughness of micro channel are crucial to carry on laminar flow in the micro fluidic devices (Tian and Finehout, 2008). In the past, micro fluidic chips were usually fabricated by photo-lithography and etching processes. However, these two methods are difficult to produce three dimensional shaped channels requested for the advanced functionalities of a micro fluidic chip. Micro injection moulding approach is then developed to overcome the shortcomings of above two fabrication approaches (Yun et al., 2008). Micro injection mould is commonly manufactured by the micromilling process. However, this process will generate unwanted

burrs on the mould. These burrs will be replicated on the structured surface of the final products in the moulding process and result in many problems such as component assembling difficulties, degrading functions and even injury of the workers (Lee and Dornfeld, 2001; Ramachandran et al., 1994). Therefore, deburring process become an imminent task to achieve good edge quality and smooth surface roughness on the precision moulds.

In this paper, a laser deburring process is developed to obtain high precision micro fluidic injection mould. The effectiveness of this new deburring approach has been confirmed by the measurement result of the edge quality and surface roughness of the micro channels on the mould by a whit light interferometer and a SEM.

2 Development of laser deburring process

The removal of burrs on the metal mould by laser is through a kind of thermal processing process which can be illustrated in Figure 1. Firstly, the laser beam is focused on the target surface. So the laser thermal energy is absorbed by the free electrons in the metal material during the interaction of laser pulse radiation. After that, the thermal energy will be transferred from the electrons to the lattices of the metal materials by thermal conductivity but some energy will disappear by thermal diffusion. The produced thermal energy will be used to melt or break metal materials to implement the removal of burrs from the metal mould. Laser energy density and laser power are two critical laser machining parameters for obtaining high quality mould by laser deburring. They can be calculated through a two-temperature model (TTM) (Wellershoff et al., 1999). In this model, the metal electrons and metal lattices are treated as two separate heat baths with temperature T_e and T_l respectively. The diffusion equation between the metal electrons and the metal lattices can be described as:

$$C_e \frac{\partial T_e}{\partial t} = -\frac{\partial Q(z)}{\partial z} - \gamma\left(T_e - T_l\right) + S \tag{1}$$

$$C_l \frac{\partial T_l}{\partial t} = \gamma\left(T_e - T_l\right) \tag{2}$$

where C_e, C_l, and z are the capacities of the metal electron and the metal lattice and the ablation rate to the target surface, respectively. $Q(z)$ is the electron heat flux and it can be calculated as: $Q(z) = -k_e \partial T_e / \partial z$. k_e is the metal electron thermal conductivity. S is the absorbed energy. As a nanosecond laser source is used in this paper, the metal electrons and metal lattices are in thermal equilibrium state, i.e., $T_e = T_l$. Therefore, equation (1) can be simplified as:

$$C_e \frac{\partial T_e}{\partial t} + \frac{-ke\partial Te / \partial z}{\partial z} = S \tag{3}$$

The absorbed energy S in equation (3) can be expressed as:

$$S = I(t) A_b \alpha e^{-\alpha z} \tag{4}$$

where $I(t)$ is the laser intensity. A_b and α are the surface transmissivity and optical penetration depth, respectively. The temperature of the metal electrons can be described as integration of equation (1):

$$T_e = \left[\frac{2I(t)At\alpha e^{-\alpha z}}{\dot{C}_e} \right]^{\frac{1}{2}} \tag{5}$$

The temperature of the metal lattice can be simplified as $T_1 \approx T_e t/C_1$. The temperature of the metal lattice can also be determined by the average cooling time of the electrons $\left(t = C_e T_e / 2\right)$, so it will have

$$T_1 \approx T_e^2 \frac{C_e}{2C_1} \approx \frac{F\alpha}{C_1} e^{-\alpha z} \tag{6}$$

where F is the laser energy density. The ablation threshold, $F_0 \approx T_1 C_1/\alpha$ can be described by the Arrhenius-type equation. Equation (6) can be written as:

$$F \approx F_0 e^{\alpha z} \tag{7}$$

The ablation threshold and the optical penetration depth are the metal material parameters. The ablation rate can be assumed to be equal to the height of burrs to be removed per pulse. Therefore, the energy density can be obtained through equation (7).

According to the definition of the energy density, the power of the laser system (P) to be used in the laser deburring process can be obtained as:

$$P = FF_r A \tag{8}$$

where F_r and A are the laser frequency and area of the laser spot respectively.

Figure 1 Schematic Illustration of the laser metal interactions in the laser deburring process

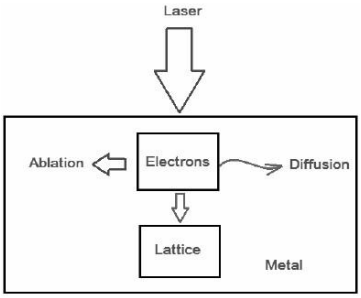

3 Micromilling and laser deburring experiment

Figure 2 showed a 3D CAD model of a micro fluidic injection mould with channels of 100 μm wide and 100 μm high. A metal mould (NAK80) was fabricated by micromilling on a CNC machining centre Takang VMC-1202 but using a high speed spindle SF3060-ST32 instead of a conventional spindle. Two metal carbide end mill tools with diameters of 1 mm and 400 μm were used for face milling and profiling respectively. In

the face milling and roughing profiling process, a spindle speed, a feed rate and a depth of cut of 25,000 rev/min, 200 mm/min and 0.05 mm were applied. In the finish profiling milling, a 0.5 mm diameter milling cutter was used and a spindle speed of 32,000 rev/min, a feed rate of 400 mm/min and a depth of cut of 0.2 mm were adopted. After the mould was machined by the micromilling processes, the edge of the micro channel was observed under a SEM (FEI Quanta3D FEG). The burrs generated on the channel were clearly seen in Figure 3. The height of burrs was measured about 10 µm by From Talysurf.

Figure 2 Micro injection mould 3D model

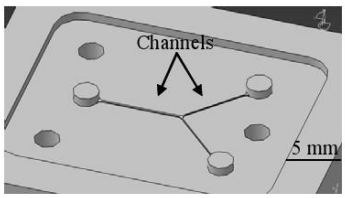

Figure 3 The burrs on the edge of the micro fluidic channels after micromilling (see online version for colours)

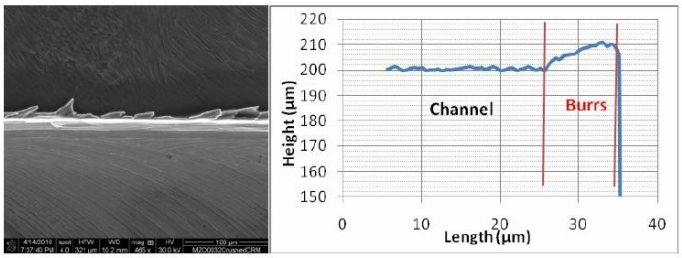

An Nd:YAG laser machine was used in the deburring process to remove the micro burrs. The maximum power, wavelength, frequency, pulse duration time and the smallest spot size of this Nd:YAG laser are 5 W, 355 nm, 15,000 Hz, 65 ns and 20 µm, respectively. The laser and workpiece are controlled by computer. The workpiece was fixed on working table and the resolution of linear stage is 1 µm. The laser deburring mechanism and schematic micro deburring process are showed in Figure 4 and Figure 5. In the laser deburring experiment, the ablation rate was assumed to be 10 µm/pulse because the height of burrs is about 10 µm. The parameters of the optical penetration depth and the ablation threshold of NAK80 were 0.3 μm^{-1} and 2.5 J/cm^2, respectively (Mannion et al., 2004; Schaffer, 2001). The determinate the cutting depth in laser machining is laser power. From equation (7), the relationship between the laser power and laser cutting depth are showed in Figure 6. The best laser power of 2.5 W was applied in the laser deburring process when using a laser frequency of 15 kHz and a spot size of 20 µm diameter. The laser cutting path followed the edge of the micro fluidic channel but with

an offset of 5 μm on the surface in order to keep the laser focus point on the burrs of the micro fluidic channel during the laser deburring processing.

Figure 4 A schematic diagram of Nd:YAG laser (see online version for colours)

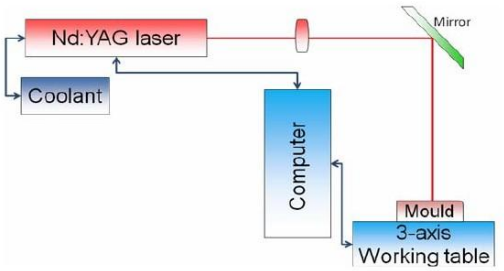

Figure 5 Schematic of micro laser deburring (see online version for colours)

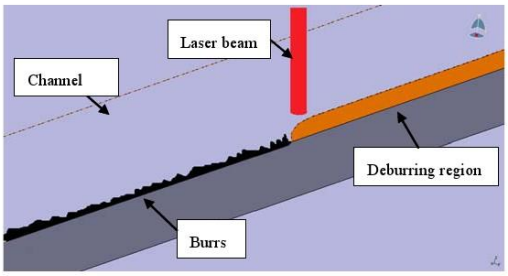

Figure 6 Theoretical laser machining depth against laser power (see online version for colours)

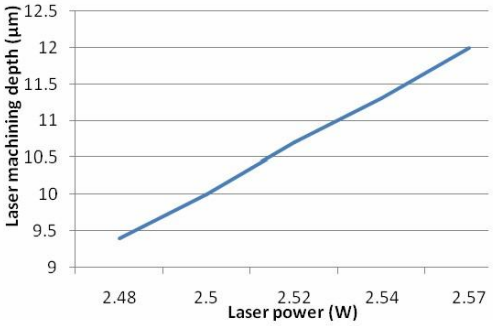

4 Result and discussion

Figure 7 showed a SEM image of an edge on the micro fluidic mould channel after the laser deburring process. It could be seen that the burrs generated in the micromilling process had been removed completely. Compared with Figure 3, the edge quality of the micro channels on the micro fluidic mould has been dramatically improved. The surface of the micro channels before and after laser deburring observed by the SEM was shown in Figure 8. It could be seen that there were some cracks generated on the machined surface after the micromilling process. However, after the laser deburring process the surface had been smooth. The surface roughness of machined surface was also measured by a white light interferometer (Zygo New View 5000). The measurement results showed that the average surface roughness (Ra) was 0.169 μm after milling process but the surface roughness was only 0.114 μm after the laser deburring process. Therefore, laser deburring process cannot only remove micro burrs on the micro fluidic channel but also achieve the surface roughness on the mould.

Figure 7 SEM image of the edge of the micro fluidic channel after laser deburring (a) after micromilling (b) after laser deburring (see online version for colours)

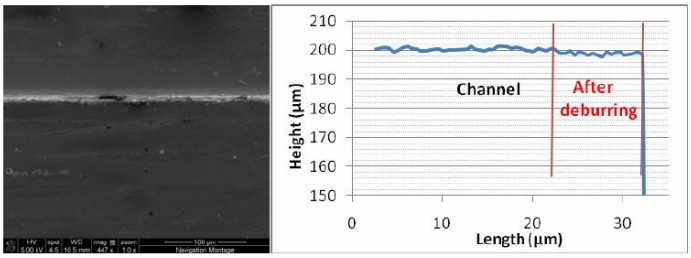

Figure 8 Machined surface topography after micromilling and laser deburring (see online version for colours)

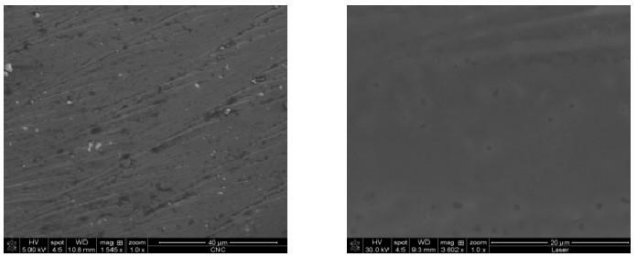

Figure 8 Machined surface topography after micromilling and laser deburring (continued) (see online version for colours)

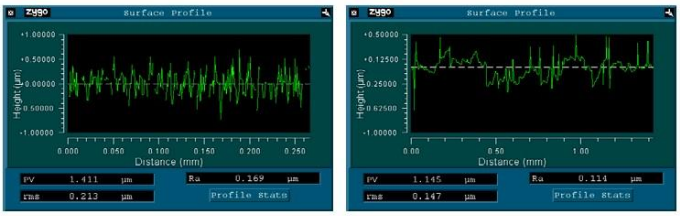

5 Conclusions

In this paper, theoretical and experimental investigations have been carried out to develop a laser deburring process to obtain high quality micro fluidic injection mould after micromilling process. It shows that the critical laser machining parameters including the laser energy density and laser power can be obtained based on a TTM model. An Nd:YAG nanosecond laser source with frequency of 15 Hz and a spot size of 5 µm is used in the laser deburring process development. The edge quality and machined surface of micro channels in the micro fluidic mould are measured by a SEM and a white light interferometer. The measurement results show that the micro burrs on the micro channels in the micro fluidic mould have been completed removed. The average surface roughness (Ra) of the machined surface was 0.169 µm but the surface roughness was only 0.114 µm after laser deburring. Therefore, laser deburring process cannot only remove micro burrs on the micro fluidic channel but also help to achieve good surface finish on the mould. Owing to the success of this experiment, future work will focus on development of a multifunctional micro machining centre that will integrate micromilling and laser machining operations to obtain high quality microproducts.

References

Lee, S.H. and Dornfeld, D.A. (2001) 'Precision laser deburring', *Journal of Manufacturing Science and Engineering*, **Vol. 123, pp.356–364.**

Mannion, P.T., Magee, J., Coyne, E., O'Connor, G.M. and Glynn, T.J. (2004) 'The effect of damage accumulation behaviour on ablation thresholds and damage morphology in ultrafast laser micro-machining of common metals in air', *Applied Surface Science*, **Vol. 233, Nos. 1–4, pp.275–287.**

Ramachandran, N., Pande, S.S. and Ramakrishnan, N. (1994) 'The role of deburring in manufacturing: a state-of-the-art survey', *Journal of Materials Processing and Technology*, **Vol. 44, pp.1–13.**

Schaffer, C. (2001) 'Interaction of femtosecond laser pulses with transparent materials', PhD thesis, Harvard University.

Tian, W.C. and Finehout, E. (2008) 'Microfluidics for biological applications', *Springer Science Business Media*, **New York.**

Tseng, F.G., Chuang, Y.J. and Lin, W.K. (2002) 'A novel fabrication method of embedded micro channels employing simple UV dosage control and antireflection coating', *IEEE 15 ICMEMS*, pp.69–72.

Wellershoff, S-S., Hohlfeld, J., Gudde, J. and Matthias, E. (1999) 'The role of electron-phonon coupling in femtosecond laser damage of metals', *Appl. Phys. A: Mater. Sci. Process.*, Vol. 69S, pp.99–107.

Yun, D.J., Seo, T.I. and Park, D.S. (2008) 'Fabrication of biochips with micro fluidic channels by micro end-milling and powder blasting', *Sensors*, Vol. 8, No. 2, pp.1308–1320.